

Copyright
by
Ashley Michelle Johnson
2004

**The Dissertation Committee for Ashley Michelle Johnson Certifies that this is the
approved version of the following dissertation:**

**Studies Toward the Development of an Electronically Switchable Ion
Exchange System**

Committee:

James A. Holcombe, Supervisor

Lynn E. Katz

Jennifer S. Brodbelt

Karen S. Browning

Keith J. Stevenson

**Studies Toward the Development of an Electronically Switchable Ion
Exchange System**

by

Ashley Michelle Johnson, B.S.

Dissertation

Presented to the Faculty of the Graduate School of

The University of Texas at Austin

in Partial Fulfillment

of the Requirements

for the Degree of

Doctor of Philosophy

The University of Texas at Austin

August, 2004

Dedication

The body of this work, and perhaps more importantly the will to complete it, are dedicated to my family whose gifts of love and support have made me whole ...

...To the memory of my grandfather who had a smile for everyone and the purest soul I will ever know, to my grandmother whose beauty and strength are more inspiring than she will ever fully understand, to my sister for being my “shipmate” and sharing with me her passion and creativity, to my father for allowing the whole world to become my “little pink box” and to my mother for always encouraging me to look for pictures in the clouds.

Acknowledgements

I would like to begin by extending a big “Thank you!” to everyone who helped me scientifically along the way – Thomas Kreschollek, Tim Smith, Todd McEvoy and Keith Stevenson for their help in constructing the glassy carbon electrodes and obtaining AFM images; Bill Balsanek for always being so available when I needed to collect ICP data; Michelle Chaumont, Bob Michie and Alan Campion for teaching me to use their Raman microscope and Dwight Romanovicz for helping me acquire the SEM images. Thank you to Gulay for being my favorite Turk and for seeing only great things in my cup. Thank you to Mike for the ice cream, the wine and, most importantly, your shoulder. I would especially like to thank Lisa for being my partner in crime and for our innumerable “How exactly does that isotherm thing work again?” and “What do you think about this story?” conversations. I would also like to thank Dr. Holcombe for his continued guidance over the past several years and for introducing me to the beauty of the “back-of-the-envelope” calculation – no matter how big an envelope might be needed to complete it. Finally, I would like to extend a special thank you to Benvenuto Cellini for helping me finally figure out a good answer to the inescapable “What do you want to be when you grow up?” question.

Studies Toward the Development of an Electronically Switchable Ion Exchange System

Publication No. _____

Ashley Michelle Johnson, Ph.D.

The University of Texas at Austin, 2004

Supervisor: James A. Holcombe

Early studies toward the development of a chemical-free means of reclaiming metals from an ion exchange system were begun by exploring the option of controlling metal-ligand interactions electrochemically. Poly-L-cysteine (PLC), a soft acid cationic metal chelator, was explored as an option for an electroactive ligand for use as an electronically switchable ion exchange system. Initial studies were conducted by immobilizing PLC onto a glassy carbon electrode creating a modified electrode. The modified electrode was characterized using electrochemical techniques, atomic spectroscopy and molecular spectroscopy.

Initial studies were conducted with poly-L-cysteine immobilized onto controlled pore glass and packed in a microcolumn for low pressure liquid chromatography experiments. Flow parameters, as well as the ability of poly-L-cysteine to act as a preconcentration agent, were established.

Electrochemical methods, specifically cyclic voltammetry, were used to confirm polymer attachment and to estimate that near monolayer coverage on the glassy carbon electrode surface existed. Further studies examined the kinetics of electron transfer through the use of large amplitude potential steps to demonstrate consistency with other types of modified electrodes. The pK_a of the polymer was determined to be between 7.5 and 8 by using surface charge density as a function of pH.

The poly-L-cysteine modified electrode, as well as an electrode modified with cysteine monomers, was evaluated for its metal binding capabilities. Using Cd^{2+} as a target metal, optimal binding conditions were established. Binding experiments were repeated with Co^{2+} , Cu^{2+} , Ni^{2+} and Pb^{2+} , as well as competitive binding studies comprised of binding in the presence of all five metals. Quantitative release of bound metals was achieved by repeatedly pulsing the potential from open circuit to a number of anodic potentials.

Raman microscopy was used to probe the redox states of PLC, confirm the complexation of Cd^{2+} to the thiol groups of PLC and to establish an average formal reduction potential for PLC of -0.3 V vs. SHE. The possibility of multiple formal potentials was explored through the use of mathematical models based on the Nernst equation. The models suggest that many formal potentials do exist although the exact nature of the distribution could not be determined.

As a plausible electronically switchable ion exchange option for heavy metal oxyanions, pyrrole was electropolymerized and investigated as a ligand for toxic chromate remediation. Polypyrrole, which bears a structural similarity to poly-L-histidine, a previously studied chromate chelator, was shown to have potential to both remediate and speciate Cr(VI) from Cr^{3+} .

Table of Contents

List of Tables	xii
List of Figures.....	xiv
Chapter 1: Introduction	1
1.1 Trace Metals as an Environmental and Medical Concern	1
1.2 Trace Metal Fixation and Sequestration in Biological Systems.....	2
1.2.1 Proteins	2
1.2.2 Metallothioneins.....	3
1.3 Current Metal Remediation Technology	5
1.3.1 Bulk Methods.....	6
1.3.2 Ion Exchange	7
1.3.3 Electrodeposition	8
1.3.4 Electrical Ion Exchange.....	9
1.4 Incorporation of Biologically-based Systems into Metal Remediation Technology.....	9
1.4.1 Biological Organisms.....	10
1.4.2 Immobilized Biologically-based Biopolymers	11
1.4.2.1 Poly-L-cysteine	11
1.5 Electronically Switchable Ion Exchange System.....	14
1.5.1 Remediation of Cationic Species	16
1.5.2 Remediation of Anionic Species.....	17
1.6 Research overview.....	18
Chapter 2: Flow Rate Studies and Preconcentration using Poly-L-Cysteine Immobilized onto Controlled Pore Glass	19
2.1 Introduction.....	19
2.2 Experimental	21
2.2.1 Instrumentation	21
2.2.2 Reagents	23
2.2.3 Effects of Loading Flow Rate on Column Capacity	25
2.2.4 Effects of Stripping Flow Rate on Metal Recovery	27

2.2.5 Preconcentration of Cd^{2+} using PLC-CPG	28
2.3 Results and Discussion	31
2.3.1 Effects of Loading Flow Rate on Column Capacity	31
2.3.2 Effects of Stripping Flow Rate on Metal Recovery	33
2.3.3 Preconcentration of Cd^{2+} using PLC-CPG	37
2.4 Conclusions	38
Chapter 3: Electrochemical Studies of Immobilized Cysteine and Immobilized Poly-L-Cysteine.....	40
3.1 Introduction.....	40
3.2 Experimental	41
3.2.1 Instrumentation	41
3.2.2 Reagents	42
3.2.3 Creation of Modified Electrodes.....	42
3.2.3.1 Fabrication of Glassy Carbon Electrodes	42
3.2.3.2 Immobilization of Glycine, Cysteine and PLC	44
3.2.4 Characterization of Modified Electrodes.....	46
3.2.4.1 Atomic Force Microscopy	46
3.2.4.2 Cyclic Voltammetry	47
3.2.4.3 Chronoamperometric Determination of Kinetic Rate Constants.....	47
3.2.4.4 Determination of the pK_a of PLC and Cys.....	48
3.3 Results and Discussion	48
3.3.1 Atomic Force Microscopy	48
3.3.2 Cyclic Voltammetry	50
3.3.3 Chronoamperometric Determination of Kinetic Rate Constants	53
3.3.4 Determination of the pK_a of PLC.....	56
3.4 Conclusion.....	60
Chapter 4: Evaluation of Metal Binding to Modified Electrodes.....	61
4.1 Introduction.....	61
4.2 Experimental	62
4.2.1 Instrumentation	62
4.2.2 Reagents	63

4.2.3 Correlation of the Electrochemical Redox Method with a Chemical Redox Method.....	63
4.2.4 Evaluation of Cd ²⁺ Binding to PLC-GCE and Cys-GCE.....	66
4.2.5 Effect of Reduction and Oxidation Voltage on Cd ²⁺ Binding Capacity on PLC-GCE.....	67
4.2.6 Evaluation of Cu ²⁺ , Co ²⁺ , Pb ²⁺ and Ni ²⁺ Single-metal and Mixed-metal Solutions.....	68
4.3 Results and Discussion	70
4.3.1 Correlation of the Electrochemical Redox Method with a Chemical Redox Method.....	70
4.3.2 Evaluation of Cd ²⁺ Binding to PLC-GCE and Cys-GCE.....	71
4.3.3 Effect of Reduction and Oxidation Voltage on Cd ²⁺ Binding Capacity on PLC-GCE.....	74
4.3.4 Evaluation of Cu ²⁺ , Co ²⁺ , Pb ²⁺ and Ni ²⁺ Single-metal and Mixed-metal Solutions.....	76
4.3.5 Comparison of PLC-GCE with Previous Immobilized PLC Systems	79
4.4 Conclusion.....	81
Chapter 5: <i>in situ</i> Raman Microscopy Investigation of PLC-GCE.....	83
5.1 Introduction.....	83
5.2 Experimental	85
5.2.1 Instrumentation	85
5.2.2 Reagents	86
5.2.3 Calibration of Raman Microscope	86
5.2.4 Depth Profile Analysis	87
5.2.5 Observation of Oxidation and Reduction of PLC-GCE.....	88
5.2.6 Determination of Raman Band Intensities.....	88
5.2.7 Verification of Cd ²⁺ Binding to Thiols.....	89
5.3 Results and Discussion	89
5.3.1 Depth Profile Analysis	89
5.3.2 Observation of Oxidation and Reduction of PLC-GCE.....	91
5.3.3 Determination of an Average Formal Potential	98
5.3.4 Verification of Cd ²⁺ Binding to Thiols of PLC	106
5.4 Conclusions	107

Chapter 6: Exploratory Investigation of Polypyrrole Films as Conductive Anion Exchangers.....	109
6.1 Introduction.....	109
6.2 Experimental	112
6.2.1 Instrumentation	112
6.2.2 Reagents	113
6.2.3 Formation of Ppy Films on Glassy Carbon Electrodes	114
6.2.4 Scanning Electron Microscopy of Ppy Films	114
6.2.5 Evaluation of Cr ³⁺ and Cr(VI) Binding.....	114
6.3 Results and Discussion	115
6.3.1 Scanning Electron Microscopy of Ppy Films	115
6.3.2 Evaluation of Cr ³⁺ and Cr(VI) Binding.....	121
6.4 Conclusions.....	123
Chapter 7: Conclusions and Future Work	125
7.1 Overview.....	125
7.2 Concerns for Scale-up.....	128
7.3 Feasibility of Other Possible Systems.....	129
Appendix	131
Data Analysis Macro for Breakthrough Analysis	131
References	136
Vita.....	148

List of Tables

Table 1.1 Maximum Contaminant Levels, Health Effects and Man-made Sources of Various Metals in Water [1]	2
Table 1.2 Enzymes and their Respective Inorganic Cofactors [2].....	3
Table 2.1 Calibration of peristaltic pump for 0.89 mm i.d. and 1.85 mm i.d. Pharmed tubing (Cole-Parmer). The Varian SIPS 20 pump used has a maximum speed of 100 rpm.....	26
Table 2.2 Time and volume required for 50%, 75%, 90% and 95% of the strip peak to be eluted from the column at 1, 3 and 5 mL/min.....	37
Table 2.3 Cd ²⁺ recovery for control and experimental conditions listed following the loading of 200 µg of Cd ²⁺	38
Table 3.1 Kinetic rate constants for electron migration in immobilized PLC.....	56
Table 4.1 ETV heating cycle used for metal analysis by ETV-ICPMS.....	65
Table 4.2 Argon plasma and quadrupole parameters for metal analysis	65
Table 4.3 Isotopes monitored for multi-metal analysis by ETV-ICPMS.....	69
Table 4.4 Comparison of chemical and electrochemical treatment of 1.5 mm diameter PLC-GCE for Cd ²⁺ binding capabilities. For chemical treatments (0.01 M DTT, pH 7; 0.1 M HNO ₃ ; 0.001 M o-IB, pH 7), the electrode was exposed for 1 min. Electrochemical potential steps were held for 30 s.....	70
Table 4.5 Cd ²⁺ binding analysis for Cys-GCE and PLC-GCE.....	72
Table 4.6 PLC-GCE capacity for Cd ²⁺ with decreasing reduction voltage.....	74
Table 4.7 Ionic radii of selected metal ions [64]	77
Table 4.8 Metals per PLC chain, assuming d.p. ~50, and Cys residues per metal as determined by ETV-ICPMS.....	79
Table 4.9 Metal Binding Capacities in nmol/cm ² from PLC immobilized on controlled pore glass [31], Carbopack-X [37] and a glassy carbon electrode. No data was available for Co ²⁺ binding to PLC immobilized onto Carbopack-X.....	80
Table 4.10 Formation constants of acetate and the metal ions studied [68].....	81

Table 5.1 Literature values for the reduction of cystine.....	98
Table 5.2 Average formal potential of PLC as determined by Raman microscopy data (I), a linear distribution model of multiple E ⁰ s (II) and a Gaussian distribution model of multiple E ⁰ s (III).....	105
Table 6.1 Binding capacities for Cr ³⁺ and Cr(VI) on the 4 ppy electrodes	122

List of Figures

Figure 1.1 Sequence and Cadmium Binding Clusters for Rabbit Liver MT 2 [4]. Cysteine residues are notated by filled circles.	5
Figure 1.2 Proposed ESIE System	16
Figure 2.1 Structure of PLC	20
Figure 2.2 Three valve FIA system used for sample introduction comprised of a six-way sample selection valve (Rheodyne) a SIPS 20 (Varian) peristaltic pump and two two-way slider valves (Rheodyne) in line with a microcolumn and flame atomic absorption spectrometer.....	22
Figure 2.3 Surface functionalities present on the CPG at each stage of the four step PLC immobilization procedure.	25
Figure 2.4 Example of typical calibration scheme for preconcentration experiments.....	29
Figure 2.5 Actual calibration procedure used for preconcentration of Cd^{2+} using PLC-CPG	30
Figure 2.6 Cu^{2+} capacity at increasing loading flow rates. 1 mL/min of 0.1 M HNO_3 was used to strip the metal from the column in all cases.....	31
Figure 2.7 Stripping efficiency for acid-activated column loaded to capacity with 10 ppm Cu^{2+} at 2 mL/min and stripped at 1, 2, 3, 4 and 5 mL/min. Percentages indicate total recovery of the metal from the strip analysis as compared to the breakthrough capacity.	34
Figure 2.8 Strip profiles versus time	35
Figure 2.9 Strip profiles versus volume	36
Figure 3.1 Electrode construction showing (A) cross-section and (B) end view.	44
Figure 3.2 Electrode Modification Procedure	46
Figure 3.3 8 μm x 8 μm Tapping-mode Atomic Force Microscopy Images of Polished Glassy Carbon Electrode (top) and PLC-modified Glassy Carbon Electrode (bottom)	49
Figure 3.4 Cyclic voltammograms of modified electrodes.	51
Figure 3.5 Peak current response to scan rate changes.	53

Figure 3.6 Current as a function of time for potential steps from 0 mV vs. Ag/AgCl to either -600 mV or +600 mV vs. Ag/AgCl.	54
Figure 3.7 Anodic CV at increasing pHs. These CVs were used for both pK_a determination methods.....	57
Figure 3.8 Voltammetric determination of pK_a . Data corresponding to PLC-GCE is connected by a solid line and plotted in reference to the left-hand axis. Data corresponding to Cys-GCE is connected by a broken line and plotted in reference to the right-hand axis.	58
Figure 3.9 Peak potentials of Immobilized PLC as a function of solution pH.....	60
Figure 4.1 Experimental pathways for metal binding analysis.....	67
Figure 4.2 Effects of oxidative pulsing on the release of Cd^{2+} . (A-30 1 s pulses, B-20 1 s pulses, C-10 1 s pulses, D-5 1 s pulses, E-1 30 s pulse).....	75
Figure 4.3 Multi-metal binding results from strip analysis as determined by ETV-ICPMS. Capacities for single metal and multi-metal solutions are shown. Multi-metal binding was released by either 0.5 mL of 0.1 M HNO_3 or 5 +600 mV potential steps into 0.5 mL 0.2 M KCl.	76
Figure 5.1 Design of cell for <i>in situ</i> Raman microscopy studies.....	85
Figure 5.2 Si calibration of Raman Microscope.....	87
Figure 5.3 Optical images of the glassy carbon electrode surface obtained using a 5X objective, left, and a 20X objective, right.....	90
Figure 5.4 Sample Raman spectrum and difference spectra obtained by depth profile analysis.	91
Figure 5.5 Raman spectrum of a polished glassy carbon electrode.....	92
Figure 5.6 Sample Raman spectrum showing peaks of interest: 450 (disulfide), 800 (thiol), 1360 (D band of GCE) and 1580 cm^{-1} (E_{2g} band of GCE). This spectrum was acquired while the working electrode was held at 0 V vs. SHE.	93
Figure 5.7 Signal averaged Raman spectrum using raw data from Figure 5.6. The curve was generated by performing a 50 point moving average to demonstrate to effective increase in the signal to noise ratio by averaging 50 data points.	94
Figure 5.8 Background corrected Raman signals for the fully oxidized (solid line) and the fully reduced (dotted line) polymer, both shown after a 50 point moving average was performed. The transition due to the disulfide bond can be seen at approximately 440 cm^{-1} . The transition due to the reduced thiols can be seen at approximately 790 cm^{-1}	95

Figure 5.9 Observation of Reduced Thiols. Normalized Raman intensity is shown as a function of electrode potential for the thiol transition, occurring at approximately 800 cm^{-1} (average of 3 replicates).	96
Figure 5.10 Observation of Oxidized Disulfides. Normalized Raman intensity as a function of electrode potential for the disulfide stretch, occurring at approximately 450 cm^{-1} (average of 3 replicates).	97
Figure 5.11 Use of the Nernst equation for the thiol-disulfide system using Raman scattering of SH (820 cm^{-1}) and SS (460 cm^{-1}) to calculate values on the abscissa.	100
Figure 5.12 Distribution of local sites used in simulations. The solid line represents a uniform distribution of redox sites while the dashed line represents redox sites with a Gaussian distribution ($\sigma = 0.1$, $\overline{E^o} = -0.24$).	103
Figure 5.13 Fractional concentrations of [SH] (\square) and [SS] (\square), as determined by Raman microscopy with resulting E^o distribution models. The uniform distribution model is shown by a solid line and the Gaussian distribution model is shown by a dashed line.	104
Figure 5.14 Cd^{2+} binding to thiol groups of PLC. The solid line represents spectrum acquired in the presence of Cd^{2+} . Points represent a spectrum acquired in the absence of Cd^{2+} .	107
Figure 6.1 Chemical structures of histidine, left, and pyrrole, right.	110
Figure 6.2 Charge storage mechanism for polypyrrole.	112
Figure 6.3 Electrode 1, grown with F^- as the counterion. Top image shows entire electrode. Bottom image is a close-up view of the film itself.	116
Figure 6.4 Electrode 2, grown with ClO_4^- as the counterion. Top image shows entire electrode surface seen from the side. Bottom image is a close-up view of the film itself.	117
Figure 6.5 Electrode 3, grown with BF_4^- as the counterion. Top image shows an end view of the entire electrode surface. Bottom image is a close-up view of the film itself.	118
Figure 6.6 Electrode 4, grown with p-toluenesulfonate as the counterion. Top image shows the entire electrode surface seen from the side. Bottom image is a close-up view of the film itself.	119
Figure 6.7 Side view of the thickness of the film grown on electrode 1.	120

Figure A.1 An example of a typical breakthrough curve collected by flow injection analysis-flame atomic absorption spectroscopy.....	132
Figure A.2 User input fields for report page of data analysis macro	133
Figure A.3 Screen shot of the breakthrough worksheet within the macro. Raw data collected by FIA-FAAS or FIA-ICPMS is entered in the first two columns. The remaining calculations are completed by the macro.	134

Chapter 1: Introduction

1.1 TRACE METALS AS AN ENVIRONMENTAL AND MEDICAL CONCERN

Heavy metals, unlike organic contaminants, represent a recirculating environmental problem. Metals can not be degraded and therefore must be removed via isolation and recovery. For many heavy metal contaminants, acceptable drinking water standards governed by the United States Environmental Protection Agency (USEPA) lie in the ppm to ppb range. In many cases, the maximum contaminant levels (MCL) are set as such due to known health concerns for humans. Most recently, the MCL for total arsenic was dropped from 50 ppb to 10 ppb. All drinking water sources are required to be in compliance with this new level by January of 2006. While the MCL reduction for total As is significant, the ultimate goal, as with most toxic contaminants, is to have drinking supplies containing no detectable levels of toxic metals. The origin of these metal contaminants includes both the erosion of natural deposits and man-made sources. The previous information is summarized in Table 1.1 [1].

Table 1.1 Maximum Contaminant Levels, Health Effects and Man-made Sources of Various Metals in Water [1]

	MCL (mg/L)	Potential Health Effects from Ingestion of Water	Man-made Sources of Contaminant in Drinking Water
As	0.010 as of 01/06	-Skin damage -Circulatory problems -Risk of cancer	-Runoff from orchards and electronics production wastes
Cd	0.005	-Kidney damage	-Discharge from metal refineries -Runoff from waste batteries and paints
Cr _{total}	0.1	-Allergic dermatitis	-Discharge from steel and pulp mills
Cu	1.3	-Gastrointestinal distress -Liver or kidney damage	-Corrosion of plumbing
Pb	0.015	-Developmental delays -Kidney Problems	-Corrosion of plumbing
Hg (inorganic)	0.002	-Kidney damage	-Discharge from refineries and factories -Runoff from landfills and croplands
Se	0.05	-Hair or fingernail loss -Circulatory problems	-Discharge from petroleum refineries and mines

1.2 TRACE METAL FIXATION AND SEQUESTRATION IN BIOLOGICAL SYSTEMS

1.2.1 Proteins

Many proteins, including at least 30% of all enzymes, require the coordination of an inorganic ion to function properly [2]. These proteins are often referred to as metalloproteins. Metalloproteins exhibit a broad range of functions including acting as

electron carriers, metal storage and transport, oxygen binding, metal sensors and cofactors for enzymatic activity [3]. One of the most recognizable, and well-understood, metalloproteins is hemoglobin. Hemoglobin, consisting of four subunits each containing an Fe^{2+} ion, serves as the primary transporter of oxygen in biological systems [2]. In addition to the previously mentioned functions, metals, specifically Ca^{2+} also play crucial roles in protein folding and structure [3]. In each of these cases, but particularly with enzymes, the metal ion necessary for function is quite specific. Some common enzymes requiring inorganic cofactors are listed in Table 1.2.

Table 1.2 Enzymes and their Respective Inorganic Cofactors [2]

Cofactor	Enzyme
Fe^{2+} or Fe^{3+}	Catalase
	Peroxidase
Cu^{2+}	Cytochrome oxidase
Zn^{2+}	Carbonic anhydrase
	Alcohol dehydrogenase
Mg^{2+}	Hexokinase
	Glucose-6-phosphatase
Mn^{2+}	Arginase
	Ribonucleotide reductase
Ni^{2+}	Urease

1.2.2 Metallothioneins

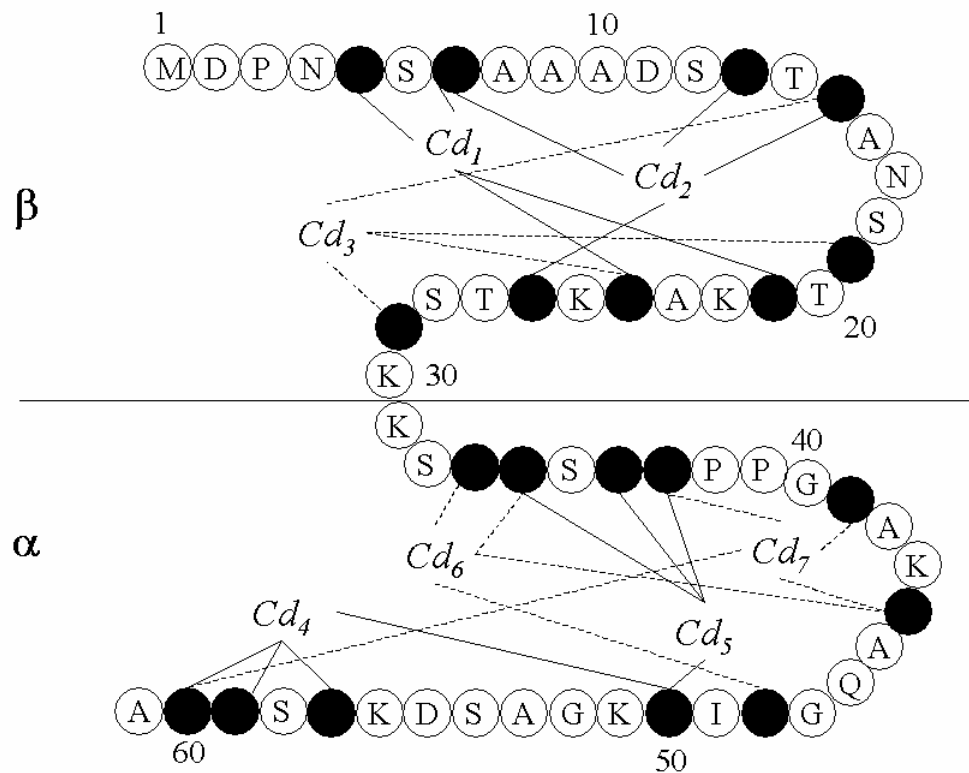
Metallothioneins are a unique class of ubiquitous, low molecular weight (approximately 6000-7000 Da) proteins with several distinctive characteristics. Most

notably, they have a high ratio of sulfur-containing residues (20 cysteine:60 total residues) and, when complexed, contain approximately 20% metal by weight (i.e. 7-12 metal cations per protein). Common functions of this subclass of metalloproteins include toxic metal sequestration and essential metal fixation. While metallothioneins have relatively little structure as compared to many other proteins, they form two distinct α and β clusters when complexing a metal cation such as Cd^{2+} or Zn^{2+} as shown in Figure 1.1. Due in large part to their indiscriminate structure, metallothioneins can accommodate a number of coordination geometries upon introduction of a metal including linear, trigonal and tetrahedral. When binding Cd^{2+} , the α cluster forms as Cd_4S_{11} and the β cluster forms a Cd_3S_9 [4].

This arrangement is the favored thermodynamic state allowing all Cd^{2+} to be tetrahedrally coordinated. In addition to Cd^{2+} and Zn^{2+} , metallothioneins have been shown to complex Ag(I), Au(I), Cu(I), Cu(II), Hg(II), Pt(II) and Bi(III) in biological systems. Unlike enzymes which rely on competitive release, metals bound to metallothioneins are easily extracted as well as readily exchanged with other cations.

The metal-thiolate complexes formed within a metallothionein exhibit both rapid kinetics of metal exchange and a large thermodynamic affinity with log K values reaching 17 [4]. Although less common than single metal-metalllothionein complexes, mixed metal-metalllothionein complexes can exist especially during neonatal development and following heavy metal exposure. Interestingly, as sequences can vary from species to species, certain amino acid residue motifs are conserved. These are Cys-Cys, Cys-X-Cys, and Cys-X-X-Cys, where X can be a number of other amino acid residues.

Figure 1.1 Sequence and Cadmium Binding Clusters for Rabbit Liver MT 2 [4]. Cysteine residues are notated by filled circles.



1.3 CURRENT METAL REMEDIATION TECHNOLOGY

Initially, metal remediation from highly contaminated sources proceeds using bulk methods. These methods, while successful in remediating large quantities of metal, can not bring many systems below regulatory levels mandated by agencies such as the USEPA. In many cases, a second technology is required to bring the bulk-treated source

into compliance. These technologies, referred to as “polishing” steps, often involve chemical extraction or adsorption to achieve required conformity with regulatory policy.

1.3.1 Bulk Methods

The most common forms of physical treatment methods are phase separation, (e.g. filtration and sedimentation), phase transition, (e.g. distillation, evaporation or physical precipitation), and phase transfer, (e.g. extraction or sorption). Phase separation methods are often aided by the inclusion of a chemical additive to act as a flocculating agent or coagulant resulting in a more effective filtration procedure. Phase transition methods are primarily used for solvents and organic contaminants like waste oil. Common methods of phase transfer treatment include leaching, supercritical fluid extraction and sorption by activated carbon. Some types of wastes, mainly organic pollutants, can be treated by incineration or biodegradation as well.

In addition to the aforementioned physical treatment methods, there are also chemical methods for the bulk treatment of water and wastewater. These include neutralization, chemical precipitation, oxidation/reduction, electrolysis, hydrolysis, chemical extraction, ion exchange and photolysis. Of these the most useful chemical treatment methods for inorganic contaminants are chemical precipitation, where the introduction of a chemical, most often hydroxide, induces precipitate formation of insoluble metal hydroxides; oxidation/reduction, where the oxidation state of the target metal is changed to a less toxic form; electrolysis, where metal ions can simply be plated onto an electrode; chemical extraction, where a metal can be made more mobile via a chemical reaction or complexed with a chelating agent, such as EDTA; and ion exchange, where a toxic metal ion is exchanged for an innocuous ion.

Many treatment schemes include a combination of these physical and chemical techniques in order to maximize the effectiveness of the treatment process. In many cases, some of these methods only target one major class of pollutants while the water may be contaminated with multiple classes of pollutants [5].

1.3.2 Ion Exchange

In the ion exchange process, one ion desorbs from a given substrate while another ion adsorbs. The substrate can be derived from natural materials, such as clays or minerals, but more often they are synthetic polymer resins. These resins are generally highly crosslinked to achieve a large surface area, but porous enough for solution flow. In addition, they are modified to include fixed, charged functional groups within the resin. Functional groups can be either cation or anionic in nature depending on the charge of the ion of interest. Common groups include sulfonates for cation exchange and quaternary amines for anion exchange. Loosely bound counter ions of opposing charge are incorporated into the resin. These counter ions are then able to be exchanged with target ions in solution. Ion exchange can proceed as either heterovalent ion exchange, when the two exchanging ion have different formal charges, or as homovalent ion exchange, when the two exchanging ions have the same formal charge. However, electroneutrality of the resin must be conserved which requires more than two ions to be exchanged when heterovalent exchange takes place.

The regeneration of an ion exchange column is essentially identical to the analyte adsorption process except the analyte is intentionally replaced by H^+ , OH^- or in some

cases Na^+ or Cl^- . For most ion exchange resins, adsorbate recovery is quite efficient, often exceeding 95%. Although some adsorbates can irreversibly bond to the resin, it typically has little effect on analyte capacity [6].

Unfortunately, many current ion exchange systems lack the specificity often desired in a remediation technique. In the case of a resin which can bind several metals, much of the total binding capacity is occupied by analytes which are not of interest. This problem is often compounded in the presence of salty matrices like seawater.

1.3.3 Electrodeposition

Electrodeposition, or electrolysis, is another commonly used remediation method for metal ions. The metal ions are electrochemically reduced at a cathode while an oxidation reaction takes place at an anode. Electrolysis is especially applicable towards the remediation of cadmium, copper, gold, lead, silver and zinc. However, the presence of some anions, such as cyanide, can greatly reduce the effectiveness of electrolysis due to stabilization by complexation [5].

Bulk electrolysis can also be used in a flow mode where the solution is passed through a large surface area electrode, usually porous in nature, such as fine mesh screens or packed carbon powders. Flow electrolysis systems often offer both rapid conversions and high efficiencies of remediation. Cell design for these large scale bulk electrolysis methods is more critical than many other electrochemical techniques primarily in order to minimize uncompensated resistance. Ideally, these systems would simultaneously minimize the length of the electrode while maximizing flow velocities. Depending on the circumstances, electrolysis can be carried out by either controlled-potential, where the

potential of the working electrode is held constant throughout treatment, or controlled-current techniques, where the current through the cell is held constant. Despite the large scale of these electrolysis cells, the basic electrochemical fundamentals governing reactions at electrode surfaces hold true [7].

1.3.4 Electrical Ion Exchange

Interestingly, several of the problems inherent to the two previously mentioned techniques can be overcome by merging their advantageous qualities into a single method. The earliest electrical ion exchange systems incorporated a resin into an electrode via a binder [8-11]. In these cases, an electrochemical potential promoted ion migration to the cathode surface where the ion exchange resin could then retain the metal ion. The system could then be regenerated by a change in polarity thereby driving the metal cations away from the electrode surface. Noted benefits of this type of system have included low energy operation as compared to electrolysis, high metal selectivity governed by the combination of potential and exchange properties, the ability to preconcentrate, the production of minimal waste volume and the prospect of continual operation [10]. However, despite the apparent advantages of electrical ion exchange, the efficiency of these systems is highly dependent on the matrix and its metal components.

1.4 INCORPORATION OF BIOLOGICALLY-BASED SYSTEMS INTO METAL REMEDIATION TECHNOLOGY

Even with the development of ever increasing technological improvements to physical and chemical treatment of waters and wastewaters, it is seemingly logical to also

consider further exploring the mechanisms already incorporated into biological systems – particularly with the drive towards “environmentally-friendly” chemistry. Some of these approaches have investigated the use of intact organisms while many others concentrate their efforts on isolating the constituent aspects of biological organisms that make them effective trace metal binders.

1.4.1 Biological Organisms

Initially, many efforts in bioremediation centered on intact biological systems. Just a little over 20 years ago, researchers first began to notice the propensity of certain species of plants to uptake and accumulate abnormally high amounts of heavy metals. These plants, known as hyperaccumulators, have spurred the development of what has become known as phytoremediation. In phytoremediation, plants known to be hyperaccumulators of a target analyte are introduced into a contaminated site providing low-cost, *in situ*, environmentally-friendly remediation. Since the beginnings of phytoremediation, researchers have found species that can accumulate cadmium, lead, copper, mercury, cobalt, nickel, manganese, zinc, chromium and selenium (e.g. [12-18]).

Other attempts to harness the efficiency of bioremediation have focused on the use of single cell systems such as algae, yeast or bacteria which can each be immobilized onto a solid substrate for use in a flow scheme. These studies have demonstrated the removal of copper, lead, nickel, zinc, iron, manganese, molybdenum, strontium, vanadium, selenium, arsenic and cobalt (e.g. [19-26]).

1.4.2 Immobilized Biologically-based Biopolymers

As an alternative to intact biological systems, other studies have explored the remediation capabilities of the components which likely dominate the metal binding mechanisms. As discussed previously, proteins are perhaps the most effective metal ion binders within biological systems. Since the function of proteins is directly derived from its predisposed tertiary structure, proteins which become denatured are no longer effective as metal binders. However, the functionalities of the constituent amino acids of a protein will retain some degree of affinity for metal ions regardless of the loss of protein function. These naturally occurring amino acids offer a variety of moieties for potential metal binding including carboxylate, as in glutamate and aspartate, amines, as in lysine, imidizoles, (e.g. histidine) and thiols, (e.g. cysteine). More recent research has begun to exploit the power of biologically-based systems by using amino acid monomers as well as short chain amino acid homopolymers in hopes of achieving the capabilities of bioremediation without the drawbacks inherent to using entire organisms.

1.4.2.1 Poly-L-cysteine

Poly-L-cysteine (PLC) was first synthesized chemically in the 1950s from monomers in solution [27]. More recently, PLC has been studied as a trace metal chelator both in batch solution experiments [28, 29] as well as immobilized onto a chromatographic support [29-34] or microfiltration membranes [35].

Batch work by Holcombe et al. established PLC to be a strong complexing agent for heavy metals such as cadmium, copper and zinc [28]. Formation constants, in the form log K, were spectroscopically determined to be at least 8 and 9.5 for Cd^{2+} and Zn^{2+} ,

respectively. While these batch studies were able to provide early insight into the nature of PLC as a heavy metal chelator, the poor solubility of the polymer in neutral solutions presented problems for further study. Subsequent research efforts using PLC as a metal remediation tool have focused on the development of bonded phase ion exchange systems.

With PLC covalently attached to silica substrates, such as controlled pore glass (CPG), low solubility is no longer a concern, and the robust nature of CPG provided an excellent substrate for peptide immobilization [33]. The PLC modified CPG particles were packed into small low pressure liquid chromatography columns supplying a system which could be used in conjunction with flow injection analysis. PLC-CPG was investigated as a preconcentration agent for Cd^{2+} primarily due to the large $\log K_f$ values. Using Langmuir isotherms, the maximum $\log K_f$ (pH=7) for Cd-PLC was estimated to be 13 although the majority of binding sites were shown to have $\log K_f$ values between 4 and 11.

Further studies sought to compare the preconcentration capabilities of PLC with those of a more traditional system, 8-hydroxyquinoline (8HQ) [31]. Both chelators were immobilized onto CPG and packed into columns and successfully complexed ppb levels of Cd^{2+} and Pb^{2+} from a synthetic seawater sample. The ability to bind ppb levels of heavy metal analytes despite the presence of a total of 12,050 ppm Na^+ , K^+ , Mg^{2+} and Ca^{2+} is due to their high selectivity against group IA and IIA metals. PLC, however, demonstrated added selectivity of some heavy transition metals over others. PLC was able to chelate ppb level amounts of Cd^{2+} and Pb^{2+} in the presence of 500 ppm Co^{2+} and Ni^{2+} matrices, while the 8HQ retained essentially no Cd^{2+} and very little Pb^{2+} .

An investigation into the effects of oxidation on the chelating abilities of PLC was also conducted previously [30]. The thiol groups of PLC are prone to oxidation to form disulfide bonds. While thiol groups are excellent metal chelators, disulfides are not. Dramatic reductions in column capacity were seen when the column was exposed to such oxidizing agents as 1% H₂O₂, dissolved O₂ and Cu²⁺. Full column capacity could be regained by chemical reduction with dithiothreitol.

The physical response of PLC to differing chemical environments was explored using *in situ* liquid cell atomic force microscopy [36]. During the analysis, PLC was exposed to a reducing agent, a metal-containing solution and an acidic pH. The average height of the polymer while in each of these environments led to a further clarification on the proposed binding mechanisms. When reduced, i.e all disulfide bonds reduced to thiol groups, the polymer reached its maximum height of about 40 nm. When exposed to Cd²⁺, the average polymer height was reduced to 20 nm indicating that the polymer was likely wrapping itself around the metal ions. In acidic conditions, the polymer was reduced in height once again, to a height of 10 nm and consistent with expectations for a tight, α -coil confirmation. It was postulated that below pHs of ~ 7, essentially all the thiol groups should be protonated, resulting in a fairly hydrophobic structure that assumes a conformation that minimizes its solvation.

Previous work with PLC also employed an alternative to CPG as a chromatographic support [37]. PLC was covalently attached to porous carbon particles and packed into a column for flow injection analysis metal binding experiments. These experiments further confirmed the behavior seen on CPG.

For use in microfiltration membranes, silica and cellulose based membrane materials were functionalized by PLC [35]. The major advantage these membranes exhibited over the previously used CPG and porous carbon systems was high sorption capacities. The PLC functionalized membranes could accommodate on the order of mg of metal per cm² of surface area as compared to µg of metal per cm² of surface area for CPG [28-31, 33] and porous carbon [28-31, 33, 37]. Overall, these studies have generated a broad, fundamental understanding into the metal binding characteristics of PLC.

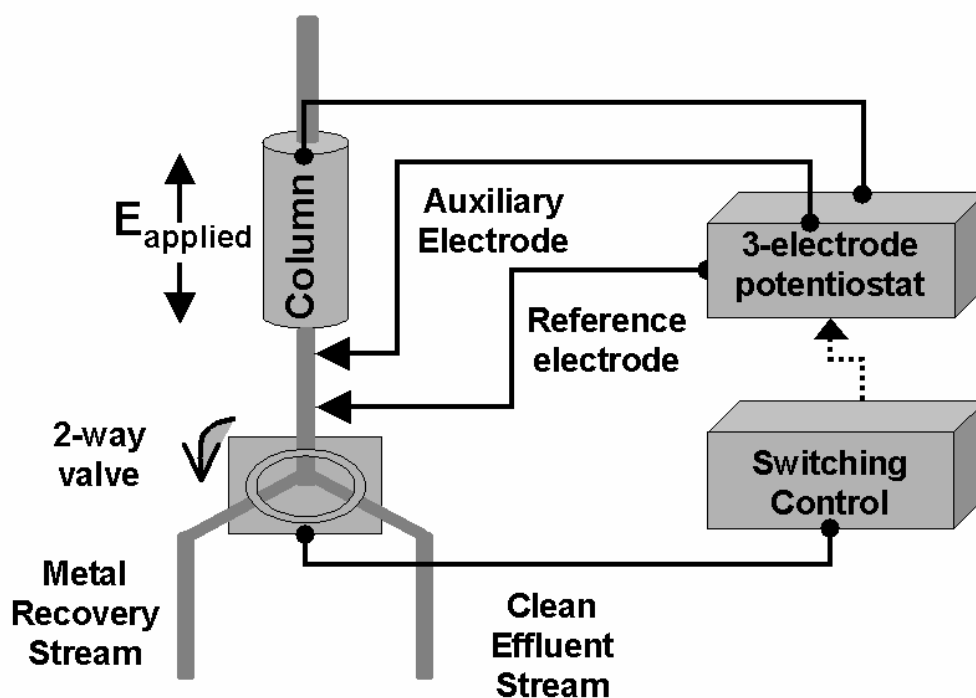
1.5 ELECTRONICALLY SWITCHABLE ION EXCHANGE SYSTEM

As discussed, PLC presents with some unique characteristics for trace metal preconcentration and remediation. In addition to its metal binding trends, PLC exhibits a dramatic reduction in metal binding capacity when it is chemically oxidized. It is conceivable that this change could also occur using electrochemical methods, i.e. using voltages or currents instead of additional chemicals. In this manner, an essentially “chemical-free” remediation system could be developed. The system, if scaled up to a column-based system could be referred to as an electronically switchable ion exchanger (ESIE). With ESIE in-line, a metal-contaminated liquid stream could be passed through the ion exchange column consisting of a strong redox active metal chelator system immobilized on a high surface area substrate *that is electrically conducting*. In the absence of a potential placed between the column and an auxiliary electrode, the column functions like an ion exchanger with the metal binding characteristics of the immobilized

chelator. The remediated effluent stream from the column then flows to the intended destination (*e.g.*, discharge stream, water distribution system, etc.). Eventually, the column binding capacity will be reached. At this time a valve in the effluent stream redirects flow to a recovery tank, and an electrochemical potential is placed across the column to “spoil” the ligand binding capability resulting in the release of metals into the column’s mobile phase and passage to the recovery tank. It is possible that efficient release could make the solution volume within the column containing the released metal as small as a single column dead volume. After the metal is removed, the column is electrochemically “reactivated” (*e.g.*, reduced) to restore it to the “binding mode”. The potential is then removed, the effluent valve is switched and column again functions as an in-line metal extraction system.

ESIE presents a novel, reversible, reusable method for metal extraction from waste streams by exploiting both the chelating and redox properties of the ion exchanger. Optimal flexibility is inherent to the system since the selection of the immobilized chelator provides the desired selectivity for metal removal while “spoiling” the K_f of the *chelator* through electrochemistry permits recovery with less dependence on the target metal. A proposed model for the ESIE system is schematically represented in Figure 1.2.

Figure 1.2 Proposed ESIE System



1.5.1 Remediation of Cationic Species

Initial work towards the development of a feasible ESIE system targeted toxic metal cations. Due to both thorough previous characterization and redox characteristics, the first chelator chosen for ESIE was poly-L-cysteine (PLC). Earlier work with PLC immobilized on surfaces such as controlled pore glass (CPG) [28, 30-32, 36] and carbon [28, 30-32, 36, 37] provided information regarding binding preferences, binding strength

and chemically-induced release efficiency. Additionally, studies focused on the role of oxidation and reduction chemistry into the binding capacities of PLC had been completed using chemical oxidizing (e.g. o-iodobenzoate, $O_{2(g)}$ and hydrogen peroxide) and reducing agents (e.g. dithiothreitol) [30]. In all cases, maximum metal binding capacities were seen when PLC was fully reduced and oxidation reduced the metal binding capacities.

From this previous work, several important aspects of PLC were determined. PLC can be immobilized onto a variety of surfaces, including those which are conductive. PLC is an effective metal cation chelator, particularly of the soft acid metals, reaching log K values of ~ 13 while maintaining fast, on-demand metal release. Immobilized PLC exhibits essentially no capacity for cations when oxidized to disulfides, but regains the original capacity once reduced.

1.5.2 Remediation of Anionic Species

In addition to the development of a cationic ESIE system, studies were undertaken to create a prototype system for the chemical-free remediation of toxic anions, particularly the metal oxyanions. Targeting these analytes, particularly Cr(VI) and As(V), can lead to a powerful speciation tool allowing for a more complete understanding into the distribution and bioavailability of particular species. Previous work into the speciation and remediation of Cr(VI) and As(V) which took advantage of the benefits of biohomopolymers focused on poly-L-histidine (PLH) [38]. The functional side group of PLH consists of an imidazole ring which becomes positively charged upon protonation. This protonated form of PLH binds both CrO_4^{2-} and AsO_4^{3-} while demonstrating relatively little capacity towards Cr^{3+} and As^{3+} [38-40].

Due to structural similarities as well as appealing electrochemical characteristics, polypyrrole (ppy) was chosen for further study as an anionic ESIE candidate. Ppy has been extensively electrochemically characterized [41-46] and has also been investigated as a chromatographic support for electrochromatography [47-49]. In addition, pyrrole is easily polymerized *in situ* to a variety of conductive supports, including carbon [41, 44-46].

1.6 RESEARCH OVERVIEW

In order to proceed toward the development of an electronically switchable ion exchange system, previous work was expanded to include a variety of new studies. Initially, flow parameters were determined to maximize the preconcentration capabilities of PLC immobilized onto porous silica. The subsequent studies involving PLC were conducted with PLC immobilized on a glassy carbon disk electrode. A series of electrochemical experiments were undertaken to characterize the PLC-modified electrode. Metal binding studies were completed to determine the capacity of the PLC-modified electrode for 5 divalent cations. Raman microscopy was used to explore the nature of the thiol-disulfide conversion. Finally, polypyrrole was investigated as a potential ligand for the remediation of anionic species, specifically Cr(VI).

Chapter 2: Flow Rate Studies and Preconcentration using Poly-L-Cysteine Immobilized onto Controlled Pore Glass

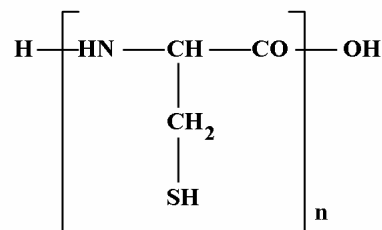
2.1 INTRODUCTION

Individually, preconcentration and flow injection analysis are both highly effective analytical tools. When used together, they become even more powerful. Preconcentration can lower the practical limit of detection for a given instrument by enhancing the original signal. The added benefit of matrix elimination improves the quality of analysis especially for some elemental analytical techniques, such as inductively coupled plasma mass spectrometry and electrothermal atomization atomic spectroscopy, which can be highly sensitive to matrix effects. Incorporating flow injection can provide highly automated and rapid sample throughput to help decrease overall analysis time. The capability for efficient analyte speciation as well as the reduction of waste volume is also of great interest for metal remediation. The combination of preconcentration and flow injection analysis (FIA) also provides an effective tool to evaluate and characterize metal-binding systems including those composed of biologically-based polymers immobilized on a solid support. An important parameter for FIA systems is the solution flow rate. Flow rates can greatly impact adsorption behavior of analytes onto particles.

Previously, a variety of solid supports from polymeric resins to activated carbon have been used as substrates for ion exchange and metal remediation systems. One such support, controlled pore glass (CPG), has offered a more rugged alternative to resins which are subject to unfavorable solvent effects, such as shrinkage and swelling. CPG is a porous silica substrate which is commercially available in a range of mesh sizes and pore diameters to accommodate a range of applications. As an added benefit, CPG has a large surface area, (e.g. 50-200 m²/g) with average pore diameters ranging from 15-50 nm.

Proteins and their constituent amino acids have long been known as effective metal binders. The variety of chemical moieties available as R groups provides an array of metal binding affinities. One of the more interesting amino acids is cysteine with its thiol side chain. Thiols, by nature, are extremely chemically reactive in addition to being redox active. L-cysteine can be chemically polymerized to form poly-L-cysteine [27], (Figure 2.1).

Figure 2.1 Structure of PLC



Poly-L-cysteine (PLC) provides the same metal binding affinity as L-cysteine but with increased binding strength due to the possibility of multi-dentate chelation, with log K_f s reaching 13 [30, 37]. PLC has been shown to be an excellent chelator of a suite of heavy metals, specifically the soft acid metals such as Cd and Pb [28-31, 33, 37]. However, the metal binding capacity of PLC is greatly mitigated by the oxidation of the thiol groups to disulfides. Oxidized PLC exhibits little to no affinity to heavy metal cations [30]. The binding strength of PLC contributes to its ability to act as an effective preconcentration agent. Another important aspect of PLC that adds to its preconcentration efficacy is the propensity for facile, on-demand release of the bound metal. Metal release is achieved by a combination of two mechanisms – proton displacement of the bound metal and a dramatic tertiary structure change of PLC. Under acidic conditions the protonated thiols cause the PLC to be much more hydrophobic and subsequently force it to coil to the surface thereby disrupting its tertiary structure and releasing the bound metal.

2.2 EXPERIMENTAL

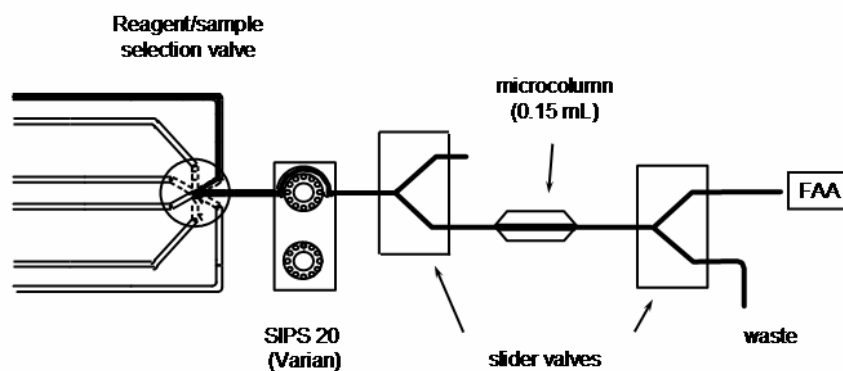
2.2.1 Instrumentation

A Varian model AA-875 atomic absorption spectrometer with an air/acetylene flame was used for Cu and Cd determinations. The hollow cathode lamps were operated at the recommended currents. The Cu and Cd absorption lines of 324.8 nm and 228.8 nm, respectively, were employed with a monochromator bandpass of 0.5 nm. All pH measurements were made with a digital pH/mV/ORP meter (Cole-Parmer). The flow

injection system that was used for these studies consists of a peristaltic pump (Varian SIPS), a pneumatic 6-port rotary valve (Rheodyne) for sample/reagent selection and two pneumatic 3-way slider valves (Rheodyne) (Figure 2.2). All connections were made with 0.76 mm i.d. PTFE tubing. The system has been automated by in-house software controlling the pump, pneumatic valves and recording the analog data output at a rate of up to 10 Hz.

The modified CPG of interest was packed into a 3 mm i.d. x 25 mm long borosilicate column with 100 μm PTFE frits (Omnifit). A Kel-F tee was used between the column and the nebulizer to provide air compensation.

Figure 2.2 Three valve FIA system used for sample introduction comprised of a six-way sample selection valve (Rheodyne) a SIPS 20 (Varian) peristaltic pump and two two-way slider valves (Rheodyne) in line with a microcolumn and flame atomic absorption spectrometer.



2.2.2 Reagents

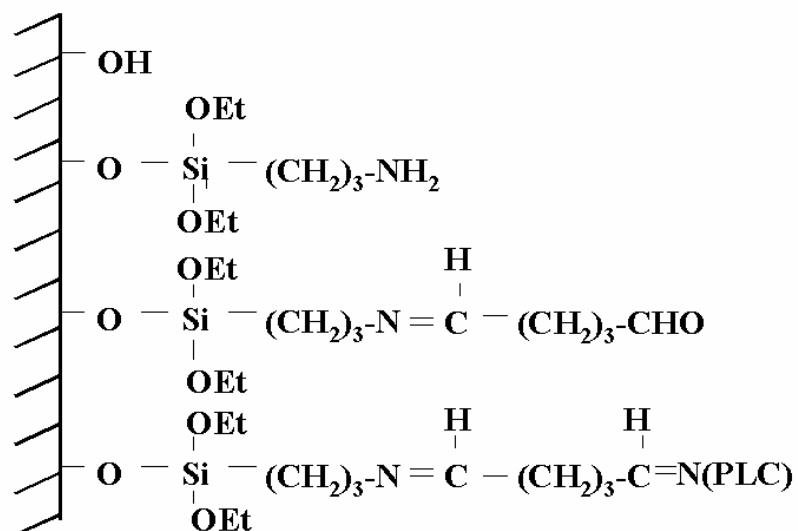
All reagent used were reagent grade, unless noted otherwise. Deionized, distilled water was used in solution preparations. All glassware was soaked overnight in 4 M nitric acid prior to use. Poly-S-CBZ-L-cysteine, PLC, (Sigma) [DP(vis) 50, MW(vis) 11,800] was used as received. Controlled pore glass, CPG, (Sigma) with an average pore diameter of 22.6 nm and mesh size 80-120 was used. Other reagents used included 3-aminopropyltriethoxysilane (98%), APS, (Sigma), gluteraldehyde (25%) (Sigma), DL-dithiothreitol, DTT, (Sigma), nitric acid, ammonium acetate (Aldrich), sodium hydroxide (Fisher Scientific) and glacial acetic acid (Fisher Scientific). Stock solutions of 1000 ppm Cd^{2+} (Assurance) and Cu^{2+} (SCP Science) atomic absorption standards were used to prepare the 10 ppm solutions for the metal binding experiments as well as calibration standards.

PLC was purchased in the form Poly-S-CBZ-L-cysteine which required the removal of the carbobenzoxy-thiol blocking group prior to use as an immobilized chelator. This was accomplished by using the procedure described by Berger [27] and modified by Miller and Holcombe [37]. In short combining 0.05 g of Poly-S-CBZ-L-cysteine, 0.2 g phenol (EM Science), 0.1 g DTT and 5 mL of 99% trifluoroacetic acid, TFA, (Acros Organics) and then heating under reflux conditions for 2 hours. After cooling to room temperature, 25 mL of a saturated solution of sodium acetate was added to precipitate the newly blocked PLC from the reaction mixture. The precipitant was then collected via vacuum filtration, rinsed with acidified DI water and diethyl ether and dried overnight under $\text{N}_{2(g)}$.

Two columns were packed – one for flow rate studies and one for the preconcentration studies. The column used for the investigation of flow rate effects was prepared only by acid activation of the CPG. The CPG surface was activated by heating under reflux conditions in 5% nitric acid for 1 hr., allowed to dry in a 95°C oven overnight and packed into a microcolumn.

The CPG onto which PLC was to be packed and used for the examination of the preconcentration abilities of PLC was further modified through reactions illustrated in Figure 2.3, which have been described previously [50]. In brief, following an identical acid activation, the CPG was reacted with 5 mL of APS in 50 mL of water adjusted to pH 3.5 with HCl, heated to 75°C for 150 min and filtered. This process was repeated twice. The filtered glass was subsequently dried overnight in a 80°C oven. The aminoalkylated glass was added to 50 mL of a 25% gluteraldehyde solution in pH 7.5 phosphate buffer and reacted under $N_{2(g)}$ for 1 hr. Following vacuum filtration, 0.1 g of deblocked PLC was added to the glass in 0.1 M pH 8.5 phosphate buffer and reacted under $N_{2(g)}$ for 2 hrs. The PLC-CPG was filtered, rinsed with DI water and dried for 48 hrs under $N_{2(g)}$.

Figure 2.3 Surface functionalities present on the CPG at each stage of the four step PLC immobilization procedure.



2.2.3 Effects of Loading Flow Rate on Column Capacity

The flow injection analysis setup shown in Figure 2.2 was used for all experiments. All pumps and tubing were warmed up preceding each experiment. Prior to use, two different i.d. tubings were used to calibrate the rpm of the pump to flow rate as summarized in Table 2.1. The flow rate was determined by flowing an acid solution through the column into a 10 mL graduated cylinder for 4 min.

Table 2.1 Calibration of peristaltic pump for 0.89 mm i.d. and 1.85 mm i.d. Pharmed tubing (Cole-Parmer). The Varian SIPS 20 pump used has a maximum speed of 100 rpm.

Flow rate	Pump speed (rpm) 0.89 mm i.d. tubing	Pump speed (rpm) 1.85 mm i.d. tubing
1	15	8
2	31	13
3	46	21
4	61	29
5	77	39
6	92	50
7	--	62
8	--	76
9	--	91
10	--	--

Before each binding experiment, the packed bed column was cleaned using 0.1 M HNO_3 for 2 min at 1 mL per min followed by 0.05 M ammonium acetate at pH 7 for another 2 min at 1 mL per min. In order to investigate the effects of loading flow rate on the capacity of an acid activated controlled pore glass, breakthrough curves were obtained at 1, 2, 3, 4 and 5 mL per min following a calibration at the corresponding flow rates using acidified metal standards that are not retained by the column. Breakthrough was generally achieved in less than 20 min, although the exact time required for breakthrough was flow rate dependant. In each case, the influent concentration was 10 ppm Cu^{2+} in 0.05 M ammonium acetate at pH 7. The in-house data collection software recorded the Cu absorbance as a function of time at a collection rate of 1 Hz. After breakthrough was reached, i.e when effluent concentration was equal to influent

concentration, flow to the AA and data collection was stopped. 2 mL of 0.5 M ammonium acetate, with no Cu^{2+} present, was introduced into the lines and the column to purge any unbound metal from the system. 0.1 M HNO_3 was then introduced on to the column to strip the bound metals. The Cu^{2+} capacity was calculated using a previously designed macro in Excel (Microsoft) and confirmed by stripping the bound metal with 0.1 M HNO_3 at 1 mL per min into a 10 mL volumetric flask. The strip solution was quantified by flame atomic absorption spectroscopy following a three point calibration curve made from Cu^{2+} standards in 0.1 M HNO_3 solution. Both the breakthrough and strip analysis for each flow rate were performed in triplicate.

2.2.4 Effects of Stripping Flow Rate on Metal Recovery

In order to evaluate the effect of flow rate on the efficiency of metal recovery, the column was loaded to capacity at 2 mL per min using 10 ppm Cu^{2+} in 0.05 M ammonium acetate at pH 7.0. The bound metal was then stripped by 0.1 HNO_3 at 1, 2, 3, 4 and 5 mL per min into a 10 mL volumetric flask. The strip solutions were quantified using flame atomic absorption as before. These experiments were also completed in triplicate for each strip flow rate.

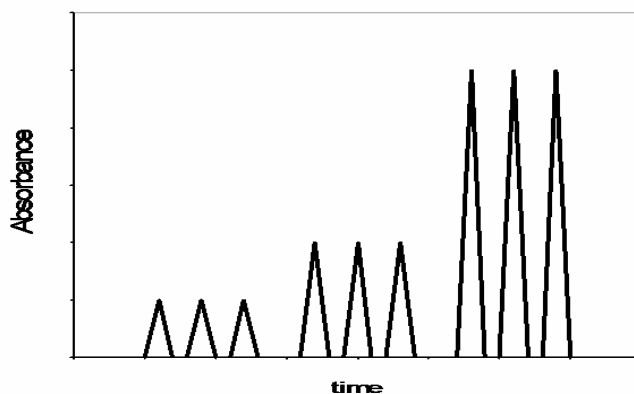
Strip profile peaks were also collected at strip flow rates of 1, 3 and 5 mL/min after loading a 10 ppm Cu^{2+} solution in 0.05 ammonium acetate (pH 7) for 3 min using a loading flow rate of 2 mL/min. As before, prior to stripping the bound metal with 0.1 M HNO_3 the lines were rinsed with 2 mL of 0.05 ammonium acetate (pH 7). Instead of collecting the bound metal in a volumetric flask, the stripped metal was allowed to flow from the column directly into the flame of the AA. Absorbance values were obtained with in-house software at a collection rate of 1 Hz.

2.2.5 Preconcentration of Cd^{2+} using PLC-CPG

A 25 cm microcolumn was packed with approximately 0.1 g of PLC modified controlled pore glass (CPG). Prior to obtaining each breakthrough curve, 0.1 M DTT (pH 9) was introduced onto the column at 1 mL/min for 10 min to reduce any oxidized disulfide bonds before metal chelation. CPG-immobilized PLC was used for the preconcentration of Cd^{2+} from a 20 ppb solution in 0.05 M ammonium acetate at pH 7. Cadmium was chosen due to the strong binding and significant capacity PLC has for that particular cation. The 20 ppb solution was introduced onto the PLC column at 2 mL per min for 10 min. After 10 min, the bound metal was stripped by 0.1 M HNO_3 directly into the nebulizer of the flame atomic absorption spectrometer resulting in a transient strip peak. The transient strip peak plotted as $\mu\text{g/mL Cd}^{2+}$ vs. mL was integrated to quantify the amount of Cd^{2+} present in the strip.

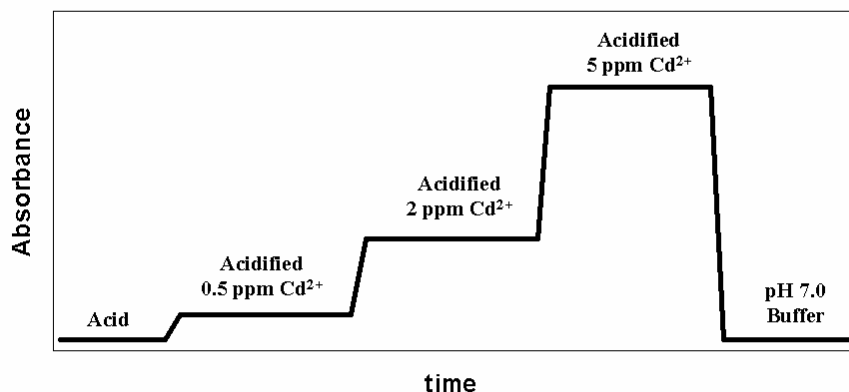
Typically, calibration standards for preconcentration experiments are made at the ppb level. The standards are loaded and stripped from the preconcentration column in the same manner as the unknown resulting in a series of transient peaks. The average peak heights are used to create a calibration curve. This general scheme is demonstrated by Figure 2.4. This process has several disadvantages – the calibration procedure is time intensive and the necessity for accurate ppb level standards can lead to concerns over metal loss to container walls. In addition, this method is inadequate if incomplete metal release occurs.

Figure 2.4 Example of typical calibration scheme for preconcentration experiments



As an alternative to the previously discussed calibration protocol, acidified ppm level standards were used to quantify the mass of Cd^{2+} that was bound to the PLC column. The calibration protocol used is demonstrated in Figure 2.5. 0, 0.5, 2 and 5 ppm Cd^{2+} in 0.1 M HNO_3 were successively introduced onto the column for 1 min each at a flow rate of 1 mL per min. The resultant absorbance was recorded by in-house data collection software at 1 Hz. Following the calibration standards, 2 mL of 0.05 M ammonium acetate at pH 7 was introduced onto the column at 1 mL per min to condition the column to the proper pH for the metal binding interaction.

Figure 2.5 Actual calibration procedure used for preconcentration of Cd^{2+} using PLC-CPG



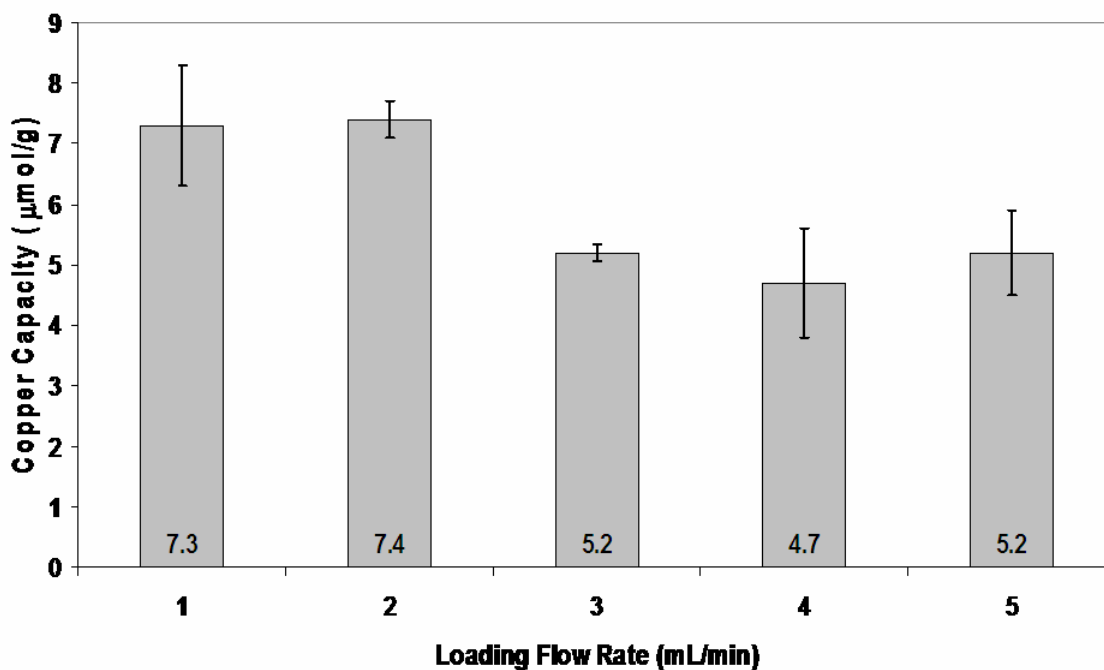
A 20 ppb Cd^{2+} solution in 0.05 M ammonium acetate at pH 7 was introduced onto the column at 1 mL per min for 10 min. After loading, lines and column were purged of any unbound metal by rinsing with 2 mL of 0.05 M ammonium acetate at pH 7. To strip, 0.1 M HNO_3 was introduced at 1 mL per min and the effluent was nebulized directly into the flame resulting in a transient strip peak. The absorbance at each point on the transient was converted to $\mu\text{g/mL}$ using the data from the acidified standard calibration curve. The time component of the strip peak was converted to volume using the determined flow rate. The peak was then integrated to determine the mass of Cd^{2+} in mg that had been retained on the column. This process was performed in triplicate for the 1 mL per min loading rate. A second analysis was also performed at 2 mL per min loading rate for 5 min and 1 mL per min stripping rate. This analysis was also conducted in triplicate.

2.3 RESULTS AND DISCUSSION

2.3.1 Effects of Loading Flow Rate on Column Capacity

The metal binding capacities calculated by using both breakthrough and strip data for Cu^{2+} on acid activated glass at various flow rates are shown in Figure 2.6. Using influent flow rates of 2 mL per min or less resulted in similar capacities. However, influent flow rates of 3 mL per min and greater resulted in a diminished capacity.

Figure 2.6 Cu^{2+} capacity at increasing loading flow rates. 1 mL/mi of 0.1 M HNO_3 was used to strip the metal from the column in all cases.



The binding of Cu^{2+} to the acid activated groups on the surface of controlled pore glass is fundamentally an adsorption process [6]. Adsorption processes generally proceed

as a combination of surface complexation reactions and phase transfer reactions. Surface complexation reactions, or “site-binding” model, are often thought to contribute to mechanisms such as ion exchange. Usually, the barriers to adsorption are equilibrium related as opposed to kinetic in nature. Mass transfer must take place through three primary mechanisms – bulk diffusion, pore diffusion and surface diffusion. The active zone of any packed bed column is the area where a dramatic concentration profile exists. This area is where the majority of mass transfer occurs and is referred to as the mass transfer zone. The mass transfer zone has two primary characteristics – its shape and its velocity. The shape of the mass transfer zone, which ultimately is the shape of the breakthrough curve, is dictated by the extent of dispersion and adsorption kinetics, particularly when equilibrium is slow to establish. Parameters affecting the shape, i.e. the broadness, of the mass transfer zone are, to some degree, dependent on solution flow rates. The velocity of the mass transfer zone is controlled by the binding strength and the maximum adsorption capacity, neither of which should be flow rate dependant. Ideally, a packed bed column would be characterized by a short, slow mass transfer zone.

Previous work with CPG packed bed columns for use as metal chelators has establish that binding equilibrium is not achieved within the time frame of a breakthrough experiment [32]. Unfortunately, packed bed columns exhibiting slow equilibrium are very difficult to model. There are ways, however, to empirically discuss the steps involved in the adsorption process and those most likely contributing to non-ideal behavior. For systems which are slow to establish equilibrium, mass transfer proceeds via the following four steps:

- 1) transport of the analyte through the bulk solution to the outer edge of the particle boundary layer;
- 2) external mass transfer, or transport from the outer edge of the boundary layer to the particle surface;
- 3) initial adsorption reaction; and
- 4) internal mass transfer, or the migration of the adsorbed analyte to the interior surfaces of the particle.

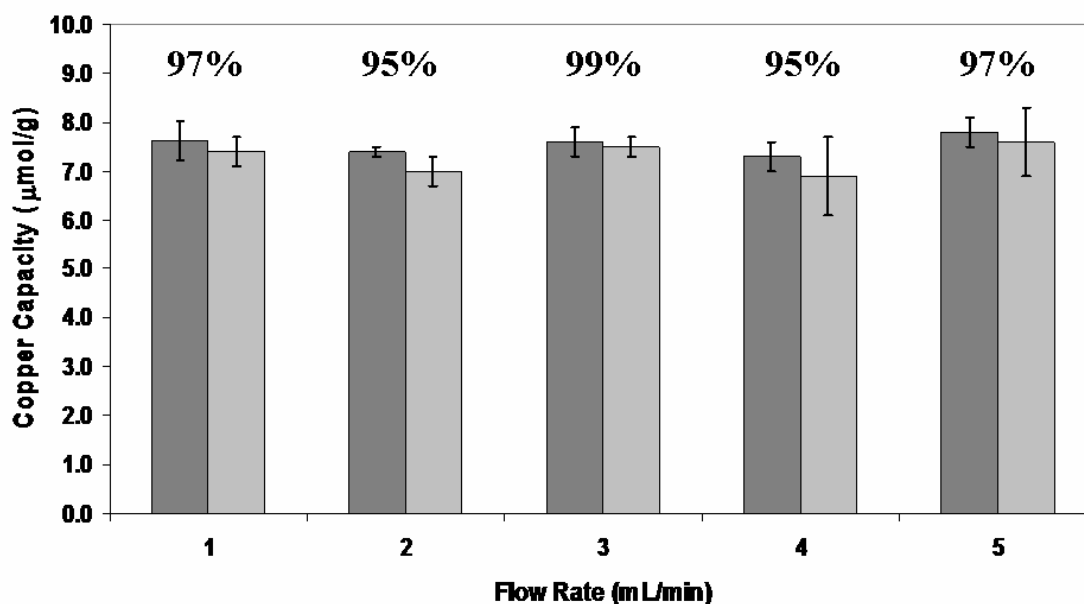
The final step is also sometimes referred to as surface diffusion or pore diffusion. Steps one and three generally offer very little resistance to the adsorption process. Steps two and/or four are most often responsible for slow equilibration. In the case of controlled pore glass, the pores of which are considered quite tortuous, it is the internal mass transfer most likely liable for the greatest resistance to equilibration. In many cases, slow equilibration results in a mass transfer zone which spans the length of the column and leads to almost immediate detection of analyte in the effluent [6]. It is conceivable that at faster influent flow rates the slow equilibration process is magnified by both the barrier to internal pore diffusion and a lengthening of the mass transfer zone.

2.3.2 Effects of Stripping Flow Rate on Metal Recovery

Following loading to capacity, the adsorbed Cu^{2+} was stripped by 0.1 M HNO_3 at influent flow rates of 1, 2, 3, 4 and 5 mL/min into 10 mL volumetric flasks and quantified by AA. The capacity as determined by the strip analysis was compared to the capacity determined by the breakthrough curves to evaluate the efficiency of metal reclamation. The results are shown in Figure 2.6. Quantitative metal recovery was achieved in all

cases regardless of the rate at which the metals were stripped. These results are contrary to the process of metal adsorption which did demonstrate flow rate dependence. This indicates that the mechanism for metal removal is probably not limited by equilibrium or kinetic barriers.

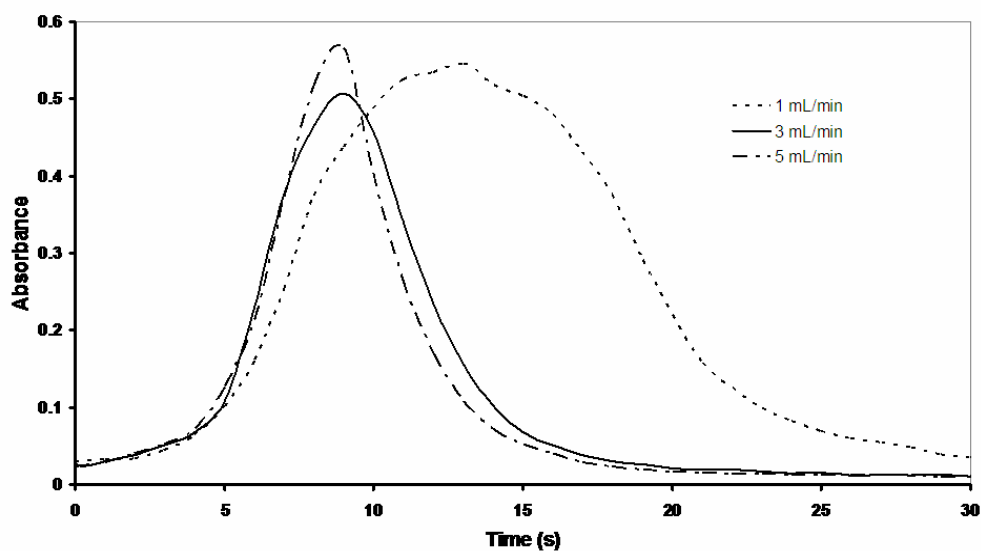
Figure 2.7 Stripping efficiency for acid-activated column loaded to capacity with 10 ppm Cu^{2+} at 2 mL/min and stripped at 1, 2, 3, 4 and 5 mL/min. Percentages indicate total recovery of the metal from the strip analysis as compared to the breakthrough capacity.



To determine whether flow rate affects the stripping process, transient strip peaks were collected by the AA after loading 10 ppm Cu^{2+} for 3 min. The resulting absorbance values were plotted in two ways – as a function of time, Figure 2.7, and as a function of

volume based on the solution flow rate, Figure 2.8. Because these peaks were not actually used for quantification and only for empirical discussion of stripping behavior, the y-axis remains as absorbance. If quantification were desired, a calibration of sensitivity as a function of flow rate would be necessary as nebulization efficiencies increase with decreasing flow rates. As expected, the faster flow rates generate narrower peaks that elute faster than the peak generated by 1 mL/min stripping rate.

Figure 2.8 Strip profiles versus time



A consequence of an increase in solution flow rate for metal removal is the amount of volume required for stripping at higher flow rates. Although using a 5 mL/min flow rate to release bound metals can strip faster, more volume is required to accomplish this goal. Minimizing the volume required, not the time required, is the primary goal of preconcentration efforts. In addition, it is also an important parameter for stripping a

reusable ion exchange column when reclamation is one objective. Table 2.2 summarizes the time and volume requirements for stripping metals at 1, 3 and 5 mL/min.

Figure 2.9 Strip profiles versus volume

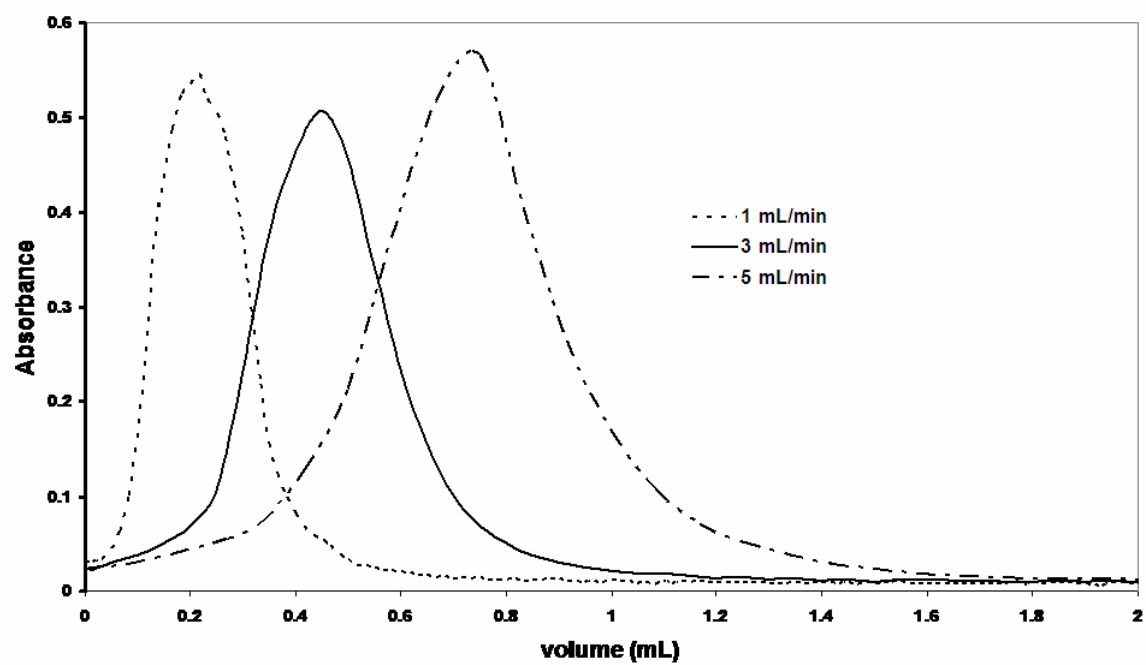


Table 2.2 Time and volume required for 50%, 75%, 90% and 95% of the strip peak to be eluted from the column at 1, 3 and 5 mL/min.

Flow Rate (mL/min)	Time (s)				Volume (mL)			
	50%	75%	90%	95%	50%	75%	90%	95%
1	14	18	25	34	0.23	0.30	0.42	0.57
3	9	11	15	18	0.45	0.55	0.75	0.90
5	8	10	13	16	0.67	0.83	1.08	1.33

According to the data presented in Table 2.2, while the elution of the strip peak at 1 mL/min requires, on average, twice as long with respect to time, less than half the volume of acid is need for the same degree of elution. These results have tangible consequences for preconcentration and remediation applications. The volume of waste solution is reduced when low flow rates are used for remediation and preconcentration; the preconcentration factor increases by a factor of 2.3 when stripping with 1mL/min vs. 5mL/min flow rates.

2.3.3 Preconcentration of Cd^{2+} using PLC-CPG

The optimized loading and stripping flow rates were used to perform a preconcentration experiment using immobilized PLC to chelate Cd^{2+} at the 20 ppb level, which is four times the maximum contaminant level governed by the current EPA drinking water standards [1]. Since it was determined that loading flow rates could be increased to 2 mL/min without sacrificing capacity and that a strip flow rate of 1 mL/min

is the most efficient for metal removal, these flow rates were used for Cd^{2+} preconcentration. A control experiment was run at previously studied flow rates (i.e. 1 mL/min for loading and 1 mL/min for stripping) for confirmation. For both flow rate conditions, quantitative recovery of the Cd^{2+} was observed. Considering the estimated volume needed for strip, the PLC column was able to preconcentrate 10 mL of a 20 ppb solution down to 0.6 mL of a 2 ppm solution in less 7 min decreasing the amount of waste by a factor of 17.

Table 2.3 Cd^{2+} recovery for control and experimental conditions listed following the loading of 200 μg of Cd^{2+} .

	Load Flow Rate (mL/min)	Strip Flow Rate (mL/min)	Cd^{2+} Recovery
Control	1	1	$98 \pm 2 \%$
Experimental	2	1	$103 \pm 6 \%$

2.4 CONCLUSIONS

Studies were conducted to obtain the most efficient flow parameters for the preconcentration of a toxic heavy metal by immobilized PLC. Acid activated controlled pore glass was used to establish the optimal flow rates. Those flow rates were then applied to Cd^{2+} preconcentration. When the flow rate was increased greater than 2 mL/min, capacity decreased. However, breakthrough experiments could be conducted at

2 mL/min without sacrificing metal binding capacity thereby reducing the time required for an experiment by half. It was also determined that, while slower stripping flow rates required more time, the resulting volume could be minimized. The validity of the use of these flow rates was confirmed by using a previously characterized chelator and obtaining quantitative recovery of the analyte metal.

Chapter 3: Electrochemical Studies of Immobilized Cysteine and Immobilized Poly-L-Cysteine

3.1 INTRODUCTION

As a prerequisite for developing an electronically switchable ion exchange column, prototype materials were investigated in a small scale environment. Because PLC had successfully been immobilized onto carbon surfaces previously [37], the chosen ligand, poly-L-cysteine (PLC), was immobilized to a glassy carbon disk creating a modified electrode. The deliberate modification of electrode surfaces has led to a vast assortment of materials which are available as electrochemical substrates for researchers. The earliest research into electrode surface modification dates back to 1973 [51]. As opposed to a column-based system, the use of a PLC-modified electrode allows for the possibility of a thorough electrochemical characterization using traditional chronoamperometric and voltammetric methods.

Modified electrodes are generally characterized by the manner in which they were created. There are four basic categories of modification:

- (1) Sorption, either physisorption or chemisorption;
- (2) Covalent attachment;
- (3) Homogenous multilayer;
- (4) Heterogeneous multilayer.

The most common examples of electrodes modified via sorption techniques are self assembled monolayers (SAMs). SAMs, particularly thiol-terminated molecules sorbed onto gold, have become a simple and reliable method for electrode modification. In the case of covalent attachment, a molecule is covalently bound to a surface group of the electrode, most commonly carbon, by standard organic reactions. This method of attachment, however, is limited by the constraints of the monolayer. The electroactive area can be increased through the use of polymeric reagents. Electroresponsive polymers can be attached to the electrode surface by covalent modification, coordinated attachment or electrostatic attachment. In other cases, a nonconductive polymer, or other substrate, can serve as a platform for the incorporation of redox molecules, such as ferrocene [52].

In this case, PLC is covalently attached to an oxidized glassy carbon disc electrode for further study.

3.2 EXPERIMENTAL

3.2.1 Instrumentation

A three-electrode potentiostat (Cypress Systems Omni-101) with a Ag/AgCl reference electrode (Cypress Systems) and a platinum wire auxiliary electrode (Cypress Systems) were used for all electrochemical experiments. Working electrodes were constructed in-house using 5 mm diameter type II glassy carbon (Alfa-Aesar). All electrochemical experiments were conducted under a nitrogen environment. All electrochemical data were obtained through commercially available software (Cypress

Systems Aquire-101). Atomic force microscopy images were collected using a Digital Nanoscope IV AFM.

3.2.2 Reagents

All reagents used were reagent grade unless noted. Deionized distilled water was used to prepare solutions, and all glassware was soaked overnight in 4 M HNO₃ prior to use. Poly-S-CBZ-L-cysteine (Sigma) [DP(vis) 50, MW (vis) 11,800] , L-cysteine (Sigma) and glycine (Sigma) were used as received. Other reagents included 1-ethyl-3-[3-(dimethylamino)propyl] carbodiimide (EDC) (Sigma); 4-morpholineethane sulfonic acid (MES), nitric acid (Sigma), ammonium acetate (Aldrich); sodium hydroxide (Fisher Scientific); disodium hydrogen phosphate (Fisher Scientific), potassium chloride (EM Science).

3.2.3 Creation of Modified Electrodes

3.2.3.1 Fabrication of Glassy Carbon Electrodes

Glassy carbon (GC) of 5mm (0.2 in) diameter was chosen to act as the working material of the electrode. The overall diameter of the electrode was chosen to be 0.65 cm. Drinking straws were collected and measured to ensure the proper size for mold material. The straw was compared to a pre-made electrode and cut to the proper length.

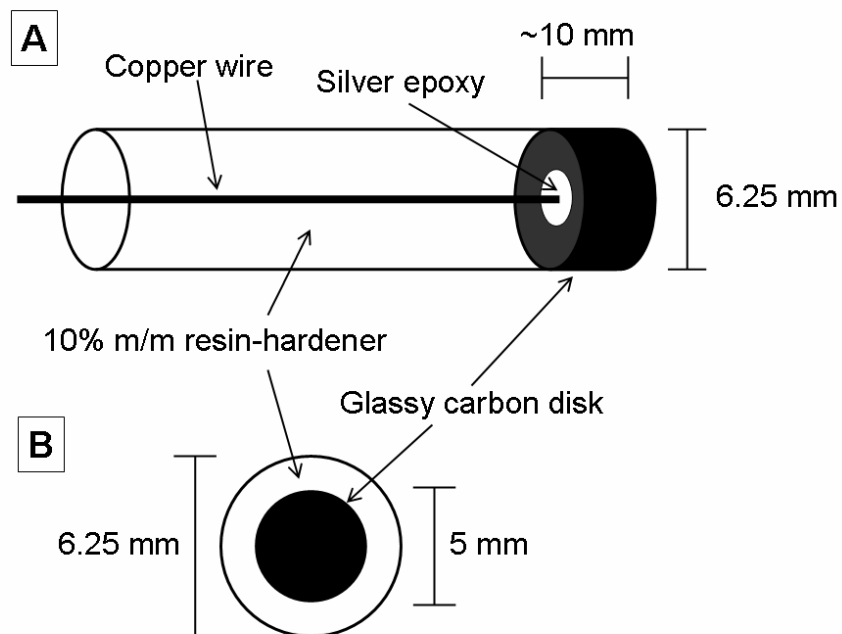
The glassy carbon rod, shipped in a length of 50 mm, was cut into approximately five 10 mm thick disks using a diamond blade. Four electrodes were constructed from the 50 mm rod. Figure 3.1 illustrates the final electrode design. Using a diamond grinding bit, a small depression was ground into one of the flat sides of the GC disk.

Gold plated electrical contact pins were purchased locally. The pins functioned as external electrical contact for the potentiostat. With the carbon cut and the pins purchased, a solid copper wire could be cut to the proper length required to take up the difference in length from the bottom of the depression in the carbon rod to the base of the pin.

The wire was affixed to the carbon rod using conductive silver epoxy. The epoxy was prepared according to label directs and heat cured. The wire was attached to the pin with regular electronic solder. The copper wire was cleaned with resin flux to remove oxidation from the surface. The rod-wire-pin combination was tested to confirm electrical conductivity via a volt-ohm meter. The connections were also checked for mechanical connections to prevent corruption of the electrode after fabrication.

The molds for the electrodes were made to have all points of the wall of the straw equidistance from any point on the longitudinal axis of the mold. Once the epoxy was mostly cured, the rod-wire-pin assembly was placed in the straw and centered using a small piece of wire wrapped around the pin. A 10% w/w resin-hardener mixture was made. The epoxy was poured slowly down the inner wall of the straw to prevent air from being trapped at the bottom, near the rod. Once the straw was full, the rod-wire-pin assembly was re-centered and secured. The epoxy was allowed to cure over night at room temperature and pressure. After curing, the straw was cut from the electrode, and the surface of the electrode prepared as desired for use.

Figure 3.1 Electrode construction showing (A) cross-section and (B) end view.

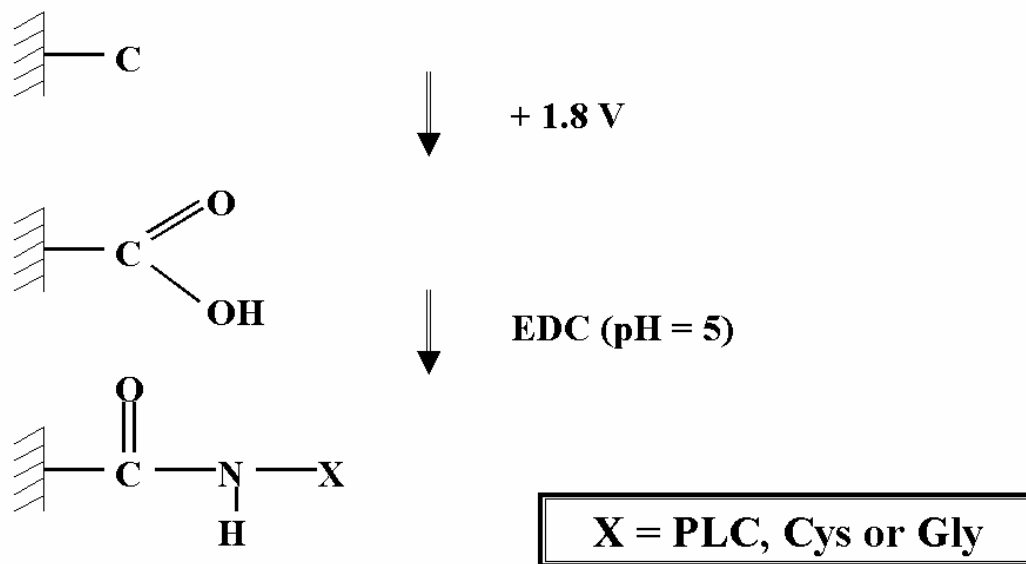


3.2.3.2 Immobilization of Glycine, Cysteine and PLC

Initially, three modified electrodes were made – one with poly-L-cysteine, one with the cysteine monomer and the last with the glycine monomer. Prior to immobilization, the carbobenzoxy group on the PLC was deblocked using a procedure described previously [37]. Before electrode modification each glassy carbon electrode was polished using 0.5 μm alumina slurry. Three 5 mm diameter glassy carbon electrodes were initially oxidized by a +1.8 V potential step in dilute sulfuric acid to create active surface groups. Activation of the acid groups on the carbon surface was performed by exposing the electrode surface to a 25 mL aqueous solution of 0.04 M 1-

ethyl-3-[3-(dimethylamino)propyl] carbodiimide (EDC) adjusted to pH 5.5 containing 0.050 M 4-morpholineethane sulfonic acid (MES) [37]. This solution was prepared immediately prior to use. The MES buffer was used to stabilize the EDC reagent. The electrodes were exposed to this solution for approximately 20 min. The electrodes were then removed from the EDC solution. One electrode was then introduced to a new solution containing 0.01 g PLC dissolved in 50 mL of 0.05 M MES buffer at pH 5. The second electrode was exposed to 0.01 g Cys in 50 mL 0.05 M MES buffer at pH 5. The third electrode was exposed to 0.01 g Gly in 50 mL 0.05 M MES buffer at pH 5. Each electrode was exposed to its respective solution for 1 h to ensure peptide bond formation between the surface active groups and the amine terminus of the PLC, cysteine and glycine to create one poly-L-cysteine (PLC-GCE), one cysteine (Cys-GCE) and one glycine (Gly-GCE) modified glassy carbon electrode. After immobilization, the electrodes were rinsed with deionized water.

Figure 3.2 Electrode Modification Procedure



3.2.4 Characterization of Modified Electrodes

3.2.4.1 Atomic Force Microscopy

In order to confirm attachment of PLC as well as general coverage characteristics, atomic force microscopy was undertaken. A 5 mm glassy carbon electrode (GCE) was polished with 0.5 μm alumina slurry for use as a control. AFM images of both the polished GCE and the PLC-GCE were collected using tapping mode under ambient conditions.

3.2.4.2 Cyclic Voltammetry

After the modified electrodes were created, initial experiments were undertaken to electrochemically characterize the immobilized species. Cyclic voltammograms of a polished glassy carbon electrode (GCE), a glycine modified glassy carbon electrode (Gly-GCE), a cysteine modified glassy carbon electrode (Cys-GCE) and a poly-L-cysteine modified electrode (PLC-GCE) were obtained by scanning from +1 V to -1 V (vs. Ag/AgCl) at 100mV/s in 0.2 M KCl at pH 7. Approximate coverages of immobilized cysteine species were calculated by integrating the Faradaic component of the voltammograms. To confirm the presence of surface redox processes as opposed to solution redox species, peak currents were determined for various scan rates on both the Cys-GCE and the PLC-GCE. The supporting electrolyte used for these experiments was 0.2 M KCl adjusted to pH 7 with concentrated KOH and concentrated HCl. Cyclic voltammograms were obtained at 10, 25, 50, 100, 150, 200, 250, 400 and 500 mV/s. The cathodic and anodic peak currents were collected in triplicate and then plotted as a function of scan rate.

3.2.4.3 Chronoamperometric Determination of Kinetic Rate Constants

Kinetic rate constants for electron transfer in PLC was evaluated by performing large potential steps, +600 mV and -600 mV in 0.2 M KCl at pH 7, and calculating a first and second order rate constant of electron exchange. The potential was stepped from 0 mV to -600 mV and from 0 mV to +600 mV while monitoring the current as a function of time for a total time of 30 s each. In each case, the potential steps were repeated 15 times and the results were averaged.

3.2.4.4 Determination of the pK_a of PLC and Cys

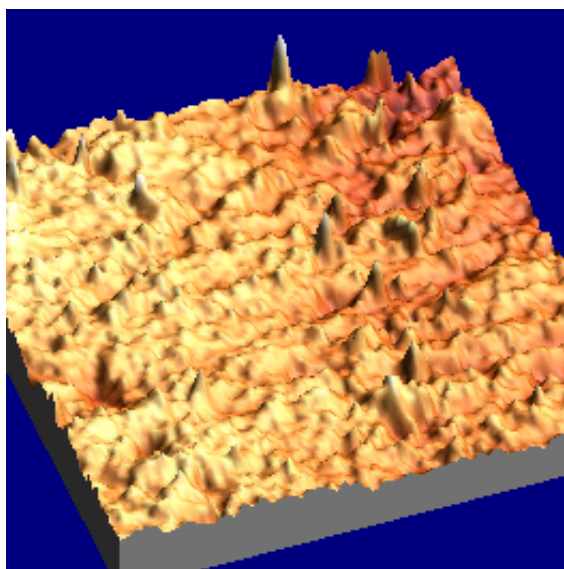
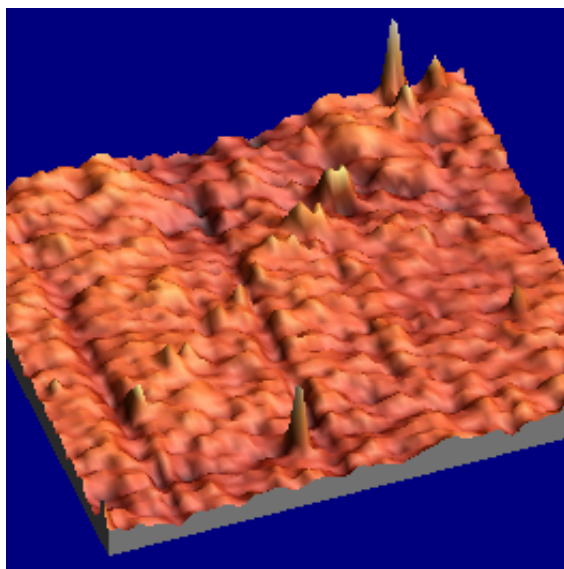
In order to electrochemically determine the pK_a of the immobilized species, anodic portions of cyclic voltammograms at pHs between 4 and 9 were integrated and a surface charge density was calculated. The voltammograms were obtained by scanning from +1 V to -1 V (vs. Ag/AgCl) at 100 mV/s in 0.05 M ammonium acetate whose pH was adjusted by adding either glacial acetic acid or 10 M ammonium hydroxide. The actual pHs, in 0.5 pH unit increments were determined using a digital pH/mV/ORP meter (Cole-Parmer). A second method of determining the pK_a of PLC based on the voltage at which the peak current appears in the cyclic voltammograms as a function of pH was used as well for further confirmation.

3.3 RESULTS AND DISCUSSION

3.3.1 Atomic Force Microscopy

The collected tapping-mode AFM images for both polished GCE and PLC-GCE are shown in Figure 3.3. The images shown are 8 μm by 8 μm . Using commercially available image analysis software, the average roughness of the GCE and PLC-GCE electrodes were determined to be 5-10 nm and 18-25 nm, respectively. The difference corresponds to the estimated height of PLC in a random coil conformation [36]. Additionally, the surface of PLC-GCE appears to be fairly uniform in height indicating the possibility of near-monolayer coverage of PLC on the surface.

Figure 3.3 8 μm x 8 μm Tapping-mode Atomic Force Microscopy Images of Polished Glassy Carbon Electrode (top) and PLC-modified Glassy Carbon Electrode (bottom)

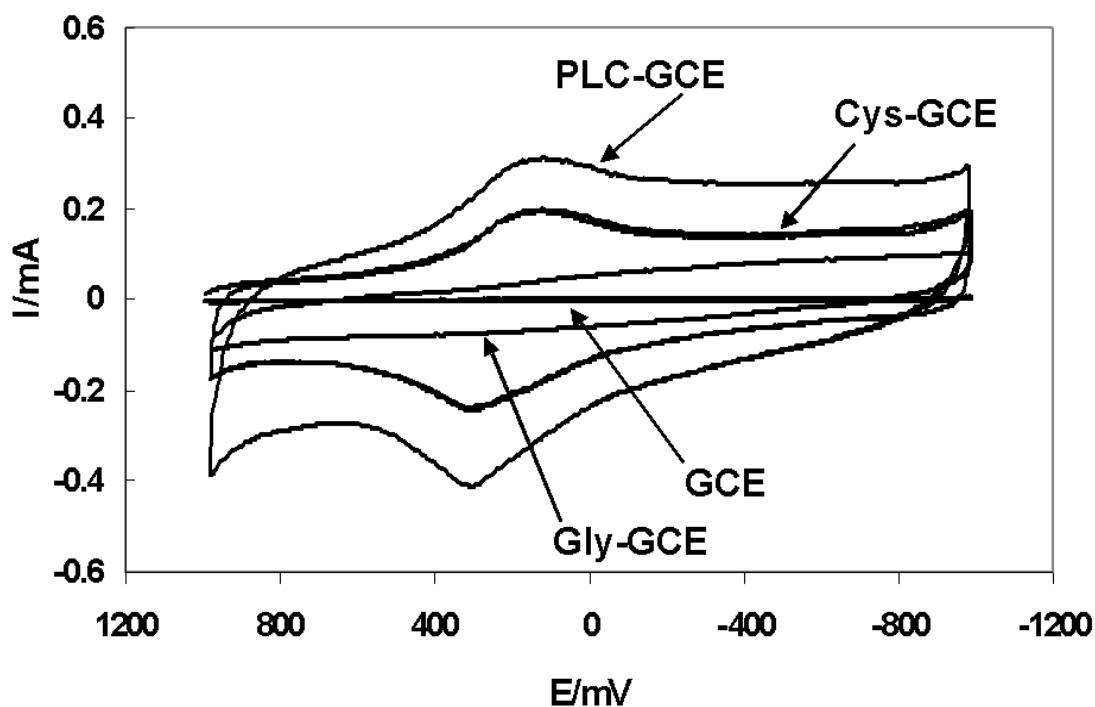


3.3.2 Cyclic Voltammetry

Initial electrochemical experiments on the three modified electrodes were carried out both to confirm the presence of each attached ligand and to characterize the electrochemical nature of the immobilized ligands. Cyclic voltammograms were obtained for both the Cys-GCE and the PLC-GCE, as well as for Gly-GCE. As seen in Figure 3.4, oxidation and reduction waves are present for both the Cys-GCE and PLC-GCE, occurring between 0 mV and +400 mV in both cases. These redox potentials correlate reasonably well with those previously reported E values for various disulfide bonds [53]. The peak-to-peak separation exhibited in the cyclic voltammograms is most likely a function of kinetic limitations or the contributions of multiple E_0 s. Also shown in this Figure is the cyclic voltammogram for the unmodified GCE and the Gly-GCE. There are no appreciable electrochemical features for the Gly-GCE, aside double-layer charging.

In ideal circumstances, when using modified electrodes, cyclic voltammetry results in a symmetric response with a ΔE_{peak} equal to 0. In reality, however, many characteristics of modified films, particularly polymeric films, lead to a variety of voltammetric peak shapes. The four most often discussed contributors to non-ideal voltammetric behavior include electron transfer and transport especially to physically remote sites, movement of polymer chains, movement of charge compensating ions and movement of solvent molecules [51].

Figure 3.4 Cyclic voltammograms of modified electrodes.



In order to approximate the surface coverage of each electroresponsive ligand, the Faradaic portion of the cyclic voltammogram was integrated. The approximate microscopic surface areas of the Cys-GCE and the PLC-GCE were estimated to be 2 cm^2 and 5 cm^2 , respectively, based on the capacitance of the oxidized electrode as determined by cyclic voltammetry [7]. Assuming a 2 electron transfer per disulfide bond, the surface coverage of the cysteine monomer on the electrode surface was calculated to be $\sim 4 \times 10^{13} \text{ molecules cm}^{-2}$ for Cys-GCE and $\sim 1 \times 10^{12} \text{ molecules cm}^{-2}$ for PLC-GCE, assuming an average of 50 Cys residues per PLC chain and complete oxidation of all

thiols. Since complete oxidation of all thiols is assumed in the calculations, the reported coverage values represent lower limit. Considering the increased steric hindrance associated with the attachment of a 50-mer as compared to a monomer, it is not unexpected that there is a significant decrease in surface coverage. Additionally, the calculated coverage of Cys and PLC is not unreasonable when compared with the 6×10^{13} molecules cm^{-2} value for monolayer coverage of a covalently attached film [51].

To further verify that the voltammetric responses seen were a result of surface immobilized species and not freely diffusing solution species, a scan rate analysis was done for each of the electrodes. Because immobilized species have a different response to scan rate changes than solution species [7], a scan rate analysis can easily differentiate between the two situations using the Randles-Sevcik equation [7].

$$i_p = (2.69 \times 10^5) n^{3/2} A D^{1/2} C v^{1/2} \quad (3.1)$$

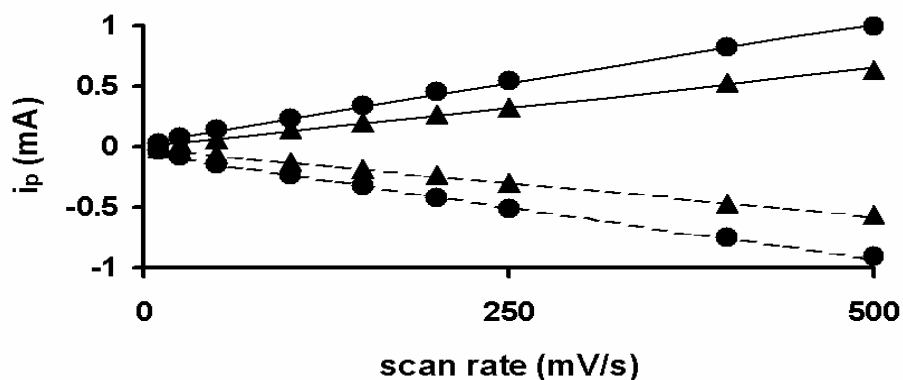
where i_p is the peak current, n is the number of electrons, A is the area of the electrode, D is the diffusion coefficient, C is the concentration and v is the scan rate. As shown in equation 3.1, the peak current of a solution species is proportional to the square root of the scan rate. The peak current of immobilized species can be related to scan rate by equation 3.2 [51],

$$i_p = \frac{n^2 F^2 \Gamma}{4RT} v \quad (3.2)$$

where F is Faraday's constant, Γ is surface coverage, R is the rate constant and T is temperature. In this case, the peak current is directly proportional to the scan rate.

Voltammograms were collected for scan rates of 10, 25, 50, 100, 150, 200, 250 and 500 mV/s. The relationship of peak current to scan rate could then be determined by the plot shown in Figure 3.5. Since the peak currents of both the Cys-GCE and the PLC-GCE exhibit a linear relationship with scan rate, the voltammetric responses were established to be those of surface-confined species.

Figure 3.5 Peak current response to scan rate changes.

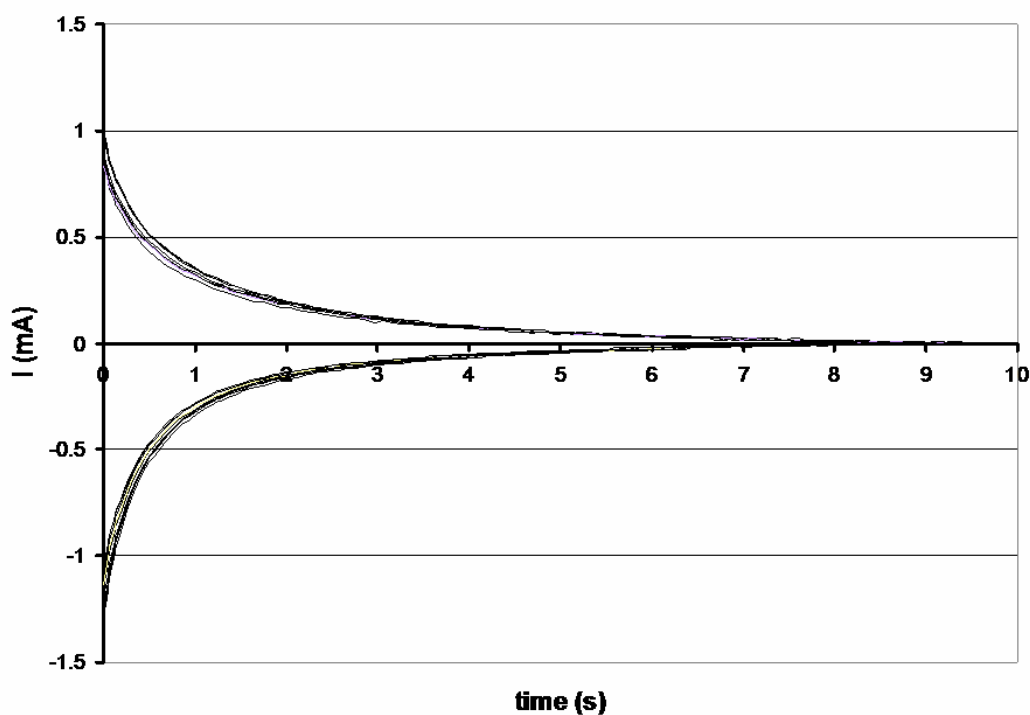


3.3.3 Chronoamperometric Determination of Kinetic Rate Constants

In most modified polymer electrode systems, electron propagation is thought to occur by means of electron self-exchange reactions between oxidized and reduced neighbors within the film. Kinetics of this electron transfer through the polymer chain

was obtained for PLC-GCE by a series of large potential steps ($\Delta 600$ mV). The potential step curves used for all the kinetic calculations are shown in Figure 3.6.

Figure 3.6 Current as a function of time for potential steps from 0 mV vs. Ag/AgCl to either -600 mV or +600 mV vs. Ag/AgCl.



Because electrons move in a diffusion-like manner [54], an electron diffusion coefficient, D_E , can be determined via the Cottrell equation. After determining that $D_E \approx 1.3 \times 10^{-12}$ cm²/s, first (k_{HOP}) and second (k_{EX}) order electron transfer rate constants for electron hopping were calculated using eq. 3,

$$D_E = k_{HOP} \delta^2/6 = k_{EX} \delta^2 C/6 \quad (3.3)$$

where k_{HOP} and k_{EX} are the first and second order electron transfer rate constants, respectively, δ is the effective distance of a single electron hop which was estimated to be 0.43 nm for intrachain hops, calculated based on bond lengths and angles [2], and 0.58 nm for interchain hops, calculated based on approximate polymer surface density, and C is the concentration of redox centers which was estimated to be 10^{-2} moles·cm⁻², calculated based on the estimated number of thiols present [55].

Rates for intrachain electron transfer as well as rates for interchain electron transfer were determined. Because of the near monolayer surface coverage, intrachain and interchain electron transfer rates, shown in Table 3.1, were roughly the same indicating that electron transfer could proceed with equal probability by either mechanism. In comparing the electron diffusion coefficient to those of other polymer systems, the D_E for the PLC-GCE system was relatively low [54]. This is mostly likely due to the fact that PLC, while immobilized, is not rigid and thereby exhibits some degree of solution-like behavior in its motion. Also, heterogeneous electron transfer may additionally contribute to the lower diffusion coefficient [54]. This sluggish electron transfer determined by the kinetic analysis may also explain why the peak-to-peak separation seen in the cyclic voltammograms is larger than one would expect for surface immobilized species. However, some contention exists regarding the accuracy of using large potential steps to measure kinetic information. Because the determined value of D_E also includes a contribution due to physical movement of redox centers and counterions, the calculated value may be at erroneously high representing an upper limit.

Table 3.1 Kinetic rate constants for electron migration in immobilized PLC.

D_E (cm^2/s)	1.3×10^{-12}
$k_{\text{HOP}_{\text{intra}}}$ (s^{-1})	4×10^3
$k_{\text{HOP}_{\text{inter}}}$ (s^{-1})	2×10^3
$k_{\text{EX}_{\text{intra}}}$ ($\text{M}^{-1}\text{s}^{-1}$)	4×10^5
$k_{\text{EX}_{\text{inter}}}$ ($\text{M}^{-1}\text{s}^{-1}$)	2×10^5

3.3.4 Determination of the pK_a of PLC

Cyclic voltammograms were obtained at pHs ranging from 1 to 12. The anodic fractions of the CVs are shown with a vertical offset in Figure 3.7. A gradual shift in the peak current towards more positive values at low pHs can be seen. Determining the pK_a of a polymer such as PLC in homogeneous solution presents experimental challenges due, in large part, to the insolubility of the fully protonated polymer. A method described previously for a carboxylic acid terminated self-assembled monolayer on gold was employed to investigate PLC-GCE. White et al. [56] presented a novel method for the voltammetric determination of the pK_a of surface immobilized acid groups. Cyclic voltammograms were obtained for both Cys-GCE and PLC-GCE at pHs from 4 to 9. The anodic portion of the voltammogram was integrated and a surface charge density was

calculated. The local maxima on the charge density plot provide estimates of the pK_a values [56]. The surface charge density variation with pH is shown in Figure 3.8.

Figure 3.7 Anodic CV at increasing pHs. These CVs were used for both pK_a determination methods.

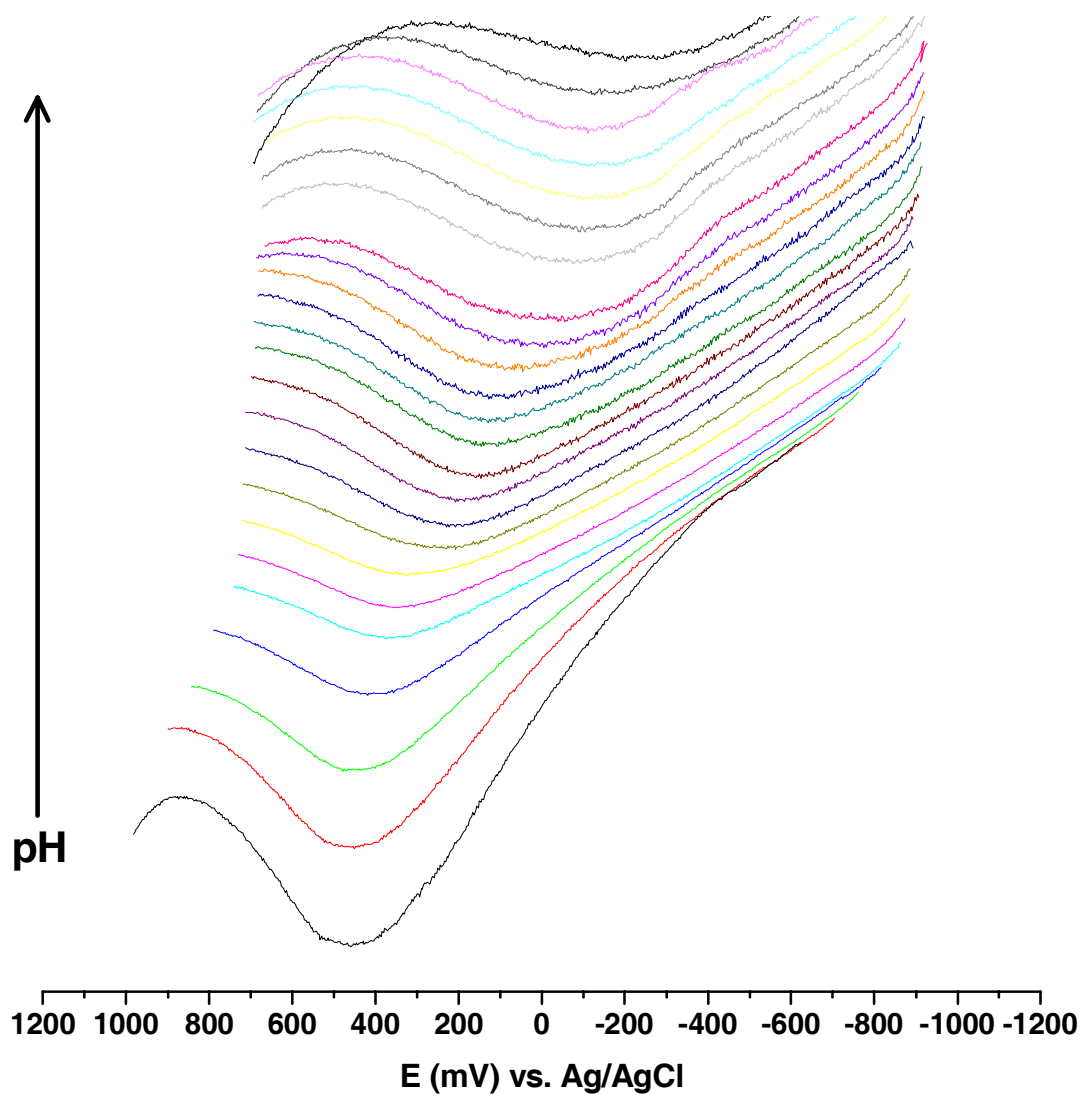
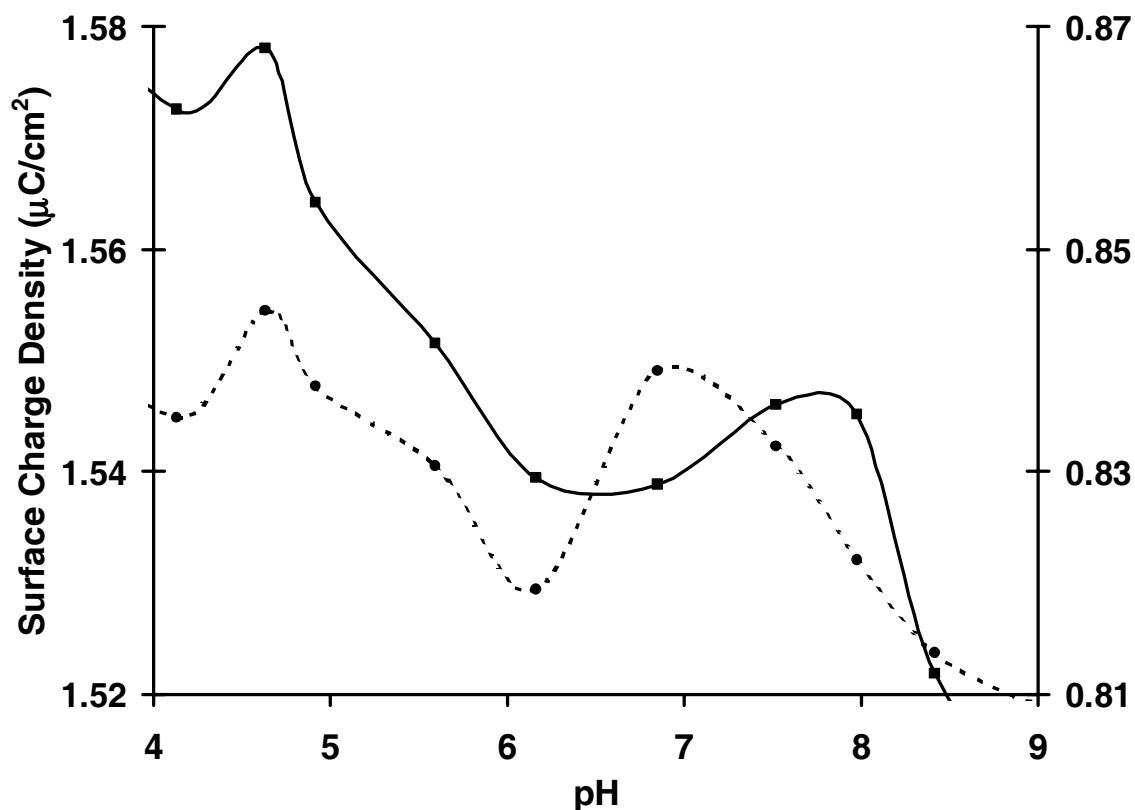


Figure 3.8 Voltammetric determination of pK_a . Data corresponding to PLC-GCE is connected by a solid line and plotted in reference to the left-hand axis. Data corresponding to Cys-GCE is connected by a broken line and plotted in reference to the right-hand axis.

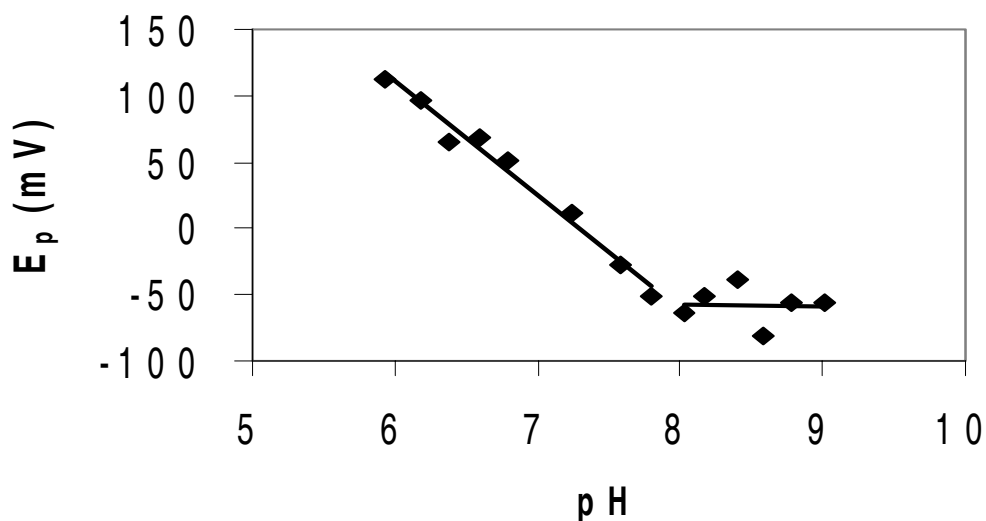


As shown in Figure 3.8, both Cys-GCE and PLC-GCE show the same maximum at $\text{pH} \sim 4.5$. This most likely corresponds to the pK_a of the terminal carboxylate of both the monomer and the polymer. The nearly 15-fold increase in Cys surface coverage would predict a similar increase on the carboxylate charge density. However, because the surface coverage of the PLC-GCE is not as dense as the Cys-GCE, it is possible that some unreacted surface carboxylates of the GCE are contributing to the magnitude of the

surface charge density for the PLC-GCE. The Cys-GCE exhibits a second maximum corresponding to the pK_a of the thiol group at $pH \sim 7$. This represents a decrease from free Cys in solution that exhibits a pK_a of ~ 8 [2]. In the case of the PLC-GCE, the peak corresponding to the thiols of the polymer does not reach a maximum until $pH \sim 8$. This peak is also slightly broader than the analogous peak for Cys-GCE. The location of the thiol peak for PLC-GCE indicates that the overall pK_a has shifted as a result of the differing environment of the constituent thiol groups combined with a reduction of the surface influence. The broadened peak may indicate that there is not a single pK_a , but many pK_a s since each thiol within the chain is contained within a different local environment.

By plotting the voltage at which the peak current appears as a function of pH (Figure 3.9), several pieces of information can be elucidated. It has been previously noted for thiol-containing compounds that the oxidation peak potentials become more negative with an increase in pH at a rate of roughly 60 mV/ pH , as governed by the Nernst equation, at pH s less than the pK_a [57]. When the solution pH becomes greater than the pK_a of the thiols, there is no correlation between the rate of decrease in peak potential and solution pH . This transition in immobilized PLC can be seen at a $pH \sim 8$, a value consistent with the results from the surface charge density method. Additionally, the slope of the line at pH s less than the pK_a is equal to 80 mV/ pH . Although this value is higher than the expected 60 mV/ pH , it may indicate the presence of repulsive forces within the molecule [54].

Figure 3.9 Peak potentials of Immobilized PLC as a function of solution pH.



3.4 CONCLUSION

Through the use of standard chronoamperometric and voltammetric analysis, physical and electrochemical characteristics of PLC-GCE, ranging from approximate coverage and pK_a to electron transfer kinetics, were determined. Results were consistent with the traits of a polymeric system with relatively slow electron transfer. Based on the previous electrochemical evaluation, PLC immobilized on carbon should be a viable system for electrochemically-mediated metal binding studies.

Chapter 4: Evaluation of Metal Binding to Modified Electrodes

4.1 INTRODUCTION

Poly-L-cysteine (PLC) can be obtained as a short chain bio-homopolymer consisting of approximately 50 repeating cysteine residues. PLC was first studied as a potential metal remediation tool [28] as a synthetic analog of the naturally occurring metallothioneins which are proteins with a disproportionately high number of cysteine residues [58]. The ability of Cys and PLC to act as an effective metal chelator has been reported previously [28, 31, 59-62]. The binding characteristics of PLC have been studied in homogeneous solution [28] as well as on substrates such as controlled pore glass where flow injection analysis (FIA) experiments using microcolumns were conducted [30-32]. PLC exhibited strong binding as well as on-demand release of metals such as Cd^{2+} , Pb^{2+} , Zn^{2+} and Cu^{2+} . The binding of Cd^{2+} to PLC is strong enough to effectively pull Cd^{2+} from EDTA as a consequence of a stability constant of ca. 10^{13} [37]. The primary group responsible for cation binding is the thiol group of the constituent cysteine residues. Because thiol groups are capable of interacting with each other to form disulfide bonds, the nature of the PLC will change under certain conditions. When all the side groups are in the reduced (*i.e.*, thiol) form, maximum metal binding is achieved. However, when the thiol groups are oxidized and engaged in disulfide bonds, binding is minimal. Previously, oxidizing agents ortho-iodobenzoate and hydrogen peroxide or a reducing agent, dithiothreitol [30], were used with the FIA to alter the oxidation state of PLC. After the column was reduced and metal bound to the chelator, rapid metal release was achieved by acid elution [32]. In addition to proton displacement, atomic force

microscopy was used to validate that a significant tertiary structure change of the PLC to a tight random coil was also a key contributor to the metal release [36]. By dropping the pH significantly below the polymer's pK_a , the thiol groups are protonated and this more hydrophobic structure coils to the surface thereby ejecting the metal completely.

Recognizing that oxidized PLC exhibits poor metal binding and should also represent a relatively hydrophobic structure, this paper explores the feasibility of ligand modifications using electrochemical potentials rather than chemical reagents for altering the binding character of PLC. In order to evaluate the ligand's response to different electrochemical environments, PLC was immobilized onto the surface of a glassy carbon electrode (GCE). Initially, the modified electrode was electrochemically characterized to determine redox behavior, electron transfer kinetics and approximate pK_a . After being electrochemically modified, the polymer was allowed to bind Cd^{2+} . The Cd^{2+} was then released both chemically and electrochemically. The capacity to bind and release Cd^{2+} was then quantified through the use of flame atomic absorption spectroscopy.

4.2 EXPERIMENTAL

4.2.1 Instrumentation

An atomic absorption spectrophotometer (Varian SpectrAA 300) with an air/acetylene flame was used for solution analysis to determine the amount of metal binding to the electrode surface. A hollow cathode lamp was operated at the current recommended by its manufacturer. The 228.8 nm line was used in conjunction with a monochromator bandpass of 0.5 nm.

For the remaining metal binding studies, a Varian UltraMass ICPMS with commercially available software was used with a modified Varian GTA-95 ETV for sample introduction. All samples were quantitatively diluted in 1% nitric acid containing 100 ppb of In for use as an internal standard. A 10 μ L aliquot of each sample was introduced into the ETV and pulse heated to 2900°C. Samples were analyzed in triplicate. Two isotopes of each analyte element were monitored to verify the absence of any isobaric interferences.

4.2.2 Reagents

All reagent used were reagent grade, unless noted otherwise. All glassware used was soaked overnight in 4M nitric acid. Deionized, distilled water was used in solution preparations. Stock solutions of 1000 ppm Cd^{2+} (Assurance), Co^{2+} (SCP Science), Cu^{2+} (SCP Science), Ni^{2+} (SCP Science), Pb^{2+} (SCP Science) and In^{2+} (SCP Science) atomic absorption standards were used to prepare the 10 ppm solutions for the metal binding experiments as well as calibration standards. Other reagents used included potassium chloride (EM Science), potassium hydroxide (Fisher Scientific), hydrochloric acid (Fisher Scientific), dithiothreitol, DTT (Fisher Scientific) and ortho-iodobenzoate, o-IB (Fisher Scientific).

4.2.3 Correlation of the Electrochemical Redox Method with a Chemical Redox Method

To confirm the efficacy of the electrochemical oxidation and reduction of PLC, Cd^{2+} binding studies were conducted using both electrochemical and previously used chemical ligand preparation. For these studies, a commercially purchased 1.5 mm glassy

carbon electrode (Cypress Systems) was modified with PLC using the previously described procedure. The electrode was placed in a 0.01 M DTT solution at pH 7 and allowed to sit for 1 min, rinsed briefly with DI water and introduced into a 10 ppm Cd^{2+} solution adjusted to pH 7. After rinsing with DI water to remove excess, unbound Cd^{2+} , the bound metal was released by exposure to 0.5 mL of 0.1 M HNO_3 . The electrode was then reduced by a 30 s -600 mV potential step, metal was allowed to bind and the bound metal was released as before. A second set of experiments were performed to evaluate electrochemical and chemical oxidation of PLC as a mechanism for metal release. The electrode was prepared for metal binding by a 30 s -600 mV potential step and Cd^{2+} was allowed to bind. The bound metal on electrode was released by either exposure to 0.5 mL of 0.001 o-IB at pH 7 or a 30 s +600 mV potential step into 0.5 mL of 0.2 M KCl at pH 7. Each set of experimental conditions were performed in triplicate. In all cases, a 10 μL aliquot of the released metal was quantified by inductively coupled mass spectrometry using electrothermal vaporization for sample introduction. Instrumental parameters used for analysis are listed in Tables 4.1 and 4.2.

Table 4.1 ETV heating cycle used for metal analysis by ETV-ICPMS

Temperature (°C)	Time (s)	Dosing Hole Position
120	20	Open
200	10	Open
200	10	Closed
2200	1.2	Closed
2200	3.0	Closed
50	11	Closed
2900	1.5	Open
2900	3.0	Open
50	14	Open

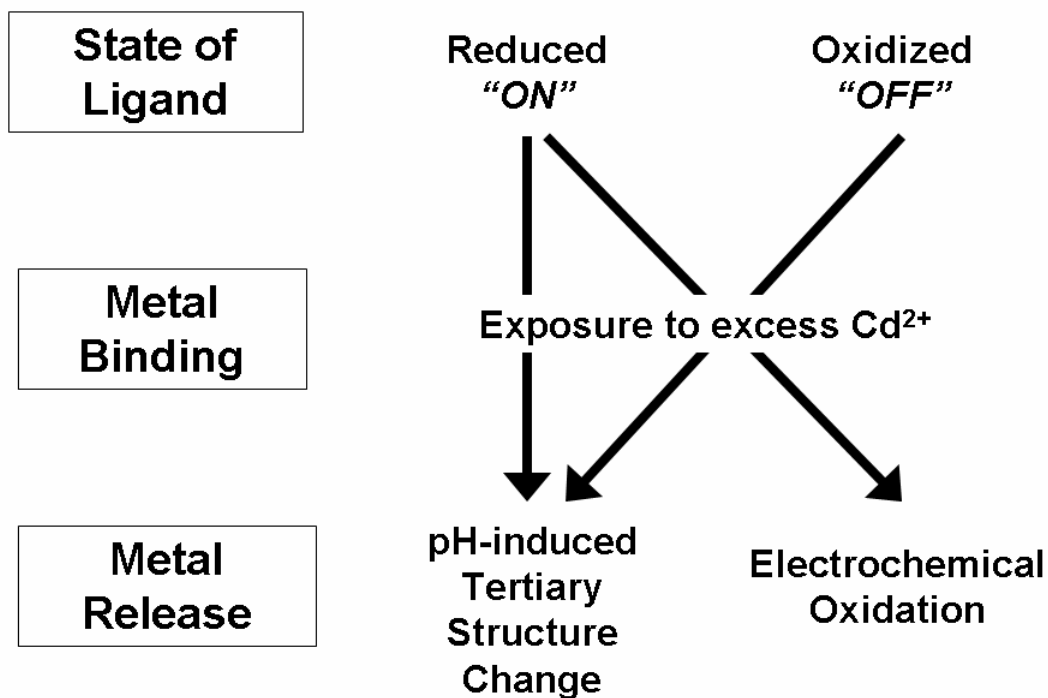
Table 4.2 Argon plasma and quadrupole parameters for metal analysis

Plasma flow	15 L/min
Auxiliary flow	1.4 L/min
Nebulizer flow	0.8 L/min
Sampling depth	11 mm
RF Power	1.2 kW
Dwell time	10000 μ s
Scan time	240 ms

4.2.4 Evaluation of Cd²⁺ Binding to PLC-GCE and Cys-GCE

In order to evaluate the metal binding capabilities of the immobilized polymer as well as the two monomers, the ligands were subjected to a series of electrochemical and chemical environments. For PLC and Cys, the ligand was first prepared for binding by either a reduction (negative potential step from 0 to -600 mV vs. Ag/AgCl) or an oxidation (positive potential step from 0 to +600 mV) in 0.2 M KCl. After initial ligand preparation, the electrode was placed in 50 mL of a 10 ppm Cd²⁺ solution in 0.01 M phosphate buffer adjusted to pH 7 with stirring for 1 min. The electrode was briefly rinsed with DI water to remove any weakly sorbed metal. The bound metal was subsequently released by one of three mechanisms for quantitation. The first release method involved soaking the electrode in 0.5 mL of 0.1 M HNO₃ for 1 min. Because Gly required no electrochemical preparation, the Gly-GCE was simply exposed to excess Cd²⁺ followed by a quantitative release in 0.1 M HNO₃. The experimental combinations are detailed in Figure 4.1.

Figure 4.1 Experimental pathways for metal binding analysis.



The released metal was quantified by discrete nebulization flame atomic absorption spectroscopy. The 0.5 mL aliquots were nebulized and their resulting peaks integrated. Calibration was achieved by integrating peaks of 0.5 mL of matrix-matched calibration standards. All metal binding experiments were repeated for a total of 5 times.

4.2.5 Effect of Reduction and Oxidation Voltage on Cd²⁺ Binding Capacity on PLC-GCE

The effect of the reduction and oxidation voltage was evaluated by repeating the metal binding experiments at decreasing reduction (i.e. -800 mV, -600 mV, -400 mV, -

200 mV and -100 mV) and oxidation (i.e. +600 mV, +400 mV and +200 mV) voltages. For the decreasing reduction voltage experiments, the electrode was reduced by a potential step from 0 mV to each of the above negative voltages for 30 s. The PLC modified electrode was then removed from the 0.2 M KCl electrolyte solution and immersed in a 10 ppm Cd^{2+} solution at pH 7 and allowed to bind for 1 min. The electrode was rinsed with DI water to remove excess Cd^{2+} . The strongly bound Cd^{2+} was released by immersing the PLC-CGE in 0.5 mL of 0.1 M HNO_3 . For the decreasing oxidation experiments, the electrode was first reduced by a potential step from 0 mV to -600 mV for 30 s. The PLC modified electrode was then removed from the 0.2 M KCl electrolyte solution and immersed in a 10 ppm Cd^{2+} solution at pH 7 and allowed to bind for 1 min. The electrode was rinsed with DI water to remove excess Cd^{2+} . The strongly bound Cd^{2+} was released into 0.2 M KCl at pH 7 by using a 30 s potential step from 0 mV to the above positive voltages. The final method utilized multiple 1 s positive potential steps (+600 mV, +400 mV and +200 mV) in 0.5 mL of 0.2 M KCl every second for 30 s, 20 s, 10 s or 5 s. All released Cd^{2+} was quantified using discrete nebulization flame atomic absorption spectrometry and a matrix-matched calibration curve. All of the above metal binding experiments were repeated for a total of 5 times.

4.2.6 Evaluation of Cu^{2+} , Co^{2+} , Pb^{2+} and Ni^{2+} Single-metal and Mixed-metal Solutions

To further study PLC as a potential electroresponsive chelator, the modified electrode was exposed to 10 ppm single metal solutions of Cu^{2+} , Co^{2+} , Ni^{2+} and Pb^{2+} for 1 min following a 30 s – 600 mV reduction pulse. The bound metal was then released in 0.50 mL of 1% HNO_3 for 1 min, quantitatively diluted 2% HNO_3 containing 200 ppb In

and analyzed by electrothermal vaporization inductively coupled mass spectrometry (ETV-ICPMS).

In order to investigate competitive effects, the PLC-modified electrode was exposed to a solution containing 10 ppm of each of the previously studied metals, Cd^{2+} , Cu^{2+} , Co^{2+} , Ni^{2+} and Pb^{2+} for 1 min following a 30 s – 600 mV reduction pulse. The bound metals were stripped one of two ways: the metals were released into 0.5 mL of 1% nitric acid for 1 min; or, the metals were released by a series of five 1 s + 600 mV pulses into 0.50 mL of a 0.2 M KCl at pH 7. In each case, the 0.5 mL samples were quantitatively diluted with 0.50 mL of 2% nitric acid containing 200 ppb of In and analyzed by ETV-ICPMS. The ETV temperature cycle used for sample vaporization is shown in Table 4.1. ICP method parameters and isotopes used for analysis are listed in Table 4.2 and Table 4.3 respectively. For all analyte metals, with the exception of Co, two isotopes were monitored to confirm correct isotopic ratios. Co only has one isotope to monitor.

Table 4.3 Isotopes monitored for multi-metal analysis by ETV-ICPMS

Co	59
Ni	60, 62
Cu	63, 65
Cd	111, 112
In	115
Pb	207, 208

4.3 RESULTS AND DISCUSSION

4.3.1 Correlation of the Electrochemical Redox Method with a Chemical Redox Method

Electrochemical methods, specifically potential step experiments, were compared to previously used chemical means of reduction and oxidation of PLC using capacity for Cd^{2+} as an indicator. Results, tabulated in Table 4.4, indicate that the electrochemical reduction yields essentially the same Cd^{2+} capacity as the 0.01 M DTT, a previously used[30] chemical reducing agent. Similar results were seen for the effectiveness of the electrochemical oxidation as compared to 0.001 M o-IB. Together these results indicate that potential steps, both reductive and oxidative, can be used to successfully reduce and oxidize the thiol groups of PLC.

Table 4.4 Comparison of chemical and electrochemical treatment of 1.5 mm diameter PLC-GCE for Cd^{2+} binding capabilities. For chemical treatments (0.01 M DTT, pH 7; 0.1 M HNO_3 ; 0.001 M o-IB, pH 7), the electrode was exposed for 1 min. Electrochemical potential steps were held for 30 s.

Ligand Preparation	Metal Release	Cd^{2+} Released (ng)
DTT	HNO_3	64 ± 17
- 600 mV	HNO_3	52 ± 10
- 600 mV	+ 600 mV	16 ± 5
- 600 mV	o-IB	22 ± 5

4.3.2 Evaluation of Cd^{2+} Binding to PLC-GCE and Cys-GCE

In order for PLC or Cys to be used as an effective metal chelator, sufficient electrochemical control of the ligand redox state must be obtained. The chelator needs to be activated, or “turned on”, to achieve maximum binding capacity, and deactivated, or “turned off”, to eliminate binding capacity. Ideally, the bound metal should be rapidly released upon ligand deactivation. To evaluate whether these control mechanisms could be realized by altering the electrochemical potential, Cd^{2+} was initially chosen as a target metal ion for binding to the modified electrode system. The glycine modified electrode served as a control for the metal binding studies because of its lack of a metal binding side chain. The capacity for Gly-GCE was <20 ng of Cd^{2+} , and even this limited capacity is likely attributable to the metal binding capability of the terminal carboxylate.

From previous studies, it is known that maximum capacity for PLC and Cys were obtained when all disulfide bonds were reduced, and very little capacity remained after the disulfide bonds were formed. Additionally, using the fully reduced form for binding, rapid and quantitative metal release could be achieved with exposure to 0.1 M nitric acid [30]. For this study, the ligands were initially prepared by either a reductive -600 mV potential step to activate the chelator or an oxidative +600 mV potential step to deactivate the chelator. After preparation, the electrodes were immersed in a 50 mL solution of 10 ppm Cd^{2+} and allowed to bind. The Cd^{2+} was subsequently released into 0.5 mL of clean solution by one of three mechanisms: a nitric acid rinse, a single oxidative potential step or a series of 30 oxidative potential steps. All results are presented in Table 4.5.

Table 4.5 Cd^{2+} binding analysis for Cys-GCE and PLC-GCE.

	<i>Pre-binding Ligand Preparation</i>	<i>Release Mechanism</i>	<i>ng Cd²⁺ released Cys-GCE (n=5)</i>	<i>ng Cd²⁺ released PLC-GCE (n=5)</i>
I	- 600 mV	acid	140 ± 20	118 ± 15
II	+ 600 mV	acid	79 ± 9	not detected
III	- 600 mV	+ 600 mV	61 ± 2	68 ± 13
IV	- 600 mV	multiple + 600 mV	62 ± 9	117 ± 10

To establish a baseline for optimal binding with quantitative release, the ligands were prepared by a negative potential step, and the bound Cd^{2+} was released by exposure to acid (See results for protocol **I** in Table 4.5). The acid strip solution for PLC-GCE contained 118 ± 15 ng of Cd^{2+} which corresponds to approximately 11 metal atoms per polymer chain. The acid strip for Cys-GCE contained 140 ± 20 ng of Cd^{2+} corresponding to <1 metal atom per Cys. By oxidizing the thiols with a positive potential step (**II**) before exposure to Cd^{2+} , the ligand should be “inactive”, i.e. non-binding. The acid strip solution for PLC-GCE contained no detectable metal indicating that very little to no Cd^{2+} binding occurred. The acid strip for Cys-GCE, however, did contain detectable levels of

Cd^{2+} (79 ng), indicating that Cys retains ~ 56% of its maximum capacity even under oxidizing conditions due, in part, to the availability of the carboxylates which are unaffected by redox state as well as possible steric inhibitions which prevent all the thiols from being involved in disulfide bond formation.

In order to study the effectiveness of electrochemical release, the ligand was “activated” by a negative pulse and the metal was released by one of two electrochemical methods – a single 30 s positive pulse or multiple positive pulses for a total of 30 s. It was initially hypothesized that the oxidative pulse would cause disulfide formation for those thiols not involved in metal binding. It was expected that the sulfides chelated to Cd^{2+} would not be oxidized by the small anodic voltage used (i.e. ca. 100-300 mV anodic of oxidative voltages for metal-free PLC.) However, it was initially anticipated that the nearby disulfide formation would impact the binding cavity, possibly through added strain placed by the disulfide-induced distortion. This might then “spoil” the metal-PLCys formation constant as the peptide proceeds to “zip up” as disulfides form. However, this was not the case. After one pulse (III), 68 ± 13 ng of metal (~ 60%) were released from the immobilized PLC and 61 ± 2 ng (~ 44%) were released from immobilized Cys. However, when pulses were repeated in quick succession for the same time period (IV in Table 4.5), quantitative release was achieved for PLC-GCE, but not for Cys-GCE. It is possible that by repeating the oxidation process many tertiary structure rearrangements are able to take place thereby significantly disturbing the metal binding pockets and releasing the bound metal ions – a process that would not be effective for the immobilized Cys monomer.

4.3.3 Effect of Reduction and Oxidation Voltage on Cd^{2+} Binding Capacity on PLC-GCE

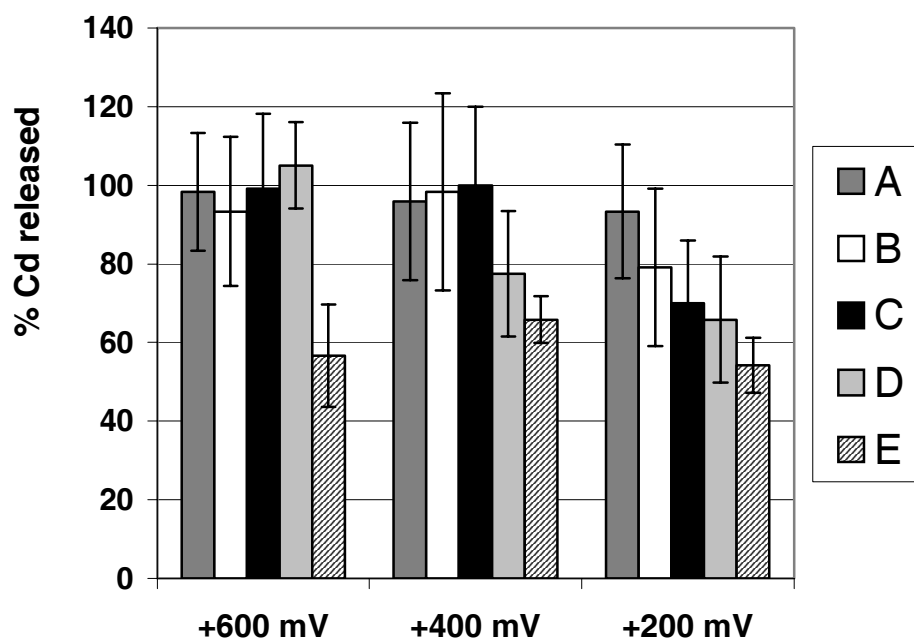
In order to optimize both reduction and oxidation conditions for the respective “turning on” of the binding mode and stripping the metal-loaded immobilized polymer, the corresponding voltages were varied. In the case of using pulsed oxidation for metal release, the number of pulses was also varied. The reduction voltages examined were – 800 mV, –600 mV, –400 mV, –200 mV and –100 mV. As shown in Table 4.6, voltages more positive than –600 mV were less effective in optimizing the binding capacity, probably as a result of incomplete reduction of the sulfurs on the Cys residues.

Table 4.6 PLC-GCE capacity for Cd^{2+} with decreasing reduction voltage.

<i>Reduction Voltage</i> (mV)	<i>ng Cd²⁺ released</i> (n=3)
-100	59 ± 5
-200	70 ± 8
-400	86 ± 5
-600	115 ± 2
-800	113 ± 9

The oxidation voltages used were +600 mV, +400 mV and +200mV. 1.0 s pulses at these potentials were applied. The number of pulses within a given release evaluation were 30, 20, 10 and 5. Additionally, one 30 s pulse was also evaluated for its effectiveness in releasing the bound metal. These results are shown in Figure 4.2. Quantitative release could be achieved by a balance of the oxidation voltages and the number of oxidations, i.e. 30 pulses at +200 mV or 5 pulses at +600 mV. It is possible that with successive oxidations thiols which were not in close enough proximity to form disulfide bonds become more sterically favored for the formation of disulfide bonds.

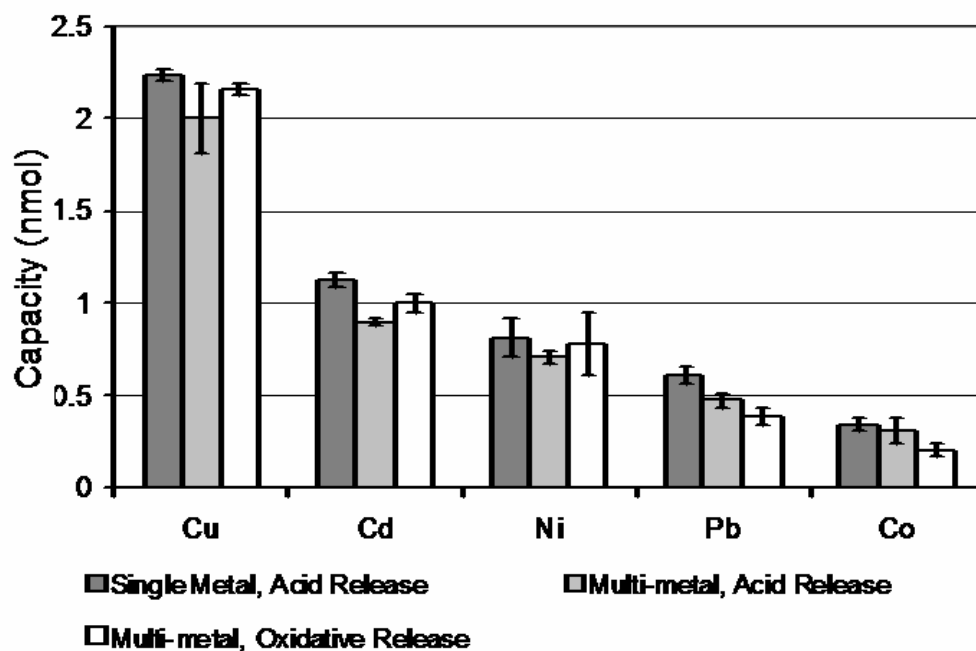
Figure 4.2 Effects of oxidative pulsing on the release of Cd^{2+} . (A-30 1 s pulses, B-20 1 s pulses, C-10 1 s pulses, D-5 1 s pulses, E-1 30 s pulse)



4.3.4 Evaluation of Cu^{2+} , Co^{2+} , Pb^{2+} and Ni^{2+} Single-metal and Mixed-metal Solutions

Results for metal binding studies for other metals are summarized in Figure 4.3. In all cases, the binding trend remained the same ($\text{Cu}^{2+} > \text{Cd}^{2+} > \text{Ni}^{2+} > \text{Pb}^{2+} > \text{Co}^{2+}$). This trend, with the exception of Pb^{2+} , closely corresponds with typical soft acid metal binding preferences that are expected of a soft acid base such as a thiol [63]. Additionally, rapid metal-thiolate exchanges have been seen in biological systems, most often with metallothioneins, in which a harder acid metal, such as Zn^{2+} , is easily replaced with Cd^{2+} which in turn can be easily replaced with Cu^+ [4].

Figure 4.3 Multi-metal binding results from strip analysis as determined by ETV-ICPMS. Capacities for single metal and multi-metal solutions are shown. Multi-metal binding was released by either 0.5 mL of 0.1 M HNO_3 or 5 +600 mV potential steps into 0.5 mL 0.2 M KCl.



In the case of Pb^{2+} , it has been observed previously that rates of exchange often show a decrease as ionic size increases [4]. Ionic radii of Pb^{2+} is 20- 200% larger than the other ions studied as shown in Table 4.7 [1], which may account for the observed discrepancy.

Table 4.7 Ionic radii of selected metal ions [64]

Metal Ion	Ionic Radii (pm)
Cd^{2+}	78
Co^{2+}	75
Cu^{+}	46
Cu^{2+}	57
Ni^{2+}	69
Pb^{2+}	119

Cu^{2+} introduces an interesting case for study. It is widely accepted that Cu(II)-thiolate complexes can be unstable and it is often assumed that Cu^{2+} enters into a redox couple with the thiols in which the Cu^{2+} is reduced to Cu^{+} and the thiol is oxidized to a disulfide. Although this mechanism is thermodynamically preferred, the conversion takes place via a binuclear $\text{Cu}_2(\text{SR})_2$ intermediate which requires steric alignment that does not always occur favorably [4]. And while, cystine generally binds transition metals

quite weakly, Cu^{2+} has been demonstrated to bind successfully to cystines [65]. The observed strong binding of Cu^{2+} needs additional studies to better elucidate its interactions when binding to PLC and, in general, thiols.

The determined metal binding capacity of each metal studied was converted to units of metals atoms per chain and cysteine residue per metal, both shown in Table 4.8. These calculations are derived from knowing the number of PLC molecules immobilized onto the surface based on electrochemical data [66] and the average degree of polymerization of PLC based on the manufacturer specification. The number of cysteine residues per metal atom can indicate the nature of the metal-ligand coordination. In the case of Cu^{2+} , the metal is able to be bound by only 2 cysteine residues probably in a linear coordination geometry. Previous spectroscopic work with the so-called “blue copper proteins” indicates that the number of cysteine residues per Cu^{2+} could range from one to six [65]. As for Cd^{2+} , evidence based on Cd^{2+} bound to metallothioneins indicates that Cd^{2+} prefers to bind in the tetrahedral coordination geometry to 4 cysteine residues [4].

Table 4.8 Metals per PLC chain, assuming d.p. ~50, and Cys residues per metal as determined by ETV-ICPMS.

	Metal atoms per PLC chain	Cysteine residues per metal atom
Cu^{2+}	23	2
Cd^{2+}	12	4
Pb^{2+}	6	8
Ni^{2+}	8	6
Co^{2+}	4	14

It is particularly interesting that the capacities for each metal remain, when evaluated in the absence of other binding metals exhibits nearly the same capacity as that observed when four other competing metal ions are present. This indicates that these binding experiments are confined to the linear portion of the Langmuir isotherm. As shown in Figure 4.3, the identical electrochemical oxidation procedure can be used to quantitatively release a variety of different metals. Thus, the redox character needed to bind and release complexed cations becomes independent of the analyte metal and is only a function of the ligand.

4.3.5 Comparison of PLC-GCE with Previous Immobilized PLC Systems

Immobilized PLC has been used previously as a heavy metal chelator. Earlier studies used PLC immobilized on controlled pore glass [28, 29, 67] and a porous carbon, Carbopack-X [37]. Metal binding capacities determined for these systems as compared

to the PLC immobilized onto a glassy carbon electrode surface are summarized in Table 4.9.

Table 4.9 Metal Binding Capacities in nmol/cm² from PLC immobilized on controlled pore glass [31], Carbopack-X [37] and a glassy carbon electrode. No data was available for Co²⁺ binding to PLC immobilized onto Carbopack-X.

	Controlled Pore Glass	Carbopack-X	Glassy Carbon Electrode
Cd	0.0064	0.0067	0.231
Co	0.0014	N/A	0.071
Cu	0.0159	0.0092	0.452
Ni	0.0032	0.0058	0.164
Pb	0.0085	0.0063	0.128

The values shown in Table 4.9 result in the following metal binding capacity trends:

CPG: Cu > Pb > Cd > Ni > Co

Carbopack-X: Cu > Cd > Pb > Ni

GCE: Cu > Cd > Ni > Pb > Co.

While the trends exhibit some variation, there is a general agreement and source of some of the inconsistency could be due to experimental error. Another variable that is not an insignificant consideration is differences in the experimental parameters,

specifically solution composition. The work on CPG and Carbopack-X was done in 0.05 M ammonium acetate while the modified electrode work was conducted using 0.2 M KCl. As shown in Table 4.10, acetate does have a significant formation constant for the metal ions in these studies which could artificially skew the binding results for experiments conducted in acetate.

Table 4.10 Formation constants of acetate and the metal ions studied [68]

Metal Ion (M)	log K_f (L=acetate)
Co ²⁺	ML 1.5
Ni ²⁺	ML 1.4
Cu ²⁺	ML 2.2 ML ₂ 3.6
Pb ²⁺	ML 2.7 ML ₂ 4.1
Cd ²⁺	ML 1.9 ML ₂ 3.2

4.4 CONCLUSION

At this point, it is plausible to use PLC as an effective metal chelator using only electrochemical potentials, as opposed to the addition of chemicals, to reversibly control the activity of the ligand without altering the redox state of the metal. Additionally, the

binding/release character of the ligand can be controlled by potentials that are independent of the metal involved in the chelation process. This is unlike, for example, remediation approaches that use bulk electrolysis where the potentials are dependent on both the analyte metal and its complexed form in solution. In short, the ligand can be easily and efficiently “turned on”, “turned off” and the metal can be completely released. While Cys offers some of the desired metal binding characteristics, it does not offer complete electrochemical control, making PLC the better choice for an electrochemically-modifiable metal binding ligand.

Chapter 5: *in situ* Raman Microscopy Investigation of PLC-GCE

5.1 INTRODUCTION

Poly-L-cysteine has become a well-established ligand for trace metal chelation and remediation. Work with PLC and the metal binding characteristics of the cysteine moiety began as early as the 1950s [27, 60]. Since then, interest in the metal binding capabilities of amino acids and their respective homopolymers has continually increased [69-82]. These homopolymers have provided a robust alternative to the delicate nature of intact proteins. PLC, in particular, presents an interesting case due to the reactivity of its constituent thiol groups. These thiol groups have proven to be excellent chelators of a suite of heavy metals including Cu, Cd and Pb [28-33, 35-37, 50, 59-61, 63, 83, 84]. Additionally, the thiol group of cysteine is naturally redox active. The formation of cystine, the oxidized version of cysteine, is crucial in biological systems contributing functions such as establishing protein quaternary structure and directing the protein folding process. Unfortunately, the high reactivity of the thiol group causes much difficulty in studying the system electrochemically.

Literature values for the formal potential of the reduction of cystine to two cysteines, shown in equation 5.1 where R represents $\text{HC}(\text{NH}_2)(\text{COOH})\text{CH}_2$, range from -0.14 to -0.39 V vs. SHE [53, 85].



Several obstacles exist in attempting to determine the electrochemical properties of both cysteine and PLC. First, the solubility of cysteine, and especially PLC, confines research and synthesis to either strongly acidic or strongly alkaline conditions which may not be ideal for the intended application or experiment [86]. Other experimental difficulties when studying cysteine in homogeneous solution include slow equilibration and sluggish electron transfer, adsorption of dissolved cysteine to solid electrodes and complicated reaction mechanisms on liquid mercury electrodes [86, 87]. At some carbon surfaces, it has been determined that the oxidation of dissolved L-cystine is electrochemically irreversible [88]. It has been previously concluded that the reversible reduction and oxidation of cysteine systems could only proceed at reasonable rates if both reactants were adsorbed to the electrode surface [89]. To overcome the previously mentioned problems, which are magnified by polymerization, PLC was covalently attached to a glassy carbon electrode surface for further characterization.

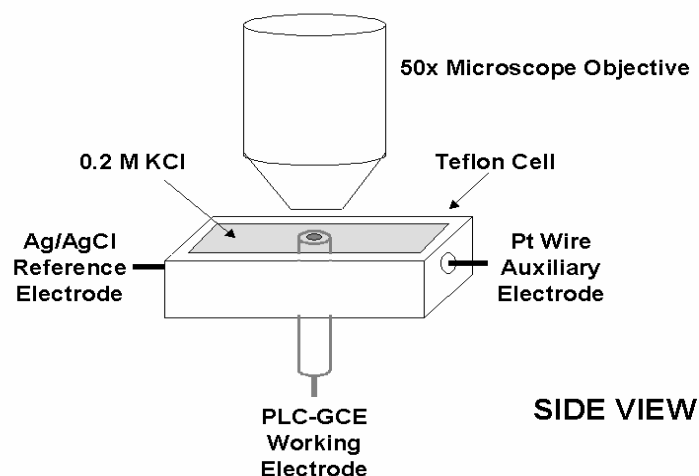
As an alternative to elucidating redox information based on electrochemical data only, the PLC-modified GCE (PLC-GCE) was investigated spectroscopically using Raman microscopy. Raman microscopy has become a preferred technique for the investigation of modified electrodes [90-98] for several reasons, most notably the ability for *in situ* work in aqueous environments. Furthermore, Raman techniques are sensitive to the region of the spectra providing characteristic information for thiol groups [64], disulfides [99] as well as metal-thiol ligand bonds [100-105].

5.2 EXPERIMENTAL

5.2.1 Instrumentation

The glassy carbon electrode was fabricated in-house and modified with a monolayer of PLC using a previously described procedure. The potential on the PLC-modified electrode was governed by a standard microprocessor-controlled three electrode potentiostat (Omni-101). A Pt wire auxiliary electrode was used in conjunction with a Ag/AgCl reference electrode (Cypress Systems) for all measurements. All Raman spectra were collected on an inVia Reflex Raman Microscope (Renishaw) using a 785 nm high power diode laser (Renishaw) and a 50x microscope objective. A custom-made Teflon cell was fabricated to house the three electrodes and the supporting electrolyte solution (Figure 5.1) that was then mounted on the microscope stage.

Figure 5.1 Design of cell for *in situ* Raman microscopy studies



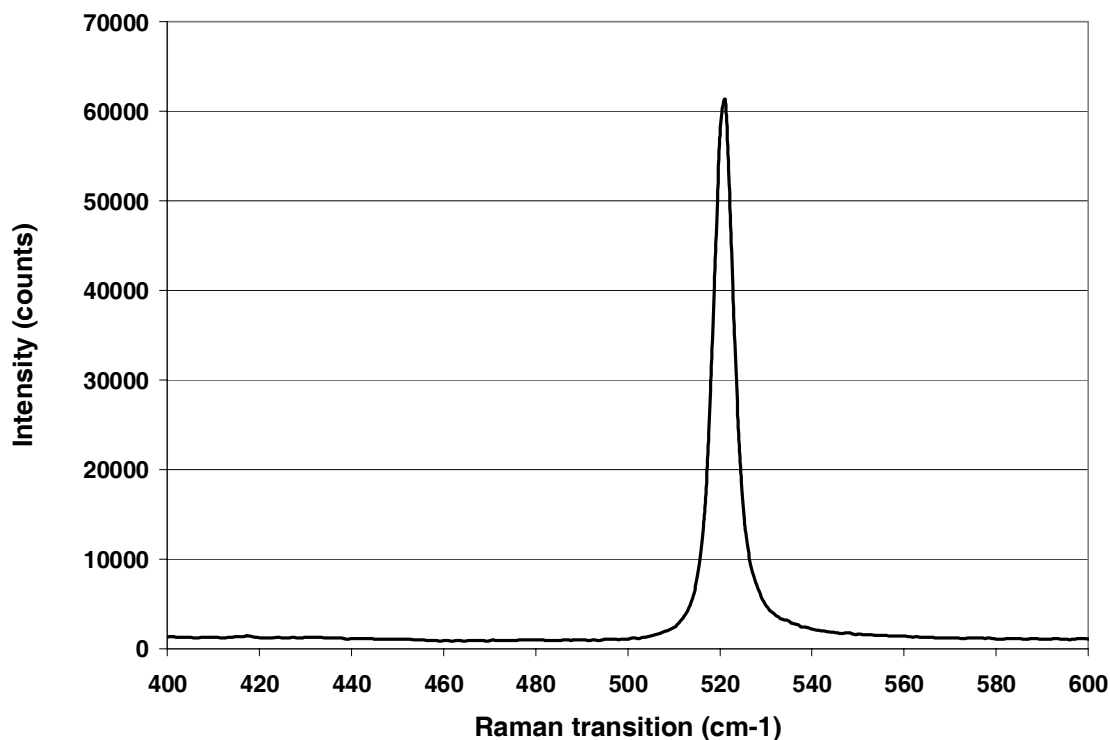
5.2.2 Reagents

All reagents used were reagent grade unless noted. Deionized distilled water was used to prepare solutions, and all glassware was soaked overnight in 4 M HNO₃ prior to use. Poly-S-CBZ-L-cysteine (Sigma) [DP(vis) 50, MW (vis) 11,800] , L-cysteine (Sigma) and glycine (Sigma) were used as received. Other reagents included 1-ethyl-3-[3-(dimethylamino)propyl] carbodiimide (EDC) (Sigma); 4-morpholineethane sulfonic acid (MES), nitric acid, ammonium acetate (Aldrich); sodium hydroxide (Fisher Scientific); disodium hydrogen phosphate, potassium chloride (EM Science). Stock solutions of 1000 ppm Cd²⁺ (Assurance) atomic absorption standards were used to prepare the 10 ppm solutions for the metal binding experiments.

5.2.3 Calibration of Raman Microscope

Prior to each use, the microscope was calibrated using an internal silicon standard using the laser parameters for each experiment. The experiment did not commence until the standard appeared at the correct transition, 521 cm⁻¹, and the number of counts exceeded 50,000. A sample calibration spectrum is shown by Figure 5.2.

Figure 5.2 Si calibration of Raman Microscope



5.2.4 Depth Profile Analysis

In order to ensure there was no changes observed in the acquired spectra due to the vertical positioning of the working electrode as compared to the microscope objective, a depth profile experiment was completed. The microscope stage was initially positioned 5 μm below optical focus. A spectrum was collected at 10 different points along the Z-axis in 1 μm increments. The Raman spectra were collected at each of the above vertical distances in the range of 200-1750 cm^{-1} . For these experiments, the laser power was set to 10% of the maximum and 3 20 s acquisitions were averaged by commercially available software (WiRE 2.0) to generate each spectra. One of the spectra was plotted as obtained. The remaining spectra were plotted as difference spectra, i.e.

each was subtracted from the sample spectra and that difference was plotted as a function of wavenumber. This analysis served only to confirm that the vertical positioning of the stage was not critical. The electrode was not immersed in any solvent or exposed to a potential.

5.2.5 Observation of Oxidation and Reduction of PLC-GCE

In order to monitor the oxidation and reduction of PLC, the electrode was first placed in 0.2 M KCl at pH 7.0 in the Teflon cell. The electrode was held at various potentials, +0.4, +0.2, 0, -0.4, -0.6, -0.8 and -1.0 V vs. SHE, by performing a potential step from -0.2 V and held for 30 s at the desired potential prior to the onset of spectral acquisition. Throughout the acquisition time, the potential was continuously held at the desired potential. The Raman spectra were collected at each of the above potentials in the range of 200-1750 cm^{-1} . For these experiments, the laser power was set to 10% of the maximum and 3 20 s acquisitions were averaged by commercially available software (WiRE 2.0) to generate each spectra. This process was repeated two additional times at different sites on the electrode surface resulting in a series of spectra at three spatially distinct regions of the electrode surface.

5.2.6 Determination of Raman Band Intensities

Due to variations in the laser intensity during data acquisition, the intensities of each spectrum were normalized to the 1360 cm^{-1} carbon peak. In addition, the spectra were each baseline subtracted using a function supplied by Origin 7.0. Because both disulfides and thiols are present to some degree at each potential, a simple blank could not be used. A range of approximately 50 cm^{-1} containing the transitions of interest were

further analyzed to obtain the corrected intensities for both the disulfide bond (450-500 cm^{-1}) and the thiol group (800-850 cm^{-1}). The corrected experimental intensity at the determined wavenumber was used for further analysis. Although Raman spectroscopy is not frequently used for elucidating quantitative information, the potential for exploring this technique to provide additional mechanistic insight to the disulfide and thiol exchange seemed worthwhile to pursue further.

5.2.7 Verification of Cd^{2+} Binding to Thiols

Following a 30 s reduction at -1.0 V to ensure complete reduction any cystine groups present, the electrolyte solution was drained from the cell and a 10 ppm (8.9×10^{-5} M) Cd^{2+} solution in 0.2 M KCl (pH 7.0) was introduced. The metal was allowed to bind for 1 min before spectral acquisition commenced. The binding of Cd^{2+} to the thiol groups of PLC was verified by evaluating the Raman spectrum from 140-300 cm^{-1} using 100% laser power and three 20 s acquisitions. As before, this process was repeated three times at different sites on the surface. Although some Raman spectrometers have difficulty acquiring data below 200 cm^{-1} , the manufacturer confirmed that the holographic notch filter used to block the intensity of the 785 nm excitation laser allowed data collection as low as 100 cm^{-1} , or up to 791 nm.

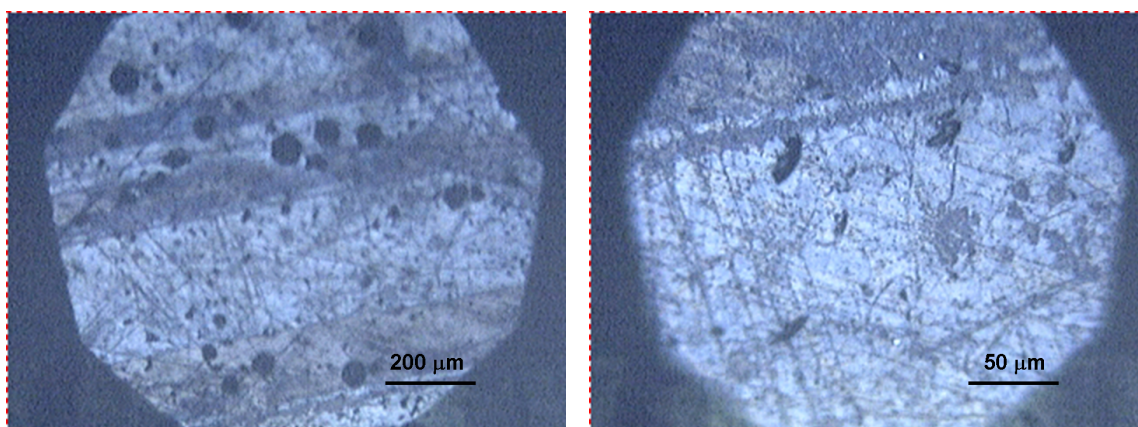
5.3 RESULTS AND DISCUSSION

5.3.1 Depth Profile Analysis

Prior to performing the depth profile analysis, optical images were obtained of the electrode surface using 2 different microscope objectives, 5X and 20X. These images are

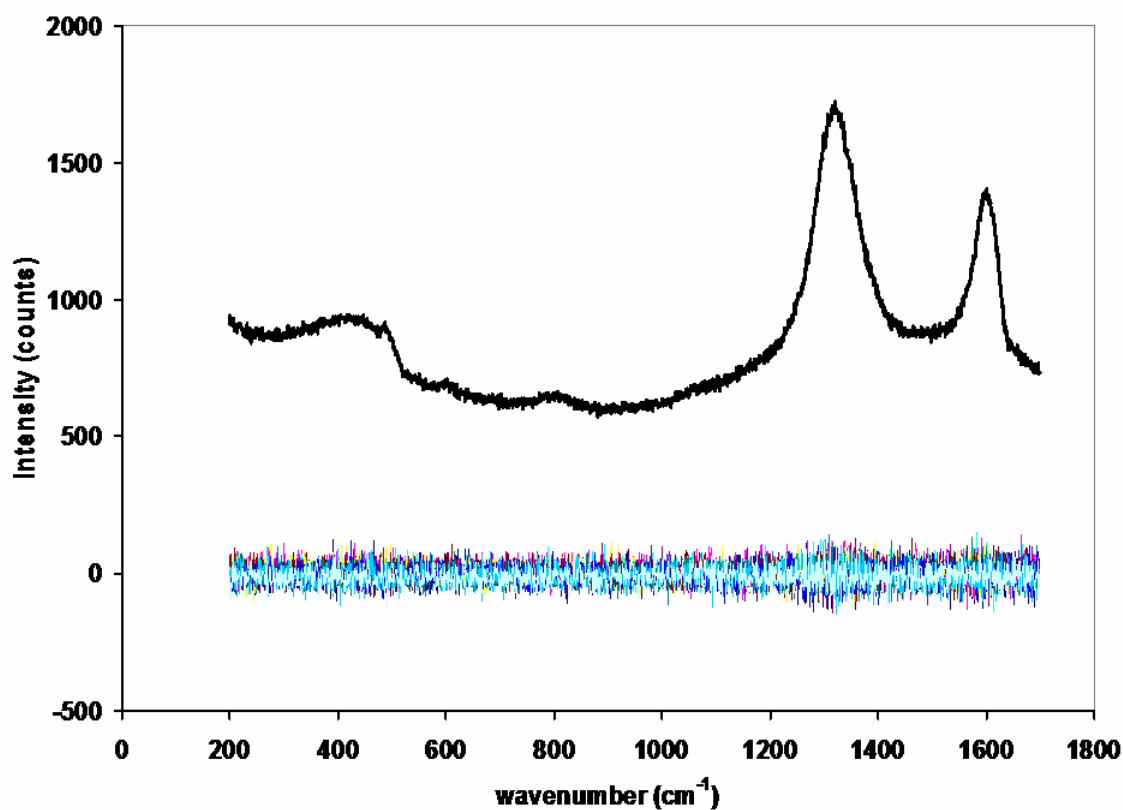
presented in Figure 5.3. The optical focus was used as a reference point for spectral acquisition as a function of position on the Z-axis.

Figure 5.3 Optical images of the glassy carbon electrode surface obtained using a 5X objective, left, and a 20X objective, right.



As seen in Figure 5.4, there are no spectral changes, other than noise, as the microscope stage was moved over 10 μm in the Z direction. This indicates that working at or very near optical focus should ensure that there are no additional or absent spectral features due to the vertical position of the microscope stage. All spectra for subsequent experiments were obtained at optical focus.

Figure 5.4 Sample Raman spectrum and difference spectra obtained by depth profile analysis.



5.3.2 Observation of Oxidation and Reduction of PLC-GCE

To serve as a blank, a spectrum of polished glassy carbon was collected as well (Figure 5.5). An example of raw Raman data for partially oxidized PLC on GCE is shown in Figure 5.6 as an example. The two pronounced peaks at 1360 and 1580 cm⁻¹

correspond to the D and E_{2g} bands, respectively, of glassy carbon surface [97, 106]. The smaller two peaks, centered at approximately 450 and 800 cm^{-1} , correspond to transitions of disulfides and thiol groups, respectively [64, 99].

Figure 5.5 Raman spectrum of a polished glassy carbon electrode

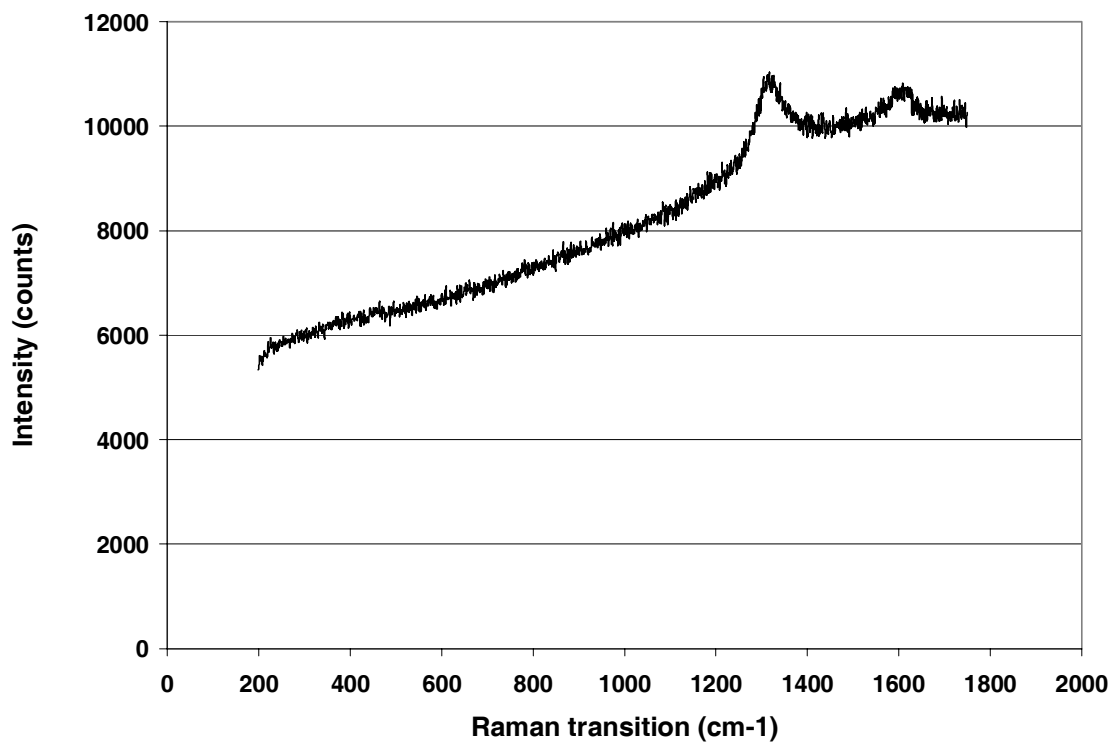


Figure 5.6 Sample Raman spectrum showing peaks of interest: 450 (disulfide), 800 (thiol), 1360 (D band of GCE) and 1580 cm^{-1} (E_{2g} band of GCE). This spectrum was acquired while the working electrode was held at 0 V vs. SHE.

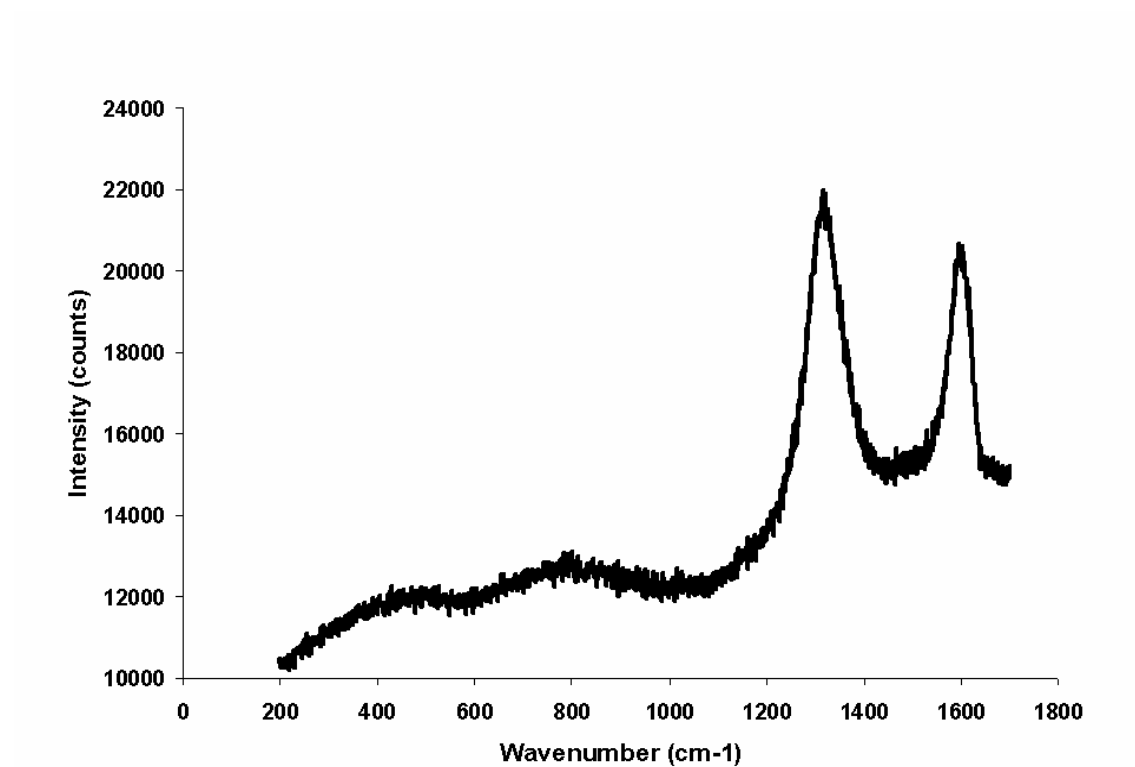
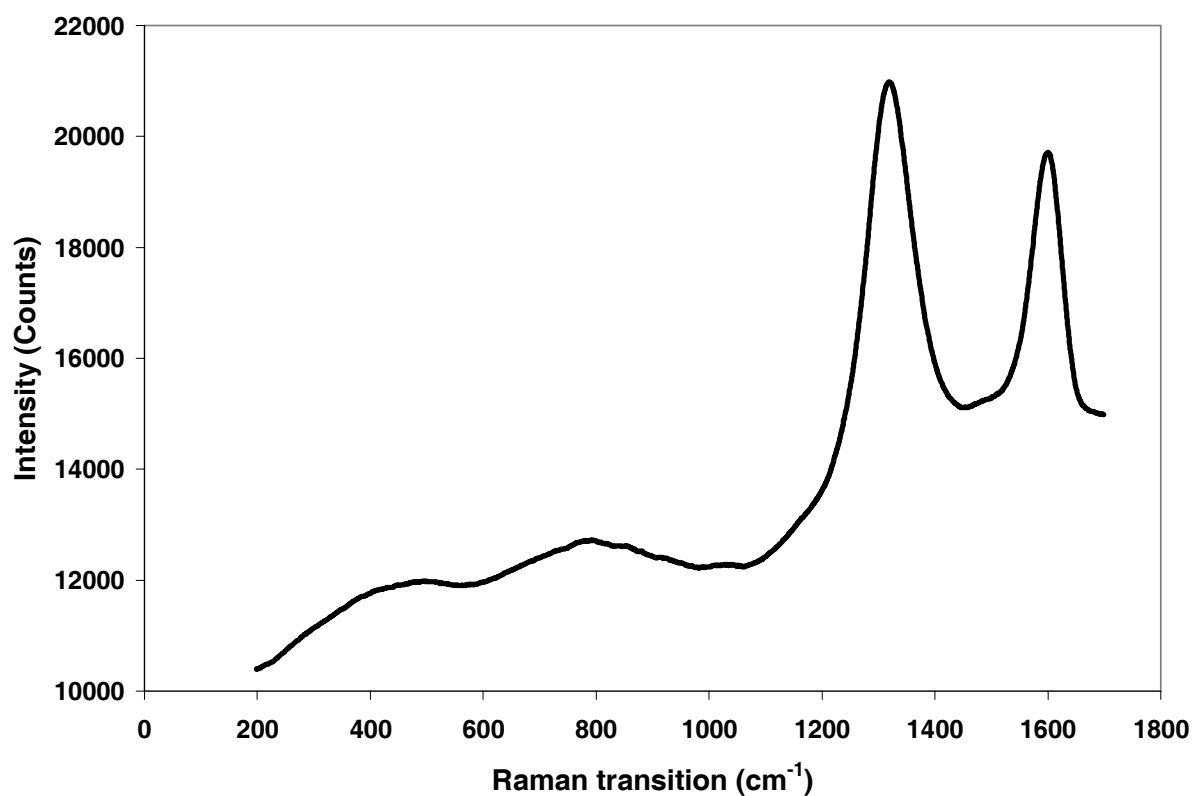
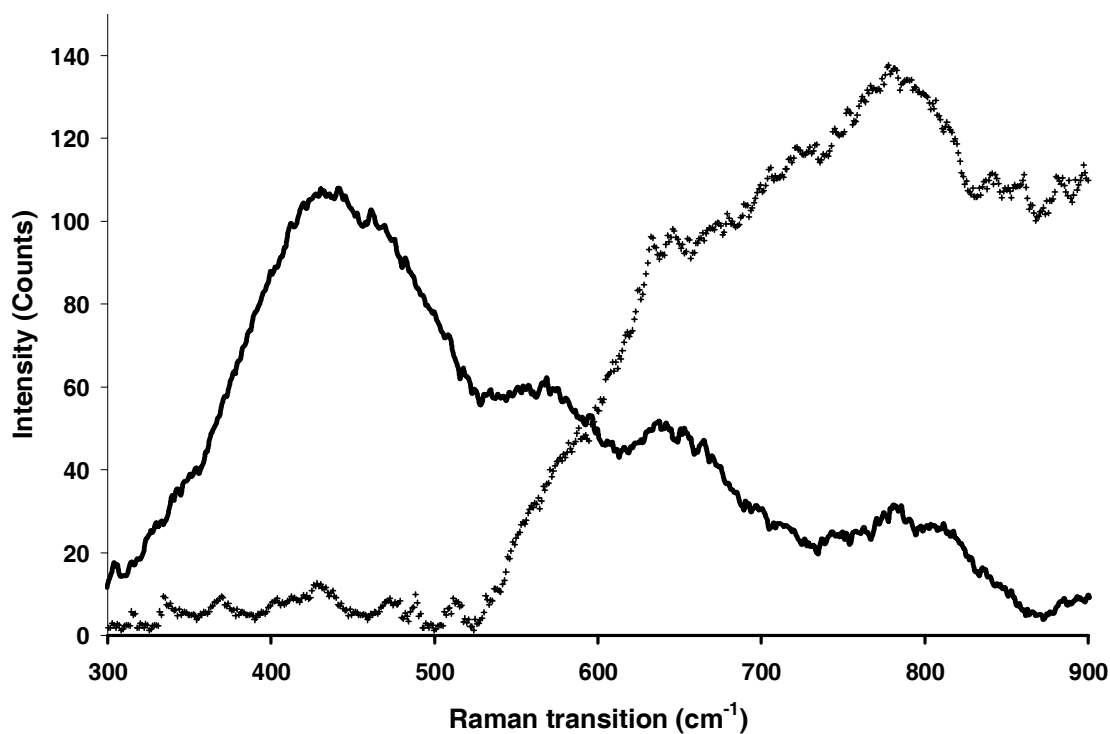


Figure 5.7 Signal averaged Raman spectrum using raw data from Figure 5.6. The curve was generated by performing a 50 point moving average to demonstrate to effective increase in the signal to noise ratio by averaging 50 data points.



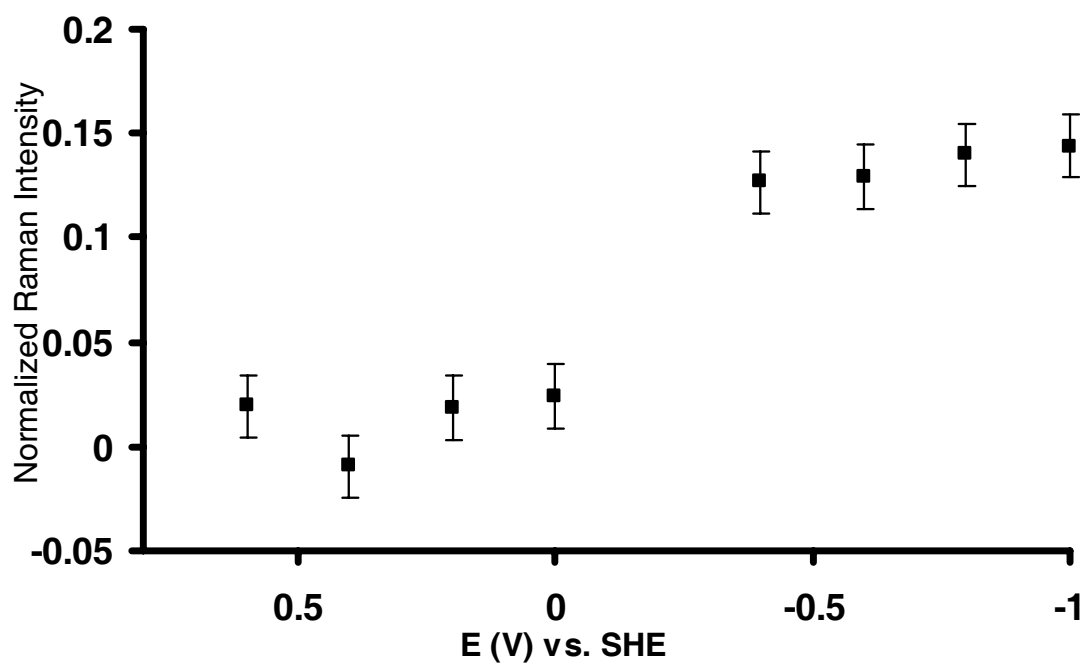
The region of interest ($300\text{-}900\text{ cm}^{-1}$) has been expanded in Figure 5.8 to demonstrate the two extremes, a fully oxidized polymer and a fully reduced polymer. Additional spectral features, though lower in intensity, are most likely attributable to other transitions within cysteine, such as the C-S stretch [64, 99].

Figure 5.8 Background corrected Raman signals for the fully oxidized (solid line) and the fully reduced (dotted line) polymer, both shown after a 50 point moving average was performed. The transition due to the disulfide bond can be seen at approximately 440 cm^{-1} . The transition due to the reduced thiols can be seen at approximately 790 cm^{-1} .



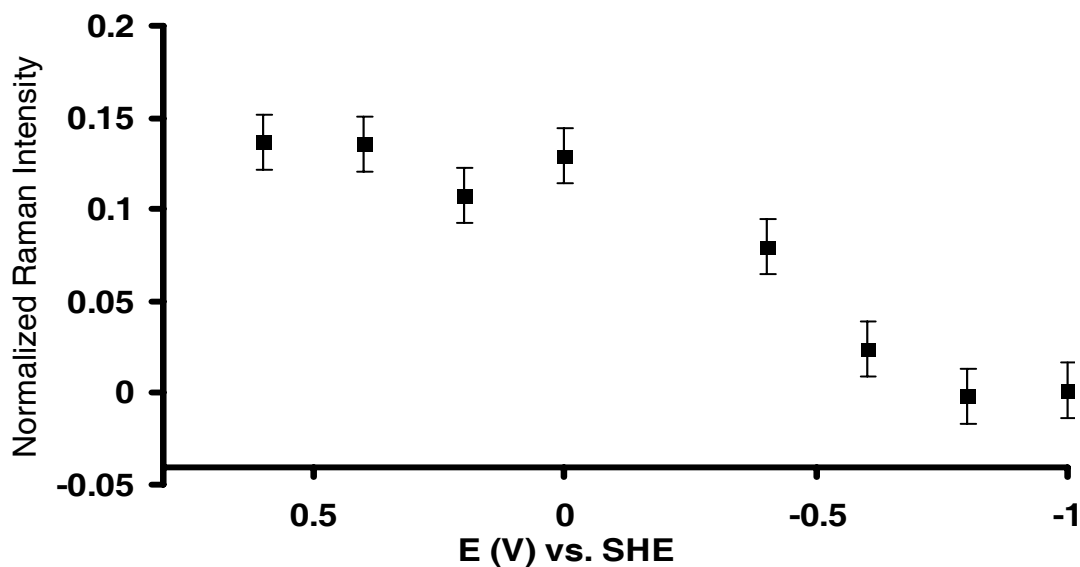
The normalized intensities at wavenumbers corresponding to the reduced thiol are shown in Figure 5.9 as a function of electrode potential. As demonstrated by Figure 5.9, the Raman intensity at these two wavenumbers reaches a maximum shortly after -0.4 V and appears to remain constant through the remaining studied potentials. The uncertainty in the data makes it difficult to say whether a maximum is reached at more negative potentials or a slight rise exists. At oxidative potentials, however, the Raman intensity falls consistently through +0.6 V indicating a loss of active thiol groups at these potentials.

Figure 5.9 Observation of Reduced Thiols. Normalized Raman intensity is shown as a function of electrode potential for the thiol transition, occurring at approximately 800 cm^{-1} (average of 3 replicates).



A similar plot was constructed for the range of wavenumbers corresponding to the disulfide stretch and is shown in Figure 5.10. At negative potentials, the Raman signal for the disulfides reached a minimum and increased steadily at more anodic potentials indicating the formation of disulfide bonds. These data confirm the expected complimentary reactions leading to the formation and reduction of disulfide bonds and the corresponding change in thiol groups.

Figure 5.10 Observation of Oxidized Disulfides. Normalized Raman intensity as a function of electrode potential for the disulfide stretch, occurring at approximately 450 cm^{-1} (average of 3 replicates).



5.3.3 Determination of an Average Formal Potential

Previous efforts to estimate the formal potential of the cystine reduction has led to a wide spread of formal potentials. Inconsistencies are generally thought to be due to the fact that cysteine strongly adsorbs to metal surfaces. Published literature values are summarized in Table 5.1.

Table 5.1 Literature values for the reduction of cystine

E°	Reference
-0.14	[85]
-0.21	[85]
-0.22	[85]
-0.222	[86]
-0.33	[85]
-0.333	[86]
-0.336	[86]
-0.34	[53]
-0.39	[85]
-0.40	[53]

In order to determine an average formal potential for immobilized PLC using spectroscopic information, Raman intensities for both disulfides and thiols were converted into respective fractional concentrations of each component with the assumptions that all sulfurs present were either present as a thiol or a disulfide and that in

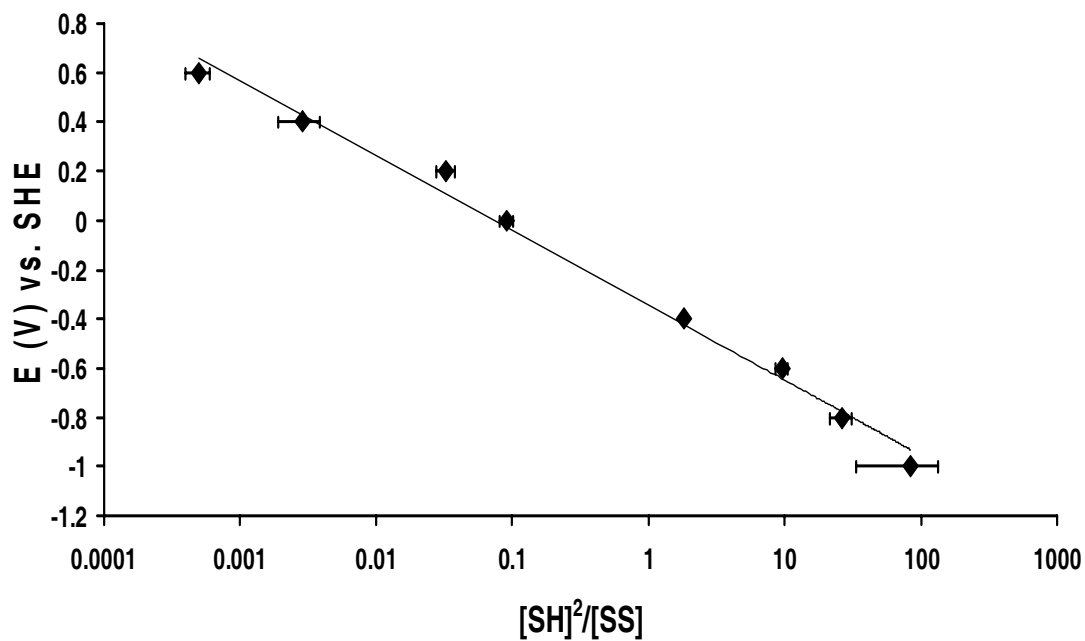
the fully reduced state the activity of the thiols was equal to 1. Assuming an activity of 1 for the fully reduced polymer ensures the validity of the following treatment, regardless of the absolute value for monolayer surface coverage of the polymer. The fractional concentrations as a function of cell potential were analyzed using the Nernst equation, shown in Equation 5.2, where α represents the fractional concentration of thiol groups. The denominator in the logarithmic term of Equation 5.2 represents the disulfide concentration, [SS], while the numerator is proportional to $[\text{SH}]^2$, i.e., the reduced form of the sulfurs.

$$E = E^o - \frac{RT}{nF} \ln \frac{\alpha^2}{\frac{1}{2}(1 - \alpha)} \quad (5.2)$$

Since it is reasonable to assume that α is proportional to [SH] and $(1-\alpha)/2$ is proportional to [SS], this equation can be used with the Raman signal intensities to approximate [SS] and [SH] to construct the plot in Figure 5.11. Full error propagation using the 90% confidence intervals from the data shown in Figures 5.9 and 5.10 was conducted to determine the error bars in Figure 5.11. The intercept suggests $E^o = -0.3 \text{ V}$ while the slope of -0.31 V implies $n = 0.05$ for the number of electrons transferred, a value which does not represent a physical reality. Because PLC is a polymeric system, it

is possible that the experimental slope is representative of a series of closely-spaced *localized formal potentials* rather than a singularly valued formal potential. This has been suggested previously for redox centers within a polymeric matrix where subtle variations in structure, solvation and environment were attributed to shifts in the local formal potential [51].

Figure 5.11 Use of the Nernst equation for the thiol-disulfide system using Raman scattering of SH (820 cm^{-1}) and SS (460 cm^{-1}) to calculate values on the abscissa.



Assuming for a given local environment i that $\alpha_i = 1$ when all the sulfurs are in the reduced form, Equation 5.2 can be rearranged to solve for the fractional amount of [SH] groups at any give potential E :

$$\alpha_i = \frac{-\frac{1}{2}\beta_i + \sqrt{\left(\frac{1}{2}\beta_i\right)^2 + 2\beta_i}}{2} \quad (5.3)$$

where

$$\beta_i = e^{\frac{-(E-E_i^o)}{RT/n_iF}} \quad (5.4)$$

and E_i^o is the local formal potential and $n_i = 2$ for reduction of the disulfide. It follows that the total number of SH and SS groups in the polymer is dependent on the potential and the fraction of the sites f_i associated with any given E_i^o . Two distributions were considered in the simulation: a uniform distribution and a Gaussian distribution. The uniform distribution possesses a flat distribution of sites between two potentials E_1^o and E_2^o .

$$f_i = k \Big|_{E_1^o}^{E_2^o} \quad (5.5)$$

where k is a constant between E_1^o and E_2^o and $k=0$ outside of this range of possible local formal potentials. The Gaussian distribution can be expressed by

$$f_i = \frac{1}{\sigma\sqrt{2\pi}} \exp\left(\frac{-(E_i^o - \overline{E^o})^2}{2\sigma^2}\right) \quad (5.6)$$

where σ is the standard deviation of the profile and $\overline{E^o}$ is the point where a maximum concentration of sites exist.

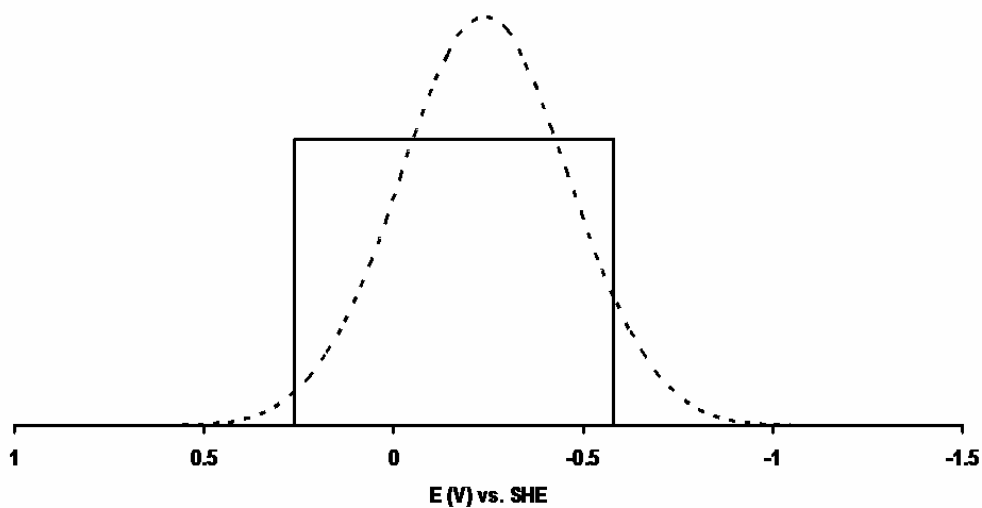
Using the two different distributions, Equation 5.3 can be solved for the various sites to allow for a simulation of the final distribution of reduced and oxidized thiols, recognizing that

$$\alpha = \sum_{i=1}^m f_i \alpha_i \quad (5.7)$$

Simulations for both types of site distributions were run, and the “shape parameters” (e.g., σ , $\overline{E^o}$, E_1^o and E_2^o) varied in an attempt to locate a distribution that provided a slope and intercept in a Nerstian plot that was equal to that found experimentally from Figure 5.9. The simulation was run for potential settings between –

1.0 and +1.0 V vs. SHE. The distributions that gave the best fit are shown in Figure 5.12 and a comparison of experimental data and that predicted in the two simulations are shown in Figure 5.13.

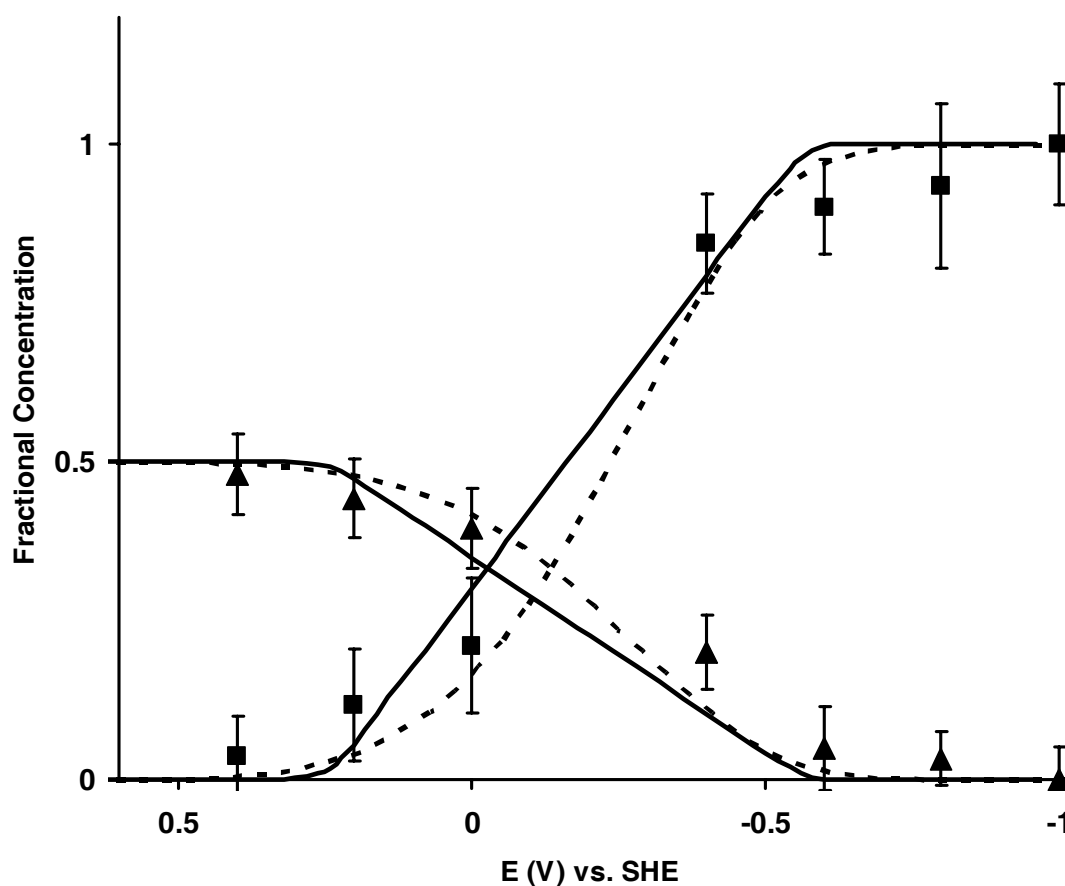
Figure 5.12 Distribution of local sites used in simulations. The solid line represents a uniform distribution of redox sites while the dashed line represents redox sites with a Gaussian distribution ($\sigma = 0.1$, $\overline{E^o} = -0.24$).



While both simulations fit the experimental data reasonably well, the uncertainty in the experimental data does not permit a definitive conclusion to be drawn regarding the “correct distribution”. However, it may be more likely that the actual distribution of formal potentials would be more similar a Gaussian distribution. Other similar

electroactive polymeric systems have been modeled with a Gaussian distribution of local formal potentials previously, although previous models have only dealt with single electron transfer systems [107-110].

Figure 5.13 Fractional concentrations of [SH] (\blacksquare) and [SS] (\blacktriangle), as determined by Raman microscopy with resulting E^0 distribution models. The uniform distribution model is shown by a solid line and the Gaussian distribution model is shown by a dashed line.



The average formal potentials of PLC immobilized on glassy carbon calculated by each of the above methods are summarized in Table 5.2. As noted, the uncertainty

associated with the spectroscopic data does not permit the precise elucidation of the site distribution function, but the results do support the presence of multiple formal potentials.

Table 5.2 Average formal potential of PLC as determined by Raman microscopy data (**I**), a linear distribution model of multiple E^0 's (**II**) and a Gaussian distribution model of multiple E^0 's (**III**).

	E^0 average
I	-0.3 ± 0.2
II	-0.16
III	-0.24

In these experiments, the physical surface coverage of PLC appeared to be relatively a constant across the surface. However, it is possible that the local surface coverage and/or nonuniform coverage across the surface could occur with a different substrate or a different preparation technique for GCE. This could impact the resulting average formal potential and the distribution for a multi-site model.

Because of the fairly uniform surface coverage in these experiments, it is assumed that both interchain as well as intrachain disulfides can be formed. As an example, it is conceivable that if the surface coverage was non-uniform, i.e., more concentrated in some areas and more diffuse in others, a shift would be seen towards intrachain interactions for the dispersed species that might yield multiple CV peaks and a difference in formal

potentials for closely packed chains and those which have greater chain-to-chain spacing on the surface.

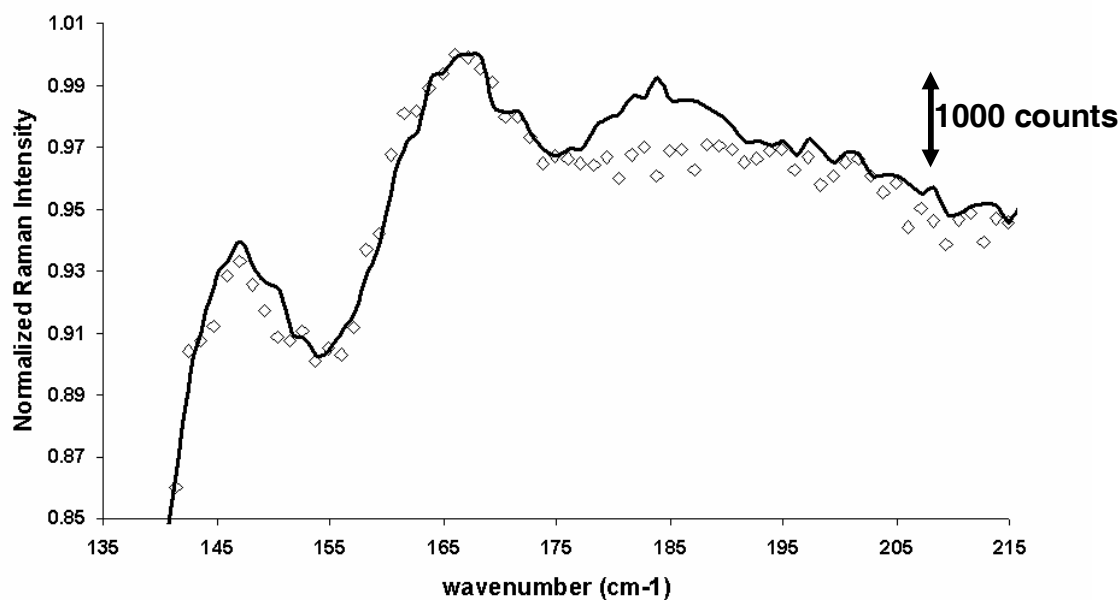
5.3.4 Verification of Cd²⁺ Binding to Thiols of PLC

It is generally accepted that the binding strength associated with cysteine-containing biomolecules and heavy metals is due to the chelation of the metal ion by the sulfurs of the thiol group. This interaction has been spectroscopically observed previously with cysteine monomers in solution [102] and chemical analogs of cysteine monomers [103] as well as in intact proteins [65]. Because these metal-ligand stretching vibrations are quite low in frequency, Raman spectroscopy becomes an ideal technique for probing that interaction. Previous work has shown that frequencies associated with the Cd-thiol stretch range from 190-300 cm⁻¹ depending on the chelating ligand [100, 102, 103], and the range of frequencies may reflect the strength of the Cd-S interaction. For example, the band location for crystalline CdS_(s) appears at wavenumbers greater than 300 cm⁻¹ [111-115].

The Raman spectra shown in Figure 5.14 were acquired at pH 7 both in the absence of Cd²⁺ and in the presence of 10 ppm Cd²⁺. In both cases, distinct peaks were seen at approximately 145 and 165 cm⁻¹. Both of these peaks can be attributed to features of cysteine [102]. In the spectrum acquired in the presence of 10 ppm Cd²⁺, an additional peak at approximately 185 cm⁻¹ appears. The appearance of Cd-S at the low end of the previously observed stretching region (i.e., 190-300 cm⁻¹) suggests a weaker ligand bond.

While PLC formation constants for Cd^{2+} can reach 10^{13} , the majority of binding sites are considerably weaker (i.e. 10^3 - 10^8) [31, 37].

Figure 5.14 Cd^{2+} binding to thiol groups of PLC. The solid line represents spectrum acquired in the presence of Cd^{2+} . Points represent a spectrum acquired in the absence of Cd^{2+} .



5.4 CONCLUSIONS

Poly-L-cysteine (PLC), a synthetic biohomopolymer which has been studied previously as a metal chelator, was immobilized onto a glassy carbon working electrode

and studied *in situ* using Raman microscopy. Previous attempts to electrochemically determine the formal potential of cystine reduction have resulted in a broad span of values. By taking advantage of the *in situ* capabilities of Raman microscopy as well as the benefits of modified electrodes, the average formal potential an otherwise challenging system was able to be determined. The analysis of the experimental data resulted in an average E° of -0.3 ± 0.2 V. The resulting data was then modeled using both a linear distribution of E° s as well as a Gaussian distribution of E° s. Using these models, the average E° was found to be -0.16 and -0.24 V, respectively. In addition, the redox behavior of cystine and cysteine was able to be verified spectroscopically. Using Raman microscopy, fractional concentrations of both thiol groups and disulfide groups were determined at various cell potentials confirming the presumed conversion of disulfides to thiol groups at negative potentials. Because metal-ligand bonds have low energy transitions, Raman microscopy proved to be an ideal tool for probing the nature of these interactions. Cd^{2+} binding to the thiol groups was confirmed by a Raman transition at approximately 185 cm^{-1} which was absent without the presence of Cd^{2+} .

Chapter 6: Exploratory Investigation of Polypyrrole Films as Conductive Anion Exchangers

6.1 INTRODUCTION

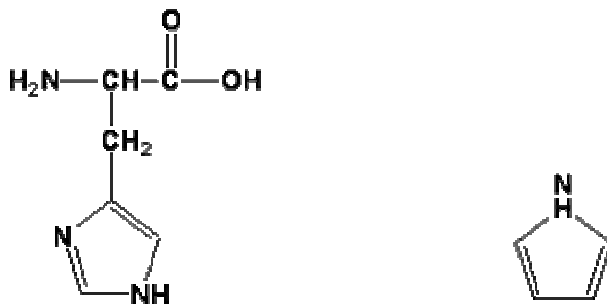
Previous efforts centered around electrochemical ligand modification have focused on polypyrrole, a well-characterized conducting polymer which can be electrochemically polymerized *in situ* in aqueous solution [41-46, 116]. In some cases, the redox state of polypyrrole was used to alter the characteristics of a chromatographic stationary phase [48, 117]. Polypyrrole is an appealing choice for several reasons including excellent, and predictable, charge-transfer properties as well as two unique charge states – one neutral and one positively charged. The positively charged state also makes polypyrrole an ideal system for use as an anion-exchange membrane [118]. Others have made use of polypyrrole as either a solid-phase microextraction system for the adsorption and desorption of target analytes [47] or as a redox reaction cell for the conversion of a toxic compound to its less toxic reduced form [49]. Some of the anions explored as target analytes have included the following: Cl^- [118], PO_4^{2-} [118], anthracene [48], caffeine [48], AMP [117], ATP [117], Cr(VI) [49], glutamate [47], perchlorate [47], dopamine [47].

In all cases, the polypyrrole is prepared for experimentation electrochemically by either potential steps or linear potential sweeps. Analyte release is achieved by chromatographic elution [48, 117], chemical elution [49, 118] or electrochemical

potentials [47]. Collectively, these previous studies have demonstrated the plausibility of constructing an ion-exchange system based on the electrochemical manipulation the component ligand. One aspect left unexplored by the body of previous work is further investigation of this polypyrrole system, or other feasible systems, as an avenue for toxic metal sequestration and remediation at the trace and ultra-trace levels, including, but not limited to, Cd^{2+} , Pb^{2+} , Hg^{2+} , Co^{2+} , Ni^{2+} , As(V) and Se(VI).

Polypyrrole (Ppy) was chosen for these studies for several reasons. Pyrrole is easily polymerized *in situ* to form the polymeric film. Also, Ppy provides an interesting organic analog to a previously studied biologically-based polymeric system, poly-L-histidine (PLH). Monomeric unit of both histidine and pyrrole are shown in Figure 6.1.

Figure 6.1 Chemical structures of histidine, left, and pyrrole, right.

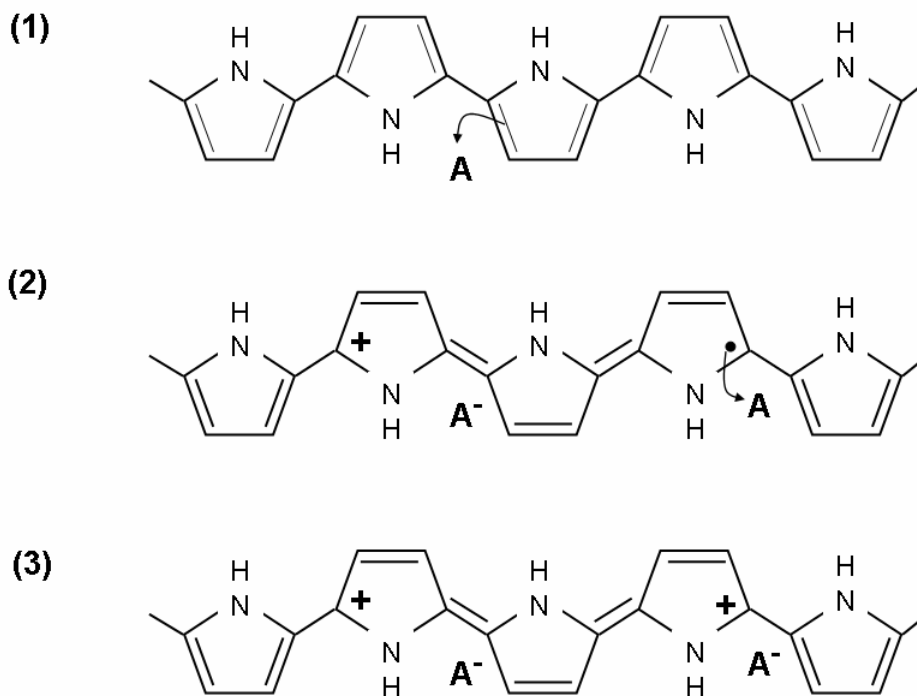


Pyrrole is structurally similar to the primary metal binding moiety of histidine, namely its imidazole ring. Because PLH has a pK_a of approximately 6, at pHs more acidic than about 5, the imidazole rings are essentially all protonated resulting in a

positively charged species. Interestingly, at pH 7 the deprotonated imidazole ring is actually able to bind cationic species such as Cu^{2+} . The protonated form of PLH demonstrated a significant capacity for Cr(VI), which is dominated by CrO_4^{2-} at 10 ppm, while exhibiting very little capacity towards Cr^{3+} providing a very powerful chromium speciation tool [38]. It was hoped that Ppy could present an electroactive analog to the success seen with PLH. Ppy, like PLH, has two distinct charge states. In the case of Ppy, however, the charge state can be controlled by electrochemical potentials. The reduced form of Ppy is electronically neutral while the oxidized form of Ppy is positively charged.

Polypyrrole, an inherently conductive polymer, has a unique charge storage mechanism which is shown in Figure 6.2. Ppy must be polymerized in the presence of a supporting anion, notated as A, which functions as reductive dopant. An electron from the backbone of the neutral Ppy chain is removed thereby resulting in a free radical and a spinless positive charge, which are together referred to as a polaron. As the oxidation process is continued, the free radical reacts with a nearby dopant molecule leaving a second spinless positive charge. The two spinless positive charges together are known as a bipolaron. The two polarons are generally thought to be spaced over four residues as shown. The localization of charge, as in the case of polarons, is often thought to be less energy efficient for the molecule than charge delocalization. In conducting polymers, however, the localization of charge leads to a significant decrease in ionization energy and appreciable increase in electron affinity which allow the molecule to store a greater number of charges than if the charge were delocalized throughout the π -system [119].

Figure 6.2 Charge storage mechanism for polypyrrole



6.2 EXPERIMENTAL

6.2.1 Instrumentation

A three-electrode potentiostat (Cypress Systems Omni-101) with a Ag/AgCl reference electrode (Cypress Systems) and a platinum wire auxiliary electrode (Cypress Systems) were used for all electrochemical experiments. Glassy carbon working electrodes (1.5 mm diameter) were commercially obtained (Cypress Systems). All electrochemical experiments were conducted under a nitrogen environment. All

electrochemical data were obtained through commercially available software (Cypress Systems Aquire-101).

An atomic absorption spectrophotometer (Varian SpectrAA 300) with a fuel rich air/acetylene flame was used for solution analysis to determine the amount of metal binding to the electrode surfaces. A hollow cathode lamp was operated at the current recommended by its manufacturer. The 357.8 nm line was used in conjunction with a monochromator bandpass of 0.5 nm for all Cr determinations.

All scanning electron microscope images were obtained using a LEO 1530 Scanning Electron Microscope.

6.2.2 Reagents

All reagents used were reagent grade unless noted. Deionized distilled water was used to prepare solutions, and all glassware was soaked overnight in 4 M HNO₃ prior to use. Pyrrole (Acros Organics) was used as received. Four different charge compensating counter ions were used during film growth: lithium perchlorate (Acros Organics), tetrabutylammonium fluoride (Acros Organics), tetrabutylammonium tetrafluoroborate (Acros Organics) and p-toluenesulfonic acid (Acros Organics). Stock solutions prepared in house of 1000 ppm Cr³⁺ from chromic acid and 1000 ppm Cr(VI) from K₂CrO₄ atomic absorption standards were used to prepare the 10 ppm solutions for the metal binding experiments. Any pH adjustments were made with either potassium hydroxide (Sigma) or hydrochloric acid (Fisher). In all cases, the supporting electrolyte for electrochemical experiments following film growth was potassium chloride (Sigma).

6.2.3 Formation of Ppy Films on Glassy Carbon Electrodes

Four glassy carbon electrodes were prepared each with an electrochemically polymerized ppy film grown with a different charge compensating counterion in aqueous conditions. The procedures used were developed from previously reported reaction conditions [42, 44, 46, 116, 120, 121]. In each case, the electrode was prepared by performing a +1.8 V vs. Ag/AgCl potential step in 0.1 M H₂SO₄ for 2 min. For all films following initial oxidation, the electrode was immersed in an aqueous solution of 0.1 M pyrrole monomer and 0.2 M supporting electrolyte and held at +0.8 V vs. Ag/AgCl for 3min. After film growth, the electrodes were stored under N_{2(g)} to limit exposure to O_{2(g)}. For ease of discussion, the electrodes will be referred to by number. Electrode 1 contains a film grown using tetrabutylammonium fluoride. Electrode 2 contains a film grown using lithium perchlorate. Electrode 3 contains a film grown using tetrabutylammonium tetrafluoroborate. Electrode 4 contains a film grown using p-toluenesulfonic acid.

6.2.4 Scanning Electron Microscopy of Ppy Films

The images were obtained by affixing the electrodes to the sample mounting platform. A ground connection was made by connecting a copper wire to each electrode pin and the sample platform. Individual instrumental parameters are listed with each image.

6.2.5 Evaluation of Cr³⁺ and Cr(VI) Binding

In order to evaluate the metal binding capabilities of the polymer films, the electrodes were subjected to a series of electrochemical environments. For each of

the ppy modified electrodes, the films were first prepared for binding by an oxidation (positive potential step from 0 to +600 mV) in 0.2 M KCl. After initial preparation for binding, the electrode was placed in 50 mL of either a 10 ppm Cr^{3+} solution or a 10 ppm Cr(VI) solution each adjusted to pH 7 with stirring for 1 min. The electrode was briefly rinsed with DI water to remove any weakly sorbed metal. The bound metal was subsequently released by a reduction (negative potential step from 0 to -600 mV) into 0.5 mL of 0.2 M KCl adjusted to pH 7.

The released metal was quantified by discrete nebulization flame atomic absorption spectroscopy. The 0.5 mL aliquots were nebulized and their resulting peaks integrated. Calibration was achieved by integrating peaks of 0.5 mL of matrix-matched calibration standards. All metal binding experiments were repeated for a total of 5 times.

6.3 RESULTS AND DISCUSSION

6.3.1 Scanning Electron Microscopy of Ppy Films

Scanning electron microscopy (SEM) is a commonly used technique for the characterization of ppy films [121, 122]. The SEM images can provide information about film morphology as well as film thickness, as both features are highly dependent on growth conditions. SEM images for this study were obtained for two primary reasons: confirmation of film growth and measurement of film thickness. Two images for each electrode are shown below. The parallel views for each set of images were obtained using similar instrument parameters making the scale bars fairly consistent for analogous

views. The specific instrument parameters as well as the scale bars are detailed on each image.

Figure 6.3 Electrode 1, grown with F^- as the counterion. Top image shows entire electrode. Bottom image is a close-up view of the film itself.

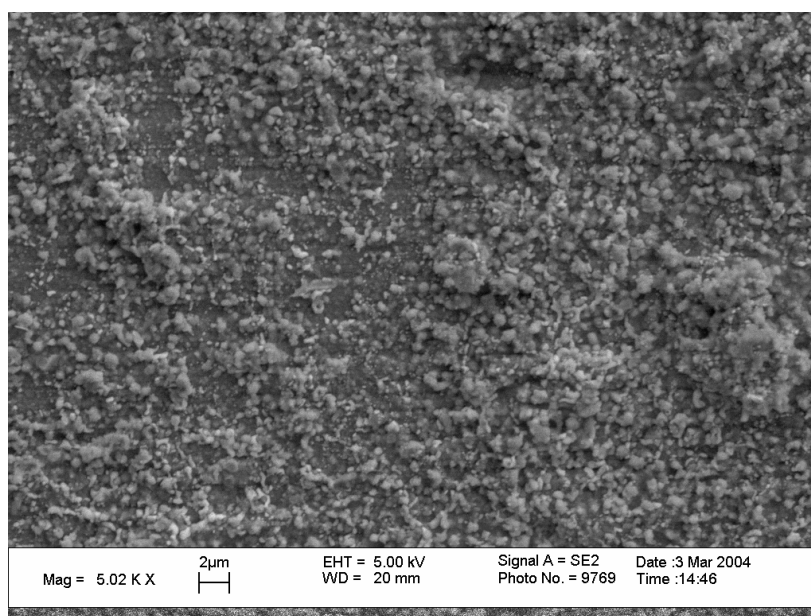
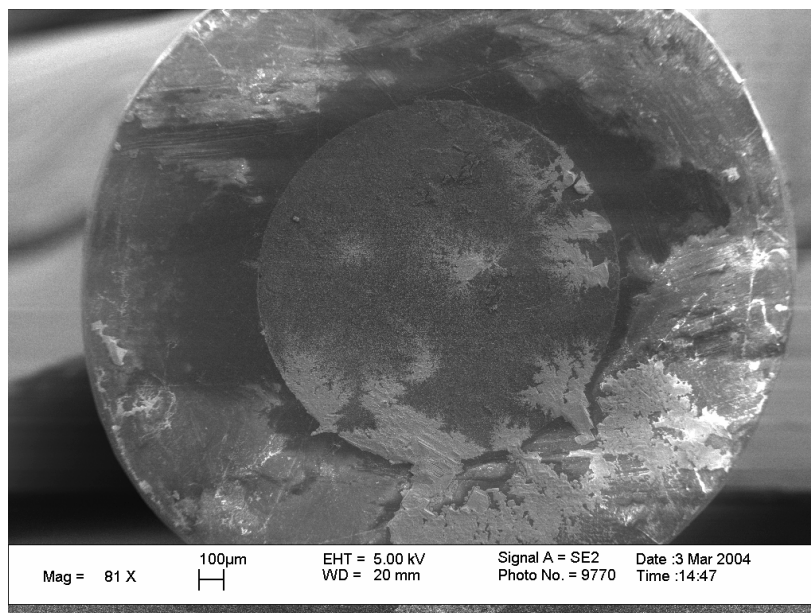


Figure 6.4 Electrode 2, grown with ClO_4^- as the counterion. Top image shows entire electrode surface seen from the side. Bottom image is a close-up view of the film itself.

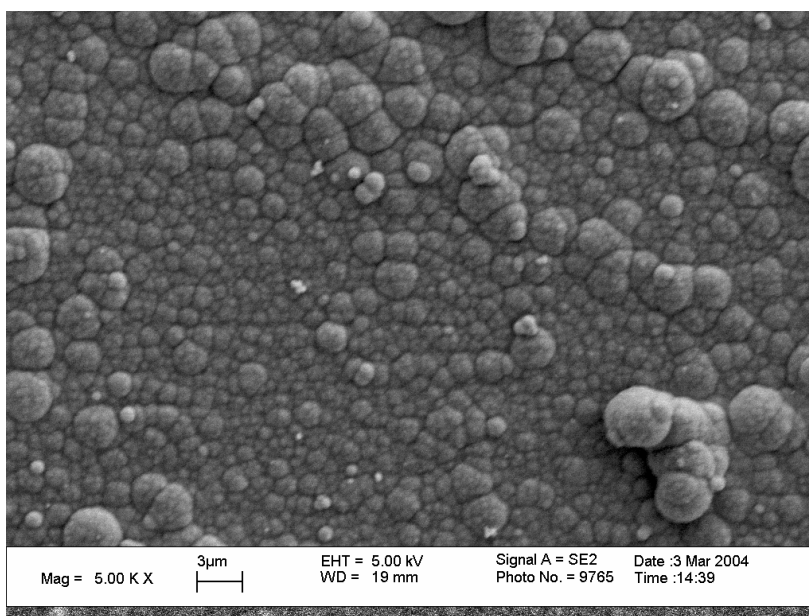
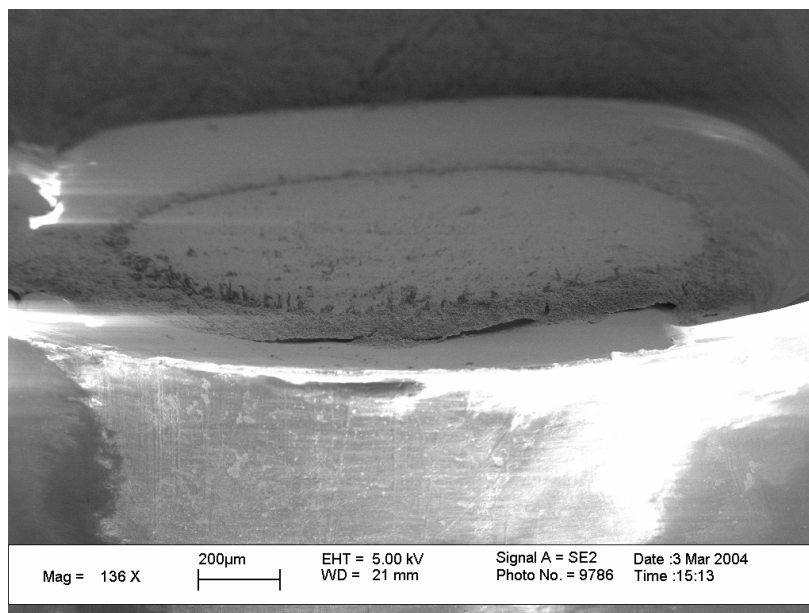


Figure 6.5 Electrode 3, grown with BF_4^- as the counterion. Top image shows an end view of the entire electrode surface. Bottom image is a close-up view of the film itself.

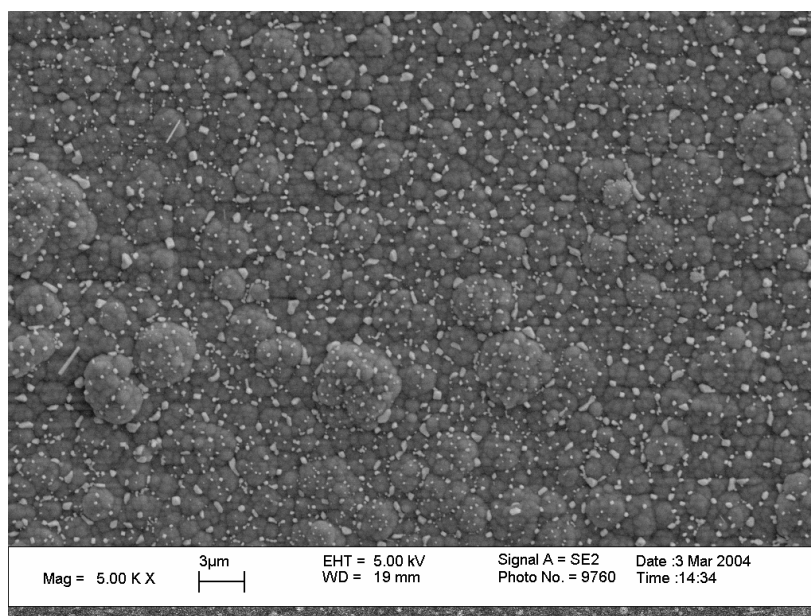
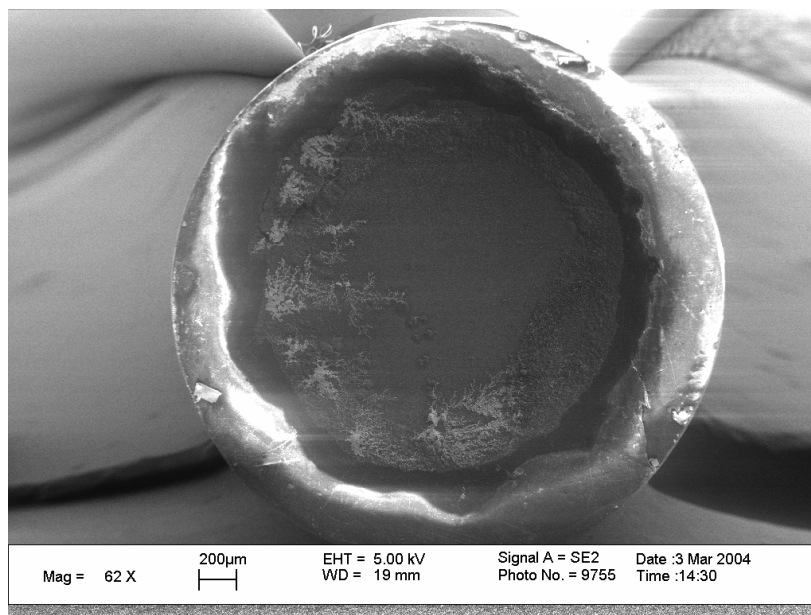
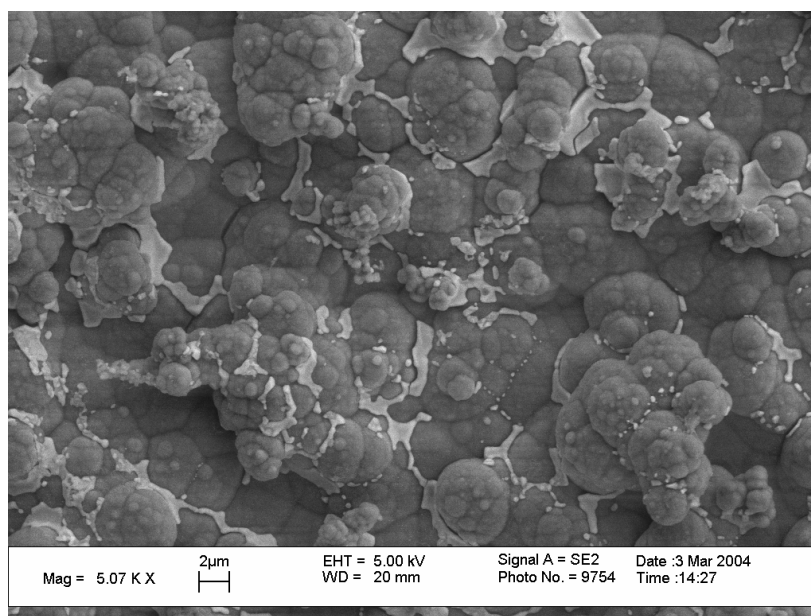
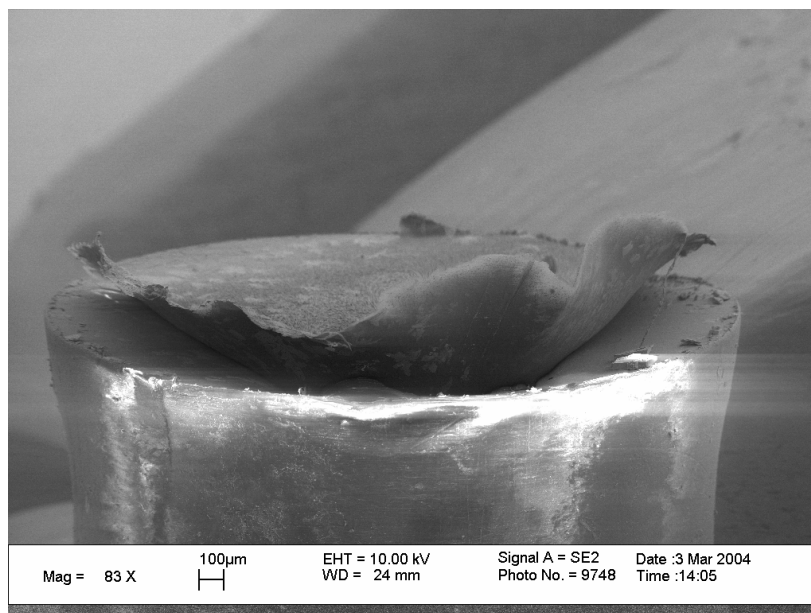
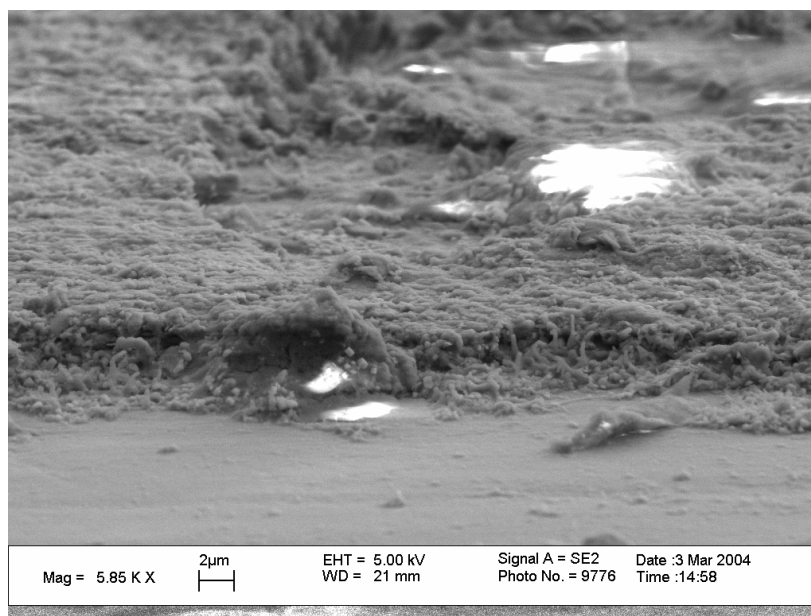


Figure 6.6 Electrode 4, grown with p-toluenesulfonate as the counterion. Top image shows the entire electrode surface seen from the side. Bottom image is a close-up view of the film itself.



The film morphologies for the four electrodes are quite different, specifically the size of the dominant features. In addition, as can be seen from the preceding images, the films grown on electrodes 2, 3 and 4 actually grew beyond area of the 1.5 mm glassy carbon disk for the same growth time. Because the PEEK portion of the electrode surface was to be used as a baseline for height measurements, height information could not be obtained for electrodes 2, 3 and 4 where the film was obscuring the PEEK surface. Additionally, the films on electrodes 2, 3 and 4 were not of uniform height adding more difficulty in determining film thicknesses. The thickness of the film on electrode 1 was estimated to be $\sim 4\text{ }\mu\text{m}$ by obtaining a side view of the film (Figure 6.7). Although actual film thicknesses could not be accurately estimated using the SEM images for electrodes 2, 3 and 4, it was evident that those three films were considerably thicker than the film grown with ClO_4^- .

Figure 6.7 Side view of the thickness of the film grown on electrode 1.

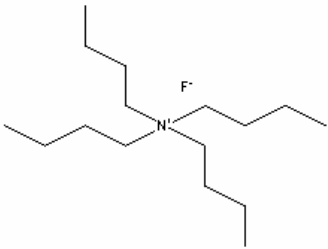
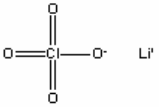
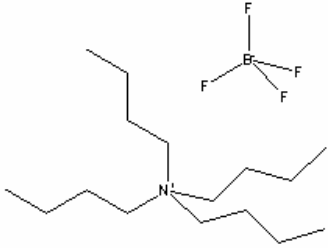
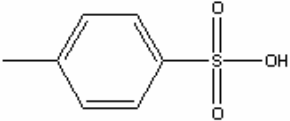


6.3.2 Evaluation of Cr³⁺ and Cr(VI) Binding

Binding experiments were carried out on all four ppy films for both the +3 oxidation state of Cr and the +6 oxidation state of Cr, which is present primarily as CrO₄²⁻ in neutral conditions for a total Cr concentration of 10 ppm. All four films exhibited similar behavior in Cr binding which are presented in Table 6.1. No film bound a detectable amount of Cr³⁺. The limit of detection for Cr in these experiments was found to be ~15 ppb using discrete nebulization atomic absorption spectroscopy with a sample volume of 0.5 mL. All four of the films did bind an appreciable amount of Cr(VI) ranging from 26 to 44 ng. Because the range of data for Cr(VI) is not too broad, all four salts used for film growth seem to be valid choices. Although, more information regarding the density of the bound metals (i.e. ng/cm³) could be ascertained with more precise film thickness results. It is possible that analyzing the binding data in these terms may expose some more pronounced differences in the capacity of these four films to bind Cr(VI).

Like poly-L-histidine (PLH) [38], ppy films do have the capability to speciate two form of Cr based on the oxidation state. As opposed to PLH, ppy has the added benefit of facilitating metal binding and release without the addition of chemicals. Although this study only explored a single oxidation and reduction voltage, ligand preparation and metal release were achieved solely through electrochemical means.

Table 6.1 Binding capacities for Cr^{3+} and Cr(VI) on the 4 ppy electrodes

Electrode	Salt used during film growth	Cr^{3+} capacity (ng) (n=5)	Cr(VI) capacity (ng) (n=5)
1		ND	27 ± 4
2		ND	26 ± 3
3		ND	44 ± 5
4		ND	35 ± 4

Previous efforts to use ppy, or other similar polymers like polyaniline, as an anion exchanger have focused on their use as a chromatographic support [47, 118, 123] not exploring its potential to for retention of materials as opposed to elution. Rodriguez et al. [49] did present the possibility that ppy films could retain Cr. However, their study used ppy in the reduced form and Cr(VI). They determined that Cr(VI) could oxidize the ppy film while reducing the Cr(VI) to the less toxic Cr^{3+} which was then incorporated into the film. Their study did not, however, address the reclamation of Cr^{3+} from the film.

The ppy films created in this study on the electrode surfaces of glassy carbon have the potential to compensate for the shortcomings of work presented by Rodriguez et al. While Rodriguez was able to remediate Cr(VI) from the source, the reclamation and disposal of the generated Cr^{3+} waste was not addressed. The currently studied system presented here is able to retain and release Cr(VI) on demand providing both a means of toxic metal reclamation and the option of preconcentration.

6.4 CONCLUSIONS

Like the previously studied biohomopolymer, PLC, ppy presents an intriguing option for use as an electrochemically switchable ion exchanger. The existence of two distinct charge states provides predictable complexation behavior. As an added benefit, ppy can be easily polymerized electrochemically *in situ*. In order to completely evaluate the effectiveness of ppy for ESIE capabilities, further studies should be conducted. The determination of the most effective voltages for both the reduction and the oxidation of the ppy films as well as a study to evaluate the effective useable lifetime of the films. It is hoped that the success demonstrated with Cr(VI) could be extended to other similar

oxyanions such as AsO_4^- and SeO_4^- . Although the four salts used for film growth in this study produced functioning films that were able to bind Cr(VI), a number of other salts could also be considered that have been used previously for the formation of ppy films for other purposes.

Chapter 7: Conclusions and Future Work

7.1 OVERVIEW

At this point, the development of a chemical-free remediation system using potential and current to operate an ion exchange systems seems plausible. Glassy carbon has proven to be a cost-effective, rugged substrate for ligand immobilization. Two electroresponsive ligands were studied for use in a prototype electronically switchable ion exchange (ESIE) system. The first, poly-L-cysteine, was investigated as a chelator of cationic heavy metals. Previous work with immobilized PLC had established it as a soft acid metal binder capable of preconcentrating trace metals from complex matrices, yet still able to achieve on-demand metal release. Prior work had also demonstrated the importance of the redox state of PLC on metal binding capacity. Maximum metal capacity was achieved when PLC was fully reduced. Oxidized PLC exhibited very little capacity toward any metal studied. Earlier work used chemicals, such as dithiothreitol and ortho-iodobenzoate, to reduce and oxidize the thiol groups of PLC. However, earlier work had never demonstrated that an oxidizing solution was capable of quantitatively removing a bound metal. The ability to reduce and oxidize PLC electrochemically would eliminate the need for additional chemicals for trace metal remediation. As an ESIE chelator, the drastically different metal binding character of each redox state can be used to govern the metal-ligand interactions. Unique to other electrochemically-based remediation techniques, the applied potential required is not dependent on the metal cation. It is dependent only on the ligand, PLC.

These studies have demonstrated the reproducible use of PLC as a heavy metal chelator using only electrochemical potentials for ligand modification. By immobilizing PLC to an electrically conductive surface, in this case, glassy carbon, a microscale remediation system was created. The system exhibited strong binding for each of the metals studied as well as effective binding within a competitive environment. Because the metal binding can be effectively “shut down” on-demand using oxidative potentials, it can be assumed that the disulfide bonds are indeed forming.

Electrochemical and spectroscopic studies were undertaken to further characterize the immobilized PLC system. Immobilized PLC, as expected, exhibited many characteristics inherent to electrodes modified with a polymeric molecule. Although some differences due to the differences in the nature of this system and those previously studied were present. Many previously studied systems are self assembled monolayers (SAMs) comprised of closely packed hydrophobic chains. In this case, each polymer is most likely well-solvated due to their surface coverage thereby resulting in slightly different electrochemical and pH-dependant characteristics. Approximate surface coverages for both immobilized PLC and immobilized Cys were determined by integrating the Faradaic current arising from cyclic voltammograms further confirming the oxidation and reduction of the sulfur species. These values were consistent with immobilized molecules for each of the respective molecular sizes. The peak current for cyclic voltammetry experiments scaled linearly with scan rate. Rate constants for electron transfer were determined via chronoamperometry to be consistent with those of immobilized polymers. The sluggish electron transfer exhibited by immobilized PLC was speculated to originate from a combination of counter ion migration, polymer

movement and electron hopping. The pK_a of immobilized PLC shifted approximately one pH unit from that of immobilized Cys monomer.

Using Raman microscopy, spectra were acquired at various electrode potentials to determine approximate ratios of thiols-to-disulfides. These ratios were ultimately converted into a Nernst plot to extract an average formal potential for the immobilized PLC system. In addition, Raman spectroscopy provided an ideal tool for probing the nature of the metal-ligand bond for this particular system, which was shown to be a Cd-S bond; albeit an apparently weak interaction.

Metal binding experiments exhibited consistency with previously used immobilized PLC systems that relied on chemical ligand preparation and metal release. Metals were able to bind and subsequently be released without the addition of previously required chemicals, such as reducing agents or acids. The reproducibility of these metal binding experiments allow for the system to be considered for scale-up to a column-type system.

One additional system that was explored was electrochemically synthesized polypyrrole. Polypyrrole is easily polymerized *in situ* under oxidizing conditions in the presence of a supporting electrolyte. The positively-charged pyrrole moieties provided electrochemically active anion binding capabilities suggesting its potential as a speciation tool for systems containing species such as chromates.

7.2 CONCERNS FOR SCALE-UP

In order for the system to be scaled-up to a larger flow-through style remediation system, an appropriate substrate must be selected. Although carbon is an obvious choice, many types of carbon, both porous and nonporous exist and must be considered. Several porous carbon substrates are currently being evaluated. A rayon-based activated carbon fabric has been studied in our laboratory, and the proposed work will characterize other forms of activated carbon and porous glassy carbon media onto which the biopolymer is immobilized. The primary criteria used to evaluate the support materials are surface coverage of the metal chelator, capacitive surface area and structure of the support itself. A few selected carbon supports should be tested in a lab-scale column setup. Column and electrode geometry will play a large role in the power requirements, so comparisons of different column configurations will be run. Also, overall process control schemes for the operation and regeneration of a column will be studied. Capacitive power usage from electrochemical modification of the column can be recovered with appropriately designed charge and discharge schemes between several columns.

The effect of several process variables such as pH and background electrolyte concentration on the column setup need to be evaluated. Background electrolyte concentration has an inverse relation with the electrochemical resistance of the column, and can greatly affect the power usage and heating of the column. An evaluation of the sensitivity of the chelating ability of the column as a function of pH will be necessary to find the range of influent streams in which the column can effectively function. Fouling of the column by irreversible binding and chemical degradation of the biopolymers are two important characteristics which affect the service life of the column, although some of

these concerns have been addressed previously in our lab for poly-L-aspartate [124]. Those processes will need to be addressed for poly-L-cystiene as well. Remediation of several synthetic and non-synthetic waters will then have to be tested in column-based studies. Synthetic mixed wastes with several metals of interest are likely the next step in order to assess competitive metal binding under real world conditions. In addition, industrial wastewaters and natural waters will need to be evaluated on the lab-scale column.

7.3 FEASIBILITY OF OTHER POSSIBLE SYSTEMS

Through previous work, novel biologically-based metal chelators have been developed [30-32, 34, 36, 38]. While immobilized PLC has proven to be a viable system, it is hoped that the ESIE concept can be generalized to incorporate the use of other previously studied short chain biopolymers such as poly-L-aspartate [34, 67, 124, 125], poly-L-glutamate and poly-L-histidine [38] which release metals by a pH induced tertiary structure change. Viability of such an assertion rests partly on previous studies showing that protonation and deprotonation of surface-bound acid species can be driven voltammetrically [56]. In addition, early work with electronic ion exchange induced the reduction of water thereby increasing the pH of the environment within the exchange resin [8-11]. A proposed research direction would expand on this body of work and exploit this local pH change to release metals from biopolymer system without the need for additional chemicals as is currently required for elution-based reclamation.

To optimize the efficient use of any ion exchange column, it is essential to ensure complete loading before reclamation is initiated. This necessitates the need to determine

when the column is at capacity or to detect the first onset of breakthrough. It would be enabling in the final embodiment of a chemical-free remediation/reclamation system to sense breakthrough with the expense and operator-based use of atomic spectrochemical analysis of the effluent stream. To this end, the incorporation of an immobilized colormetric indicator detector system which could complex a variety of heavy metals would be a logical approach for breakthrough determination [126-130]. One such dye which has been used as a general cationic detector is alizarine complexone [126-146].

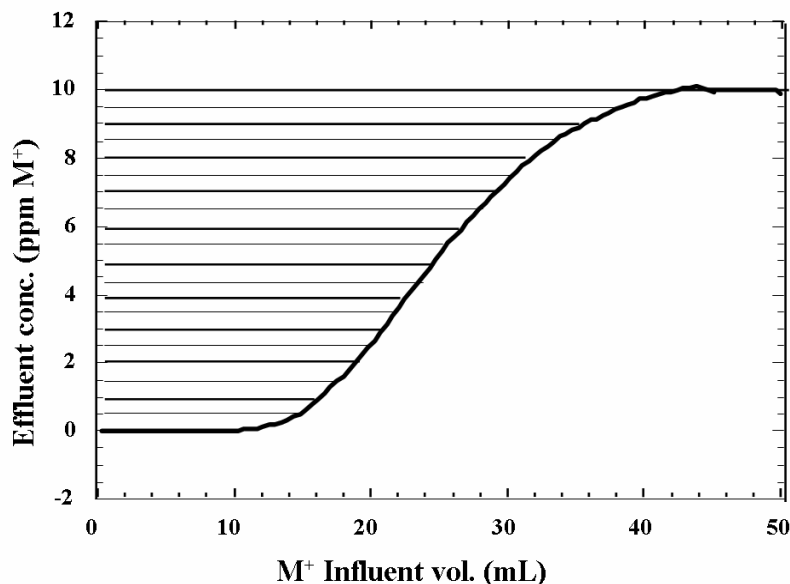
Because alizarine complexone absorbs in the visible region of the electromagnetic spectrum, a simple photodiode system could be employed for detection of metal binding to the alizarine complexone. A small column containing immobilized alizarine complexone, or other similar chromophoric chelator, could be placed on the effluent side of the binding column to detect the beginnings of breakthrough. Calibration can then be done to correlate the transmitted intensity through the immobilized of the alizarine complexone-metal complex and the effluent metal concentration.

Appendix

DATA ANALYSIS MACRO FOR BREAKTHROUGH ANALYSIS

All column-based metal binding analysis is conducted through the use of breakthrough curves and their subsequent strip quantification. Breakthrough curves, shown in Figure A.1, are simply a graphical representation of effluent analyte concentration as a function of either time or volume. The breakthrough curve represents the change in the amount of metal in the column effluent as an influent concentration of 10ppm of metal is introduced onto the column. The change in absorbance of the metal versus time is measured directly as it flows through the column. Corresponding information can also be obtained using bulk methods in the absence of a flow injection analysis system by changing the solution concentration. Breakthrough curves can also provide insights into the nature of the metal binding interaction when used in conjunction with flow injection analysis. The baseline of the curve represents the hard (or strong) sites of the chelator. The sloped region of the curve represents binding to the soft or weaker sites. The overall capacity of the column for the target metal is represented by the area above the curve. The curve can be easily converted to the more familiar Langmuir isotherm.

Figure A.1 An example of a typical breakthrough curve collected by flow injection analysis-flame atomic absorption spectroscopy.



Visual Basic was used to create a macro for automated analysis of column breakthrough data within Microsoft Excel. The file template conFigured for triplicate analysis consists of 8 worksheets – labeled Report, Calibration 1-3, Breakthrough 1-3 and Strip – and the macro code. The report page, an excerpt is shown in Figure A.2, allows the user to enter constants needed for the macro to run as well cells programmed to calculate results based on the output of the macro. Cells labeled A and C are primarily for user identification and are not required for the macro to operate. Cells labeled B and D-H are required for the calculations within the macro. Column weight in grams is placed in the cell labeled B; the molecular weight (g/mol) of the metal used is placed in the cell labeled D; the solution flow rate (mL/min) is placed in the cell labeled E; the time required for an unretained sample to be detected, known as the dead volume time (s), is placed in the cell

labeled F; the volume of the strip solution (L) is placed in the cell labeled G; the data collection rate, in s/point, is placed in the cell labeled H. Cells labeled I-K are calculated based on the macro output on the corresponding breakthrough worksheet. Cells labeled L-N are calculated based on user input from strip data.

Figure A.2 User input fields for report page of data analysis macro

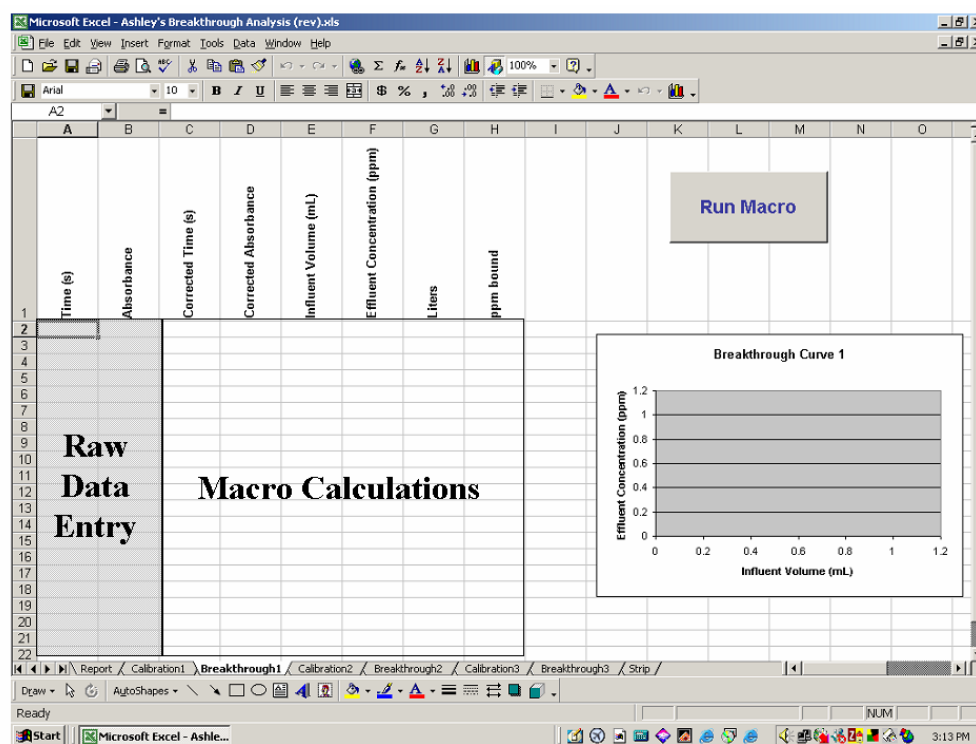
B

	Column	A			
10	Column Weight (g)	B			
	Metal	C			
	Molecular Weight (g/mol)	D			
	Flow Rate (mL/min)	E			
	Dead Volume Time (s)	F			
15	Strip Volume (L)	G			
	Collection Rate (s/pt)	H			
	Breakthrough Capacity	I ₁			
	($\mu\text{mol metal/g column}$)	I ₂			
20		I ₃			
	Average capacity	J	+	K	
	($\mu\text{mol metal/g column}$)		-		
25					
	Strip Analysis	L ₁			
	($\mu\text{mol metal/g column}$)	L ₂			
		L ₃			
30	Average Strip Analysis	M	+	N	
	($\mu\text{mol metal/g column}$)		-		

For breakthrough analysis, raw data, in the form of a two-dimensional array consisting of the time point and its resultant absorbance reading, is entered on one of the three breakthrough worksheets. The macro simultaneously corrects for the dead volume time and baseline drift, converts time into volume based on the flow rate, calculates an

effluent concentration for each absorbance using a calibration curve from the corresponding calibration worksheet and plots the data as effluent concentration (ppm) versus influent volume (mL). This process is repeated two additional times for triplicate analysis. A screen shot of this worksheet is shown in Figure A.3.

Figure A.3 Screen shot of the breakthrough worksheet within the macro. Raw data collected by FIA-FAAS or FIA-ICPMS is entered in the first two columns. The remaining calculations are completed by the macro.



Visual Basic Code is as follows:

```
Sub BreakthroughAnalysis()  
,  
' BreakthroughAnalysis Macro  
' Macro recorded 07/06/2000 by Ashley M. Johnson  
,  
' Keyboard Shortcut: Ctrl+b  
  
Range("A2").Select  
Selection.End(xlDown).Select  
s = Selection.Value  
  
Range("Z6").Select  
r = Selection.Value  
  
n = s / r  
  
Range("c2").Select  
ActiveCell.FormulaR1C1 = "=RC[-2]-R3C26"  
Range("D2").Select  
ActiveCell.FormulaR1C1 = "=(RC[-2]-(AVERAGE(R2C2:R12C2)))"  
Range("e2").Select  
ActiveCell.FormulaR1C1 = "=RC[-2]/60*R2C26"  
Range("F2").Select  
ActiveCell.FormulaR1C1 = "=(RC[-2]-R4C26)/R5C26"  
Range("G2").Select  
ActiveCell.FormulaR1C1 = "=RC[-2]/1000"  
Range("c2:g2").Select  
Selection.Copy  
Range("c3", Range("g3").Offset(rowoffset:=(n - 1))).Select  
ActiveSheet.Paste  
Range("H2").Select  
ActiveCell.FormulaR1C1 = "=((MAX(R2C6:R2000C6)-RC[-2]))"  
Selection.Copy  
Range("h2", Range("h2").Offset(rowoffset:=n)).Select  
ActiveSheet.Paste  
  
End  
Sub
```

References

1. Environmental Protection Agency, *National Primary Drinking Water Standards*. 2004.
2. Lehninger, A.L., D.L. Nelson, and M.M. Cox, *Principles of Biochemistry*. 2nd ed. 1993, New York, NY: Worth Publishers.
3. Shriver, D.F., P.W. Atkins, and C.H. Langford, *Inorganic Chemistry, Pt. 1. 2nd Ed.* 1996. 740 pp.
4. Stillman, M.J., et al., *Metallothioneins: Synthesis, Structure and Properties of Metallothioneins, Phytochelatins and Metal-Thiolate Complexes*. 1992. 443 pp.
5. Manahan, S.E., *Environmental Chemistry. 5th Ed.* 1991. 525 pp.
6. Lawler, D., *Physical/Chemical Treatment Processes for Water and Wastewater*. Vol. 2. 2002: McGraw-Hill.
7. Bard, A.J. and L.R. Faulkner, *Electrochemical Methods: fundamentals and applications*. Vol. 7. 2001. 255.
8. Bridger, N.J., C.P. Jones, and M.D. Neville, *Electrochemical Ion Exchange*. Journal of Chem. Tech. Biotechnol., 1991. **50**: p. 469-481.
9. O'Keefe, T.J. and V.A. Ettel, *The Electrolytic Recovery of Metals from Aqueous Solution*. Proceedings - Electrochemical Society, 1987. **87**(17): p. 103-117.
10. Rajeshwar, K. and J.G. Ibanez, *Environmental Electrochemistry: Fundamentals and Applications in Pollution Abatement*. 1997, San Diego: Academic Press.
11. Rudd, E.J., *Electrochemistry and the Environment -- An Overview*. Proceedings - Electrochemical Society, 1995. **95**(12): p. 23-35.
12. Ghosh, M. and S.P. Singh, *Effect of cadmium and lead on growth of Ipomea cranea - a phytoremediation study*. Pollution Research, 2003. **22**(4): p. 561-568.
13. Zhang, J., Z. Han, and Y. Wang, *Biological treatment technology for heavy metal wastewater*. Huanjing Wuran Zhili Jishu Yu Shebei, 2003. **4**(4): p. 75-78.
14. Heberling, J.A., *Phytoremediation: Transformation and control of contaminants edited by Steven C. McCutcheon and Jerald L. Schnoor*. Environmental Progress, 2003. **22**(4): p. D4.

15. Khondaker, M. and R.A. Caldwell, *Mercury uptake, translocation and volatilisation by Australian saltbush: prospects for phytoremediation*. Australasian Journal of Ecotoxicology, 2003. **9**(2): p. 129-135.
16. Liu, X.-b. and B.-s. Xing, *Phytoextraction: a cost-effective approach to metal-contaminated soils*. Journal of Northeast Agricultural University (English Edition), 2003. **10**(2): p. 182-187.
17. Liu, X.-m., Q.-t. Wu, and P.-t. Li, *Phytoremediation of heavy metal contaminated soil by hyper - accumulators: a review of researches in China and abroad*. Nongye Huanjing Kexue Xuebao, 2003. **22**(5): p. 636-640.
18. Kamnev, A.A., *Phytoremediation of heavy metals: an overview*. Recent Advances in Marine Biotechnology, 2003. **8**(Bioremediation): p. 269-317.
19. Mahan, C.A. and J.A. Holcombe, *Preconcentration of trace metals using silica-immobilized algae cells in a chromatographic separation procedure*. Spectrochimica Acta, Part B: Atomic Spectroscopy, 1992. **47B**(13): p. 1483-95.
20. Mahan, C.A. and J.A. Holcombe, *Immobilization of algae cells on silica gel and their characterization for trace metal preconcentration*. Analytical Chemistry, 1992. **64**(17): p. 1933-9.
21. Mahan, C.A., V. Majidi, and J.A. Holcombe, *Evaluation of the metal uptake of several algae strains in a multicomponent matrix utilizing inductively coupled plasma emission spectrometry*. Analytical Chemistry, 1989. **61**(6): p. 624-7.
22. Yu, X., L.-y. Chai, and X.-b. Min, *Removal of lead in wastewater by immobilized inactivated cells of Rhizopus oligosporus*. Journal of Central South University of Technology (English Edition), 2003. **10**(4): p. 313-317.
23. Rangsayatorn, N., et al., *Cadmium biosorption by cells of Spirulina platensis TISTR 8217 immobilized in alginate and silica gel*. Environment International, 2004. **30**(1): p. 57-63.
24. Pagnanelli, F., et al., *Mechanistic modeling of heavy metal biosorption in batch and membrane reactor systems*. Hydrometallurgy, 2003. **71**(1-2): p. 201-208.
25. Galli, E., et al., *Copper biosorption by Auricularia polytricha*. Letters in Applied Microbiology, 2003. **37**(2): p. 133-137.
26. Mallick, N., *Biotechnological potential of Chlorella vulgaris for accumulation of Cu and Ni from single and binary metal solutions*. World Journal of Microbiology & Biotechnology, 2003. **19**(7): p. 695-701.

27. Berger, A., J. Noguchi, and E. Katchalski, *Poly-L-Cysteine*. Journal of the American Chemical Society, 1956. **78**: p. 4483-4488.
28. Autry, H. and J.A. Holcombe, *Cadmium, copper and zinc complexes of poly-L-cysteine*. Analyst (Cambridge, United Kingdom), 1995. **120**(10): p. 2643-7.
29. Jurbergs, H.A., *Characterization of free and silica-immobilized poly-L-cysteine for trace metal chelation and preconcentration*, in Univ. of Texas, Austin, TX, USA. FIELD URL: 1997. p. 165 pp.
30. Howard, M., H.A. Jurbergs, and J.A. Holcombe, *Effects of Oxidation of Immobilized Poly(L-Cysteine) on Trace Metal Chelation and Preconcentration*. Analytical Chemistry, 1998. **70**(8): p. 1604-1609.
31. Howard, M., H.A. Jurbergs, and J.A. Holcombe, *Comparison of silica-immobilized poly(L-cysteine) and 8-hydroxyquinoline for trace metal extraction and recovery*. Journal of Analytical Atomic Spectrometry, 1999. **14**(8): p. 1209-1214.
32. Howard, M.E. and J.A. Holcombe, *Model for Nonequilibrium Binding and Affinity Chromatography: Characterization of 8-Hydroxyquinoline Immobilized on Controlled Pore Glass Using a Flow Injection System with a Packed Microcolumn*. Analytical Chemistry, 2000. **72**(16): p. 3927-3933.
33. Jurbergs, H.A. and J.A. Holcombe, *Characterization of Immobilized Poly(L-cysteine) for Cadmium Chelation and Preconcentration*. Analytical Chemistry, 1997. **69**(10): p. 1893-1898.
34. Miller, T.C. and J.A. Holcombe, *Evaluation of electroless gold deposited on porous silica for ligand attachment for metal ion-exchange*. Analytica Chimica Acta, 2002. **454**(1): p. 37-44.
35. Ritchie, S.M.C., et al., *Polycysteine and Other Polyamino Acid Functionalized Microfiltration Membranes for Heavy Metal Capture*. Environmental Science and Technology, 2001. **35**(15): p. 3252-3258.
36. Miller, T.C., et al., *An in Situ Study of Metal Complexation by an Immobilized Synthetic Biopolymer Using Tapping Mode Liquid Cell Atomic Force Microscopy*. Analytical Chemistry, 2001. **73**(17): p. 4087-4095.
37. Miller, T.C. and J.A. Holcombe, *Characterization of metal ion-exchange on modified surfaces of porous carbon*. Analytica Chimica Acta, 2002. **455**(2): p. 233-244.

38. Malachowski, L. and J.A. Holcombe, *Immobilized poly-L-histidine for chelation of metal cations and metal oxyanions*. Analytica Chimica Acta, 2003. **495**(1-2): p. 151-163.
39. Bottari, E., G. Carletti, and M.R. Festa, *Histidine and ornithine as ligands towards lead(II)*. Annali di Chimica (Rome, Italy), 1992. **82**(7-8): p. 357-70.
40. Bottari, E. and M.R. Festa, *Histidine and ornithine as ligands towards zinc(II)*. Journal of Coordination Chemistry, 1990. **22**(3): p. 237-48.
41. Diaz, A.F. and e. al., *Chemical Modification of a Polypyrrole Electrode Surface*. Journal of Electroanalytical Chemistry, 1980. **108**: p. 377-380.
42. Diaz, A.F. and e. al., *Electrochemistry of Conducting Polypyrrole Films*. Journal of Electroanalytical Chemistry, 1981. **129**: p. 115-132.
43. Labaye, D.E. and e. al., *Full Electrochemical Synthesis of Conducting Polymer Films Chemically Grafted to Conducting Surfaces*. Langmuir, 2002. **18**: p. 5222-5230.
44. Pei, Q. and R. Qian, *Electrochemical polymerization of pyrrole in aqueous buffer solutions*. Journal of Electroanalytical Chemistry, 1992. **322**: p. 153-166.
45. Petitjean, J. and e. al., *Ultra-fast electropolymerization of pyrrole in aqueous media on oxidizable metals in a one-step*. Journal of Electroanalytical Chemistry, 1999. **478**: p. 92-100.
46. Zhou, M. and J. Heinze, *Electropolymerization of pyrrole and electrochemical study of pyrrole. 3. Nature of "water effect" in acetonitrile*. Journal of Physical Chemistry B, 1999. **103**: p. 8451-8457.
47. Wu, J.e.a., *Electrochemically controlled solid-phase microextraction based on conductive polypyrrole films*. Analytical Chemistry, 2002. **74**: p. 4855-4859.
48. Ge, H.a.G.G.W., *Characterization of conducting polymeric stationary phases and electrochemically controlled high-performance liquid chromatography*. Analytical Chemistry, 1989. **61**: p. 2391-2394.
49. Rodriguez, F.J.e.a., *The efficiency of toxic chromate reduction by a conducting polymer(polypyrrole): Influence of electropolymerization conditions*. Environmental Science and Technology, 2000. **34**: p. 2018-2023.
50. Elmahadi, H.A.M. and G.M. Greenway, *Immobilized cysteine as a reagent for preconcentration of trace metals prior to determination by atomic absorption spectrometry*. Journal of Analytical Atomic Spectrometry, 1993. **8**(7): p. 1009-14.

51. Skotheim, T.A., *Electroresponsive Molecular and Polymeric Systems*, ed. T.A. Skotheim. Vol. 1. 1988, New York: Marcel Dekker, Inc. 270.
52. Zen, J.-M., A. Kumar, and D.-M. Tsai, *Recent Updates of Chemically Modified Electrodes in Analytical Chemistry*. *Electroanalysis*, 2003. **15**(13): p. 1073-1087.
53. Clark, W.M., *Oxidation-Reduction Potentials of Organic Systems*. 1960. 595 pp.
54. Murray, R.W. and Editor, *Molecular Design of Electrode Surfaces*. [In: *Tech. Chem.* 1992; 22]. 1992. 427 pp.
55. Hicks, J.F., et al., *The Dynamics of Electron Self-Exchange between Nanoparticles*. *Journal of the American Chemical Society*, 2001. **123**(29): p. 7048-7053.
56. White, H.S., et al., *Voltammetric measurement of interfacial acid/base reactions*. *Journal of Physical Chemistry B*, 1998. **102**(16): p. 2930-2934.
57. Viertler, H., J. Gruber, and V.L. Pardini, *Anodic Oxidation of Sulfur- and Selenium-Containing Compounds*, in *Organic Electrochemistry*, H. Lund and O. Hammererich, Editors. 2001, Marcel Dekker, Inc.: New York.
58. Harrison, P.M. and Editor, *Topics in Molecular and Structural Biology, Vol. 6: Metalloproteins, Pt. 1: Metal Proteins with Redox Roles*. 1985. 149-181.
59. Lenz, G.R. and A.E. Martell, *Metal Chelates of Some Sulfur-Containing Amino Acids*. *BIOCHEMISTRY*, 1964. **297**: p. 745-50.
60. Li, N.C. and R.A. Manning, *Some metal complexes of sulfur-containing amino acids*. *Journal of the American Chemical Society*, 1955. **77**: p. 5225-8.
61. Cherifi, K., et al., *Transition metal complexes of L-cysteine containing di- and tripeptides*. *JOURNAL OF INORGANIC BIOCHEMISTRY*, 1990. **38**(1): p. 69-80.
62. Shindo, H. and T.L. Brown, *Infrared spectra of complexes of L-cysteine and related compounds with zinc(II), cadmium(II), mercury(II), and lead(II)*. *Journal of the American Chemical Society*, 1965. **87**(9): p. 1904-9.
63. Berthon, G. and Editor, *Handbook of Metal-Ligand Interactions in Biological Fluids: Bioinorganic Chemistry, Volume 2*. 1995. 605 pp.
64. Lide, D.R., ed. *CRC Handbook of Chemistry and Physics, 84th Edition*. *Journal of the American Chemical Society*. Vol. 126. 2004. 1586.

65. Ferris, N.S., et al., *Resonance Raman Spectra of Copper-Sulfur Complexes and the Blue Copper Protein Question*. Journal of the American Chemical Society, 1978. **100**(18): p. 5939-5942.
66. Johnson, A.M. and J.A. Holcombe, *Poly-L-Cysteine as an Electrochemically-modifiable Ligand for Trace Metal Chelation*. Analytical Chemistry, submitted, 2004.
67. Gutierrez, E., et al., *Characterization of Immobilized Poly-L-aspartate as a Metal Chelator*. Environmental Science and Technology, 1999. **33**(10): p. 1664-1670.
68. Martell, A.E., *Critical Stability Constants*. 1974, New York: Plenum Press.
69. Malachowski, L., J. Stair, and J. Holcombe, *Immobilized Peptides/Amino Acids on Solid Supports for Metal Remediation*. Pure and Applied Chemistry, submitted, 2004.
70. Bhattacharyya, D., et al., *Novel poly-glutamic acid functionalized microfiltration membranes for sorption of heavy metals at high capacity*. Journal of Membrane Science, 1998. **141**(1): p. 121-135.
71. Denizli, A., et al., *Heavy metal ion adsorption properties of methacrylamidocysteine-containing porous poly(hydroxyethyl methacrylate) chelating beads*. Adsorption Science & Technology, 2002. **20**(7): p. 607-617.
72. Denizli, A., et al., *Metal-complexing ligand methacryloylamidocysteine containing polymer beads for Cd(II) removal*. Separation and Purification Technology, 2003. **30**(1): p. 3-10.
73. Denizli, A., et al., *Cysteinylnhexapeptide attached poly(2-hydroxyethyl methacrylate) beads for Cd(II) removal from human plasma in a packed-bed column*. Separation Science and Technology, 2003. **38**(8): p. 1869-1881.
74. Disbudak, A., et al., *Cysteine-metal affinity chromatography: determination of heavy metal adsorption properties*. Separation and Purification Technology, 2002. **26**(2-3): p. 273-281.
75. Elefterov, A.I., et al., *Ion-exchange properties of glutamic acid-bonded silica*. Journal of Chromatography A, 1997. **769**: p. 179-188.
76. Gutnick, D.L. and H. Bach, *Engineering bacterial biopolymers for the biosorption of heavy metals; new products and novel formulations*. Applied Microbiology and Biotechnology, 2000. **54**(4): p. 451-460.

77. Hestekin, J.A., L.G. Bachas, and D. Bhattacharyya, *Poly(amino acid)-Functionalized Cellulosic Membranes: Metal Sorption Mechanisms and Results*. Industrial & Engineering Chemistry Research, 2001. **40**(12): p. 2668-2678.
78. Iwata, H., et al., *Adsorption characteristics of an immobilized metal affinity membrane*. Biotechnology Progress, 1991. **7**(5): p. 412-18.
79. Kiseleva, M.G., P.A. Kebets, and P.N. Nesterenko, *Simultaneous ion chromatographic separation of anions and cations on poly(aspartic acid) functionalized silica*. Analyst, 2001. **126**: p. 2119-2123.
80. Kebets, P.A., K.A. Kuz'mina, and P.N. Nesterenko, *The heats of adsorption of metal cations on silica gel with covalently attached polyaspartic acid*. Zhurnal Fizicheskoi Khimii, 2002. **76**(9): p. 1639-1642.
81. Liu, C.Y. and P.J. Sun, *Preparation and analytical properties of a chelating resin containing cysteine groups*. Analytica Chimica Acta, 1981. **132**: p. 187-93.
82. Say, R., et al., *Preparation and characterization of the newly synthesized metal-complexing-ligand n-methacryloylhistidine having PHEMA beads for heavy metal removal from aqueous solutions*. Macromolecular Materials and Engineering, 2002. **287**(8): p. 539-545.
83. Bottari, E. and M.R. Festa, *On the behavior of cysteine as ligand of cadmium(II)*. Talanta, 1997. **44**(10): p. 1705-1718.
84. Cao, Q.-E., et al., *Study on the flow injection method for the determination of L-cysteine with a Cu(II) complex by fluorescence quenching*. Indian Journal of Chemistry, Section A: Inorganic, Bio-inorganic, Physical, Theoretical & Analytical Chemistry, 2001. **40A**(12): p. 1344-1347.
85. Torchinskii, Y.M., *Sulphydryl and Disulfide Groups of Proteins*. 1971. 229 pp.
86. Ralph, T.R., et al., *The electrochemistry of L-cystine and L-cysteine Part 1: Thermodynamic and kinetic studies*. Journal of Electroanalytical Chemistry, 1994. **375**: p. 1-15.
87. Tong, J., M.-y. Nie, and H.-l. Li, *Electrochemical oxidation of L-cysteine catalyzed by 10-ethylphenothiazine*. Journal of Electroanalytical Chemistry, 1997. **433**: p. 121-126.
88. Reynaud, J.A., B. Maltoy, and P. Casessan, *Journal of Electroanalytical Chemistry*, 1986. **114**: p. 195.

89. Zagal, J., C. Paez, and S. Barbato, *Proceedings - Electrochemical Society*, 1987. **87**(12): p. 211.
90. Chen, P., M.A. Fryling, and R.L. McCreery, *Electron Transfer Kinetics at Modified Carbon Electrode Surfaces: The Role of Specific Surface Sites*. Analytical Chemistry, 1995. **67**(18): p. 3115-22.
91. Chen, P. and R.L. McCreery, *Control of electron transfer kinetics at glassy carbon electrodes by specific surface modification*. Analytical Chemistry, 1996. **68**(22): p. 3958-3965.
92. Colvin, V.L., A.N. Goldstein, and A.P. Alivisatos, *Semiconductor nanocrystals covalently bound to metal surfaces with self-assembled monolayers*. Journal of the American Chemical Society, 1992. **114**(13): p. 5221-30.
93. Itoh, T. and R.L. McCreery, *In Situ Raman Spectroelectrochemistry of Electron Transfer between Glassy Carbon and a Chemisorbed Nitroazobenzene Monolayer*. Journal of the American Chemical Society, 2002. **124**(36): p. 10894-10902.
94. Kagan, M.R. and R.L. McCreery, *Quantitative Surface Raman Spectroscopy of Physisorbed Monolayers on Glassy Carbon*. Langmuir, 1995. **11**(10): p. 4041-7.
95. Liu, Y.-C. and R.L. McCreery, *Reactions of Organic Monolayers on Carbon Surfaces Observed with Unenhanced Raman Spectroscopy*. Journal of the American Chemical Society, 1995. **117**(45): p. 11254-9.
96. Liu, Y.-C. and R.L. McCreery, *Raman Spectroscopic Determination of the Structure and Orientation of Organic Monolayers Chemisorbed on Carbon Electrode Surfaces*. Analytical Chemistry, 1997. **69**(11): p. 2091-2097.
97. Ray, K., III and R.L. McCreery, *Spatially Resolved Raman Spectroscopy of Carbon Electrode Surfaces: Observations of Structural and Chemical Heterogeneity*. Analytical Chemistry, 1997. **69**(22): p. 4680-4687.
98. Turrell, G., J. Corset, and Editors, *Raman Microscopy: Developments and Applications*. 1996. 463 pp.
99. Akhtar, W., et al., *Fourier-transform Raman spectroscopic study of human hair*. Spectrochimica Acta Part A, 1997. **53**: p. 1021-1031.
100. Abu Sal, B., V.N. Moiseenko, and G.D. Zegzhda, *Vibrational spectra and the structure of coordination center complexes of cadmium with cysteine in solid state*. Ukrains'kii Fizichnii Zhurnal, 1999. **44**(11): p. 1347-1350.

101. Alex, S. and R. Savoie, *Raman spectroscopic study of the interactions of metallic ions with molecules of biological interest*. Spectrosc. Biol. Mol., Proc. Eur. Conf., 1st, 1985: p. 226-8.
102. Ikram, M. and D.B. Powell, *Infrared spectra of L-cysteine and its metal complexes*. Pakistan Journal of Scientific Research, 1973. **25**(1-2): p. 53-60.
103. Canty, A.J., et al., *Metal-sulfur stretching frequencies and structures of complexes of zinc, cadmium, and mercury with thiols*. Inorganica Chimica Acta, 1976. **20**(2): p. 161-6.
104. Moiseenko, V.N., et al., *Optical vibrational spectra of solid metallo-complexes of cysteine*. Optika i Spektroskopiya, 1996. **81**(3): p. 430-433.
105. Mori, M., *Raman spectrum of metal complexes*. Kagaku (Kyoto, Japan), 1979. **34**(7): p. 562-6.
106. Wang, Q. and D.D. Allred, *Low-frequency feature in the first-order Raman spectrum of amorphous carbon*. Physical Review B, 1993. **47**(10): p. 6119-6121.
107. Posadas, D., et al., *Redox Potential Distribution in the Presence of Mechanical Stress. The case of Electroactive Polymers*. Journal of Physical Chemistry B, 2001. **105**: p. 2291-2296.
108. Posadas, D., M.J.R. Presa, and M.I. Florit, *Apparent formal redox potential distribution in electroactive arylamine-derived polymers*. Electrochimica Acta, 2001. **46**: p. 4075-4081.
109. Sabatani, E. and F.C. Anson, *A revised model to account for the kinetics of thermodynamically disfavored electron-transfer cross-reactions at the interface between redox polymers and solutions*. Journal of Physical Chemistry, 1993. **97**: p. 10158-10165.
110. Sabatani, E. and F.C. Anson, *Mediated electron transfer across Nafion/solution interfaces. Comparison with Marcus theory for case involving Gaussian arrays of mediator couples*. Journal of Electroanalytical Chemistry, 1995. **386**: p. 111-119.
111. Balandin, A., et al., *Raman spectroscopy of electrochemically self-assembled CdS quantum dots*. Applied Physics Letters, 2000. **76**(2): p. 137-139.
112. Boone, B.E., *Optical characterization of CdS semiconductors by Raman spectroscopy and photoluminescence*, in Auburn Univ., Auburn, AL, USA. *FIELD URL*:. 1998. p. 148 pp.

113. Porteanu, H.E., et al., *Optical properties of CdS/HgS/CdS quantum dot-quantum well structures*. Physica Status Solidi B: Basic Research, 2001. **226**(1): p. 219-232.
114. Milekhin, A.G., et al., *Optical vibrational modes in (Cd, Pb, Zn)S quantum dots embedded in Langmuir-Blodgett matrices*. Thin Solid Films, 2002. **422**(1-2): p. 200-204.
115. Yang, Y.-j., et al., *Electrical transport and optical properties of CdS thin films*. Xiamen Daxue Xuebao, Ziran Kexueban, 2003. **42**(1): p. 39-43.
116. Li, Y., *Effect of anion concentration on the kinetics of electrochemical polymerization of pyrrole*. Journal of Electroanalytical Chemistry, 1997. **433**: p. 181-186.
117. Deinhammer, R.S.e.a., *Ion chromatographic separations using step and linear voltage waveforms at a charge-controllable polymeric stationary phase*. Analytical Chemistry, 1991. **63**: p. 1889-1894.
118. Tsai, E.W.e.a., *Anion-exchange behavior of polypyrrole membranes*. Journal of Physical Chemistry, 1988. **92**: p. 3560-3565.
119. Skotheim, T.A., et al., *Handbook of Conducting Polymers, Second Edition, Revised and Expanded*. 1997. 1112 pp.
120. Hallik, A., A. Alumaa, and J. Tamm, *Influence of ions on the polypyrrole redox process*. Tartu Ulikooli Toimetised, 1993. **966**(Publications on Chemistry XXI): p. 40-51.
121. Tamm, J., et al., *Influence of anions on electrochemical properties of polypyrrole-modified electrodes*. Russian Journal of Electrochemistry (Translation of Elektrokhimiya), 2002. **38**(2): p. 182-187.
122. Hallik, A., et al., *A comparison of redox processes for polypyrrole/dodecylsulfate films in aqueous and non-aqueous media*. Journal of Solid State Electrochemistry, 2001. **5**(4): p. 265-273.
123. Ge, H. and G.G. Wallace, *Characterization of conducting polymeric stationary phases and electrochemically controlled high-performance liquid chromatography*. Analytical Chemistry, 1989. **61**: p. 2391-2394.
124. Miller, T.C. and J.A. Holcombe, *Comparison and evaluation of the synthetic biopolymer poly-L-aspartic acid and the synthetic \"plastic\" polymer poly-acrylic acid for use in metal ion-exchange systems*. Journal of Hazardous Materials, 2001. **83**(3): p. 219-236.

125. Miller, T.C. and J.A. Holcombe, *An Ion-Exchange Microcolumn Employing Gold Minigrids as Supports for the On-Line Immobilization of Poly(L-aspartate)*. Analytical Chemistry, 1999. **71**(14): p. 2667-2671.
126. Capitan, F., M. Roman, and Y.A. Fernandez-Gutierrez, *Spectrophotometric determination of cadmium(II) with Alizarin Complexon*. Boletin de la Sociedad Chilena de Quimica, 1971. **17**(2): p. 29-34.
127. Capitan, F., M. Roman, and A. Guiraum, *Spectrophotometric determination of manganese(II) using Alizarin Complexon*. Quimica e Industria (Madrid), 1971. **17**(3): p. 15-18.
128. Tataev, O.A. and A. Isakhanova, *Analytical possibilities of Alizarine Complexone. 3. Photometric determination of nickel with Alizarine Complexone*. Fiz.-Khim. Metody Anal. Kontrolya Proizvod., 1975: p. 82-3.
129. Marti, F.B., A.C. Martin, and C.F. Gutierrez, *Spectrophotometric determinations of zinc traces*. Inform. Quim. Anal. (Madrid), 1965. **19**(6): p. 165-70.
130. Isakhanova, A.T. and O.A. Tataev, *Study of the reaction of Alizarine Complexone with some inorganic ions*. Fiziko-Khimicheskie Metody Analiza i Kontrolya Proizvodstva, 1976. **2**: p. 111-15.
131. Capitan, F., A. Guiraum, and J. Bullejos, *Spectrophotometric determination of calcium(II) with Alizarine Complexone*. Afinidad, 1975. **32**(327): p. 461-7.
132. Chaplanov, P.E., I.G. Per'kov, and G.D. Khnykin, *Spectrophotometric study of acid-base equilibriums in a Alizarine Complexone (1,2-dihydroxyanthraquinone-3-methylamine-N,N-diacetic acid)-water-sodium chloride system*. 1974, Khar'k. Gos. Univ. im. Gor'kogo, Kharkov, USSR. FIELD URL.: p. 14 pp.
133. Filippova, L.P., A.A. Minin, and Z.G. Kalugina, *Photometric study of the composition of a zinc complex with Alizarine Complexone*. Proizvod. Pirazolona Anal. Reagenty, Metody Fiz.-Khim. Anal., 1976: p. 116-18.
134. Flyantikova, G.V. and L.I. Korolenko, *Photometric and fluorimetric determination of germanium with alizarine complexone and Rhodamine 6Zh*. Zhurnal Analiticheskoi Khimii, 1975. **30**(7): p. 1349-53.
135. Krizan, M. and J. Nozaki, *Use of alizarines and their derivatives for molybdenum determination*. Mikrochimica Acta, 1975. **2**(4-5): p. 435-41.
136. Leonard, M.A. and T.S. West, *Chelating reactions of 1,2-dihydroxyanthraquinon-3-yl-methylamine-N,N-diacetic acid with methyl cations in aqueous media*. Journal of the Chemical Society, Abstracts, 1960: p. 4477-86.

137. Melikov, A.A., *Determination of cerium subgroup rare earth elements by Alizarine Complexone in the presence of diphenylguanidine*. Azerbaidzhanskii Khimicheskii Zhurnal, 1977(1): p. 114-18.
138. Mori, I., et al., *Electrophoretic determination of pK-values of indicators and their relation to color changes*. Talanta, 1972. **19**(3): p. 299-306.
139. Nazarenko, V.A., et al., *Mechanism of reactions of polyvalent element ions with organic reagents. 31. Interaction of germanium(IV) and alizarine complexone*. Zhurnal Analiticheskoi Khimii, 1975. **30**(7): p. 1354-60.
140. Qureshi, G.A., G. Svehla, and M.A. Leonard, *Electrochemical studies of strongly chelating anthraquinone derivatives*. Analyst (Cambridge, United Kingdom), 1979. **104**(1241): p. 705-22.
141. Rudenko, E.I. and V.A. Popov, *Flotation-photometric determination of fluorine using rare earth element Alizarine Complexonates*. Zavodskaya Laboratoriya, 1979. **45**(5): p. 388-91.
142. Shkrobot, E.P., N.S. Tolmacheva, and T.M. Baigulova, *Three-component compounds of fluoride with Alizarine Complexone and rare earth elements*. Nauch. Tr. NII Tsvet. Met., 1977(43): p. 12-14.
143. Stroehl, G.W. and D. Kurzak, *New cationic surfactant-dye complexes and their absorption spectra. I*. Tenside, 1969. **6**(2): p. 76-7.
144. Tataev, O.A. and A. Isakhanova, *Analytical possibilities of alizarin complexon. 4. Photometric determination of ytterbium with alizarin complexon*. Fiz.-Khim. Metody Anal. Kontrolya Proizvod., 1975: p. 84-5.
145. Tataev, O.A. and A. Isakhanova, *Possible analytical uses of Alizarine Complexone. (Communication 4). Photometric determination of ytterbium by Alizarine Complexone*. Sb. Nauch. Soobshch. Dagestan. Un-t. Kafedra Obshch. Khimii, 1975(9): p. 84-5.
146. Tataev, O.A. and A. Isakhanova, *Possible analytical uses of Alizarine Complexone. (Communication 3). Photometric determination of nickel by Alizarine Complexone*. Sb. Nauch. Soobshch. Dagestan. Un-t. Kafedra Obshch. Khimii, 1975(9): p. 82-3.

Vita

Ashley Michelle Johnson was born on May 26, 1977 in Birmingham, Alabama, to Dennis and Sharon Johnson. She attended the Lois Cowles Harrison Center for the Visual and Performing Arts graduating in May of 1995 as the valedictorian. Following high school graduation, Ashley enrolled at the University of Florida in Gainesville, Florida where she earned a Bachelor of Science degree in Chemistry graduating in December of 1998. She began graduate studies at the University of Texas in analytical chemistry in the fall of 1999 under the supervision of James A. Holcombe.

Permanent address: 1226 Brighton Way, Lakeland, FL 33813

This dissertation was typed by the author.